Journal Pre-proof

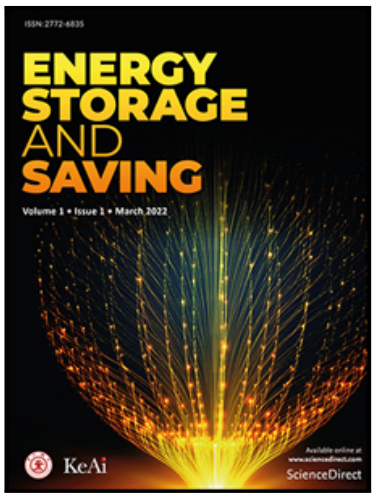

Recent development in degradation mechanisms of proton exchange membrane fuel cells for vehicle applications: problems, progress, and perspectives

Zikuo Liu , Shanshan Cai , Zhengkai Tu , Siew Hwa Chan

PII: S2772-6835(24)00012-8
DOI: https://doi.org/10.1016/j.enss.2024.02.005
Reference: ENSS 69

To appear in: *Energy Storage and Saving*

Received date: 29 November 2023
Revised date: 25 February 2024
Accepted date: 26 February 2024

Please cite this article as: Zikuo Liu , Shanshan Cai , Zhengkai Tu , Siew Hwa Chan , Recent development in degradation mechanisms of proton exchange membrane fuel cells for vehicle applications: problems, progress, and perspectives, *Energy Storage and Saving* (2024), doi: https://doi.org/10.1016/j.enss.2024.02.005

Recent development in degradation mechanisms of proton exchange membrane fuel cells for vehicle applications: problems, progress, and perspectives

Zikuo Liu[1], Shanshan Cai[1,*], Zhengkai Tu[1], Siew Hwa Chan[2]

[1]School of Energy and Power Engineering, Huazhong University of Science and Technology, Wuhan, Hubei, 430074, China

[2]Energy Research Institute, Nanyang Technological University, 50 Nanyang Avenue, 637553, Singapore

* Corresponding author. E-mail: shanshc@hust.edu.cn

Abstract

Due to its zero emissions, high efficiency and low noise, proton exchange membrane fuel cell (PEMFC) is full of potential for the application of vehicle power source. Nonetheless, its lifespan and durability remain multiple obstacles to be solved before widespread commercialization. Frequent exposure to non-rated operating conditions could considerably accelerate the degradation of the PEMFC in various forms, thus reducing its durability. This paper first analyses degradation mechanisms of PEMFCs under typical automotive operating conditions, including idling, startup-shutdown, dynamic loads, and cold start. The corresponding accelerated stress testing methods are also discussed. Then, as the impurities existed in the reaction gas source and generated from the degradation of the PEMFC itself may occur under all automotive

conditions, the degradation mechanisms caused by impurity contamination are classified and reviewed in detail. After that, the techniques proposed by researchers to enhance the durability of PEMFCs are presented from four aspects: MEA materials, bipolar plates and flow fields design, stack assembly, and cell control strategies. The challenges in the field and the prospects for the future are summarized and analyzed at the end. The aim of this work is to provide guidelines for improving the durability of PEMFCs in vehicle applications.

Keywords: Proton exchange membrane fuel cell; Vehicle; Automotive operating conditions; Degradation; Durability

List of Abbreviation

Abbreviation	Definition
AST	Accelerated stress testing
CL	Catalyst layer
COR	Carbon oxidation reaction
ECSA	Electrochemical active surface area
GDL	Gas diffusion layer
MEA	Membrane electrode assembly
MPC	Model predictive control
OCV	Open circuit voltage
OER	Oxygen evolution reaction
ORR	Oxygen Reduction Reaction
PEM	Proton exchange membrane
PEMFC	Proton exchange membrane fuel cell

PFSA	Perfluorosulfonic acid
PI	Proportional-integral
PID	Proportional-Integral-Derivative
PTFE	Polytetrafluoroethylene
SS	Stainless steel

1.Introduction

The proton exchange membrane fuel cell (PEMFC) is a clean, non-polluting energy source that offers high efficiency and power density. It is capable of replacing internal combustion engines as a transportation power source [1,2]. In recent years, researchers have made progress in improving the performance of PEMFCs, which has strengthened the competitiveness in the market [3]. In certain applications, such as vehicle power sources, PEMFCs are often subjected to non-ideal operating conditions. These severe operating conditions can considerably accelerate the ageing and degradation of PEMFCs implemented in vehicles, thus form obstacles for long-term operation of fuel cell vehicles. The lifespan of PEMFCs is still a crucial restriction that impeding the commercialization [4,5]. To expedite the implementation of PEMFC technology in the transport industry, the European Commission has suggested an aim of 7,000 to 28,000 hours for the lifespan of PEMFC systems installed on light- and heavy-duty vehicles by 2030. This aligns with the long-term ambition of 8,000 to 30,000 hours proposed by U.S. Department of Energy (DOE) [6]. Achieving competitive costs while meeting durability targets is a crucial and inevitable challenge of the research related to PEMFC.

The degradation of the PEMFC under automotive operating conditions can be generally categorized into the following forms [7,8]: (1) chemical degradation of the proton exchange membrane under idling conditions; (2) carbon support corrosion under startup-shutdown conditions; (3) mechanical degradation of the membrane and catalyst morphology under dynamic load conditions; (4) ice damage to PEMFC components during cold start. Besides, there exists poisoning failure of catalyst and accelerated membrane decomposition under impurity contamination. Some scholars have noted that in the actual operating process, different operating conditions may have varying durations, with their impacts on the durability of PEMFC classified into primary (such as load changing, start-stop) and secondary (such as idling and high power) categories [8,9]. Nevertheless, to further advance the lifespan of PEMFC, it is important to clarify the mechanism of typical automotive operating conditions and understand the specific degradation process of PEMFC. Many studies have been conducted on the durability of PEMFC, along with more comprehensive degradation analysis methods [10]. Furthermore, they have suggested various measures and strategies to boost the durability of PEMFCs in vehicles. A state-of-art literature may summarize potential techniques and provide multiple insight for the enhancement of in-vehicle PEMFC durability.

This paper presents a thorough analysis of the degradation mechanisms and strategies for improving the durability of PEMFCs under common operational conditions of vehicles, as shown in Fig. 1. Specifically, Sections 2 to 5 describe the primary degradation mechanisms related to idling, dynamic loads, startup-shutdown, cold start,

and analyze the corresponding methodology. Accelerated stress testing (AST) is commonly used in durability studies, and some representative AST methods can provide insights to other researchers on certain PEMFC durability issues. Therefore, these sections also briefly introduce the corresponding AST methods under different typical working conditions. Section 6 discusses the impact of impurities on the durability of PEMFCs, including those used in automotive applications. It is important to consider the negative effects of impurities on PEMFCs as demands for durability increase. Additionally, severe operating conditions may accelerate the formation of impurities from the PEMFC itself, which can threaten the durability of automotive PEMFCs. Therefore, it is crucial to pay close attention to this issue. Section 7 mainly discusses the potential solutions proposed by researchers for durability improvement in recent years. These possible solutions are evaluated based on the degradation mechanisms and consider the overarching problems regarding membrane electrode assembly (MEA) materials, bipolar and flow fields, stack assembly, and control strategies. This paper suggests potential design principles and approaches for highly resilient PEMFCs in vehicle applications and discusses further challenges that require more in-depth research.

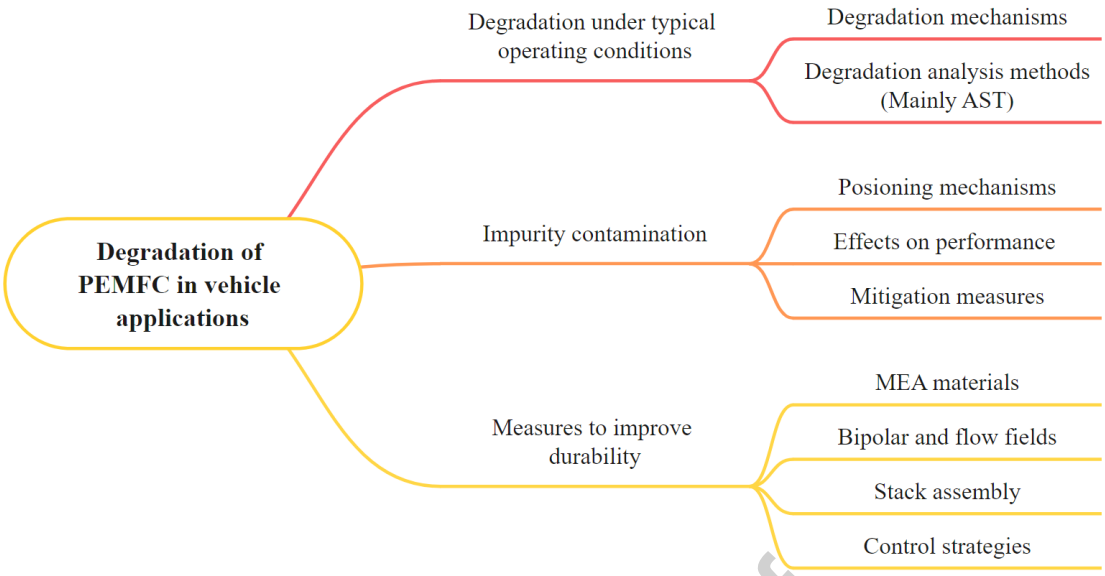

Fig. 1. The logic structure diagram of this paper.

2. Idling condition

Automotive PEMFCs need to operate at lower current densities and low power output during idling conditions. Under this condition, the high potential of the cathode and the reaction gas can cause irreversible damage to the Pt catalyst and membrane. As a result, the durability and healthy operation of the PEMFC are challenged.

2.1 Degradation mechanisms

2.1.1 Chemical degradation of the membrane

Due to the low current density and fuel consumption under idling condition, the reaction gas is transported to the other pole by penetrating the proton exchange membrane under the effect of concentration gradient. This process produces H_2O_2, which is further decomposed to produce free radicals such as ·OH and OOH [11]; with the aid of a catalyst, hydrogen and oxygen can also react directly to produce free radicals [12,13]. These reaction processes can be expressed by the following equations [14].

$$O_2 + 2H^+ + 2e^- \rightarrow H_2O_2 \#(1)$$

$$H_2O_2 + \cdot OH \rightarrow \cdot OOH + H_2O \#(2)$$

$$H_2 + \cdot OH \rightarrow \cdot H + H_2O \#(3)$$

$$O_2 + \cdot H \rightarrow \cdot OOH \#(4)$$

$$H_2 + O_2 \rightarrow 2 \cdot OH \#(5)$$

These free radicals can damage the proton exchange membrane as a direct result of which the membrane thins, the surface becomes rough, and even cracks and pinholes appear. This leads to irreversible degradation of the PEMFC, a process often referred to as chemical degradation of membranes. Here, perfluorosulfonic acid (PFSA) membrane is taken as an example to explain the damaging effects of free radicals on membranes.

The molecular structure of PFSA membranes consists of a main chain, which determines the mechanical properties of the membrane, and a side chain, which determines the electrical conductivity of the membrane through the sulfonate group located at its end [12,15] (see Fig. 2).·OH attacks the carboxyl group at the end of the main chain [16,17] and the relatively weak bonds of α-OCF_2, β-OCF_2 and C-S in the side chains [16,18]. It has been shown that β-OCF_2 breaks later than α-OCF_2, that is, the side chain breaks first at the end [12]. For H radicals, the tertiary carbon in the molecular structure of PFSA is their main target [12,19]. In addition, it has been shown that the rate of main chain disruption does not seem to change drastically due to the high stability of the O-H bond, but the disruption of the side chain is accompanied by the continuous generation of new radicals, which exacerbates the

further disruption of the side chain [20,21]. Since hydrofluoric acid is produced during most of the free radical damage to membranes, the rate of fluorine release reflects the extent to which the membrane is affected by chemical decay [22,23]. The mechanism of free radical damage to PFSA membranes and the associated reaction equations are shown below:

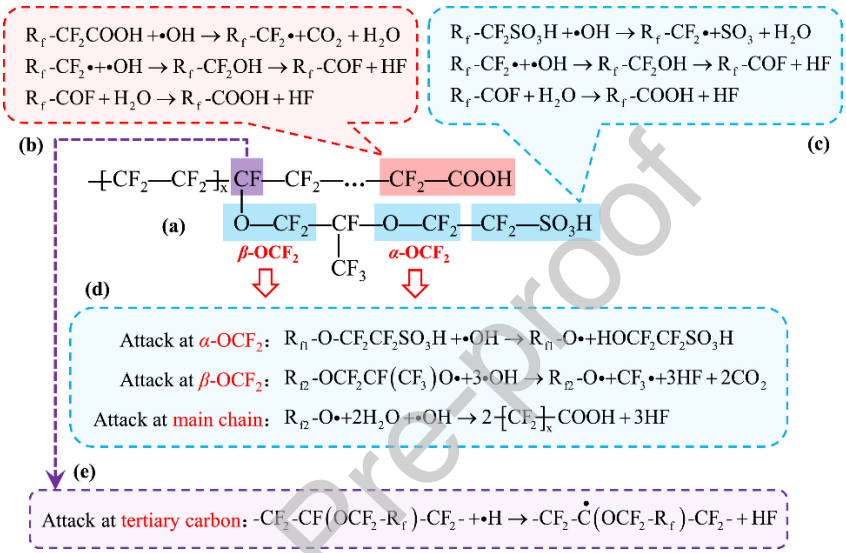

Fig. 2. Schematic diagram of the mechanism of action of free radicals attacking the PFSA membrane. Reprinted from Ref. [7] with permission of Elsevier. (a) Molecular structure of PFSA membranes containing long side chains; (b) Mechanism of attack on the carboxyl group at the end of the main chain; (c) Mechanism of attack on the terminal C-S bond of the side chain; (d) Mechanism of attack on α-OCF_2 and β-OCF_2 within the side chain; (e) Mechanism of attack on tertiary carbon branching point between the main chain and the side chain. R_f is the portion not involved in the chemical reaction.

2.1.2 Pt catalysts degradation in the catalyst layer (CL)

In addition to the chemical degradation of the membrane, high voltages under idling

conditions can have a significant detrimental effect on the CL [24,25]. This paper focuses on the decline of Pt catalysts, that is, changes in the distribution of Pt on the carbon support with its own structure, which tends to cause a significant decrease in electrochemical surface area (ECSA). Under idling conditions, high cathodic potentials cause Pt dissolution, a process that can be described by the following equations [26]:

$$Pt - 2e^- \rightarrow Pt^{2+} \#(6)$$

$$Pt + H_2O - 2e^- \rightarrow PtO + 2H^+ \#(7)$$

$$PtO + 2H^+ \rightarrow Pt^{2+} + H_2O \#(8)$$

At the cathode, smaller sized Pt particles dissolve and then deposit at larger sized Pt particles under the tendency of reduced surface energy, which will increase the average particle size of the Pt catalyst. This process is known as Ostwald ripening [27,28]. Literature [7] suggests that electrochemical Ostwald ripening (EOR) actually occurs during PEMFC operation, as the Pt atoms are less likely to be directly soluble in the ionomers. The carbon supports and ionomers in the CL act in two similar way for the Pt particles: the carbon supports act as electrical conductors among the Pt particles, and once the Pt particles are in contact or sintered, electrons can flow from the smaller particles to the larger one, which can lead to an increase in the sphericity of the aggregated particles, as observed by Sneed et al [29]. Ionomers conduct Pt^{2+}, which allows further fusion of small Pt particles to larger particles. The schematic diagram of the degradation mechanism of Pt catalysts is indicated in Fig. 3.

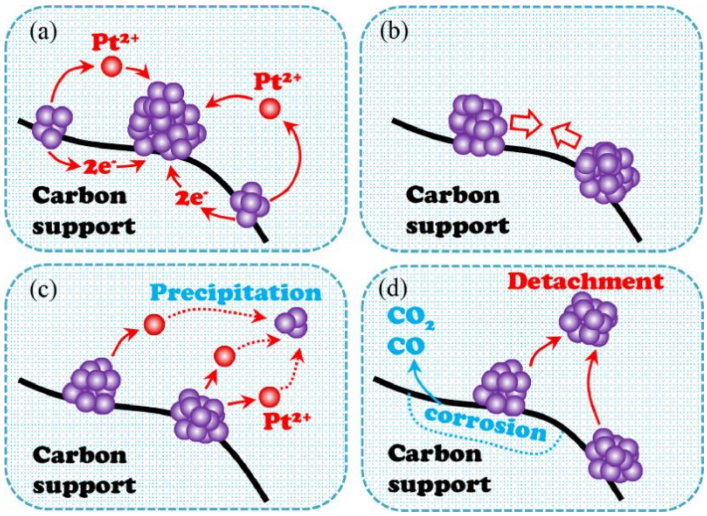

Fig. 3. Schematic diagram of the degradation mechanism of Pt catalysts. Reprinted from Ref. [7] with permission of Elsevier. (a) Electrochemical Ostwald ripening; (b) Agglomeration and sintering of Pt particles; (c) Pt catalyst migration such as dissolution, diffusion and precipitation in ionomers or membranes; (d) Pt catalyst separation.

In addition to the effect of the EOR process, agglomeration and sintering of Pt particles probably occurs. Under idling conditions, the heat released from the direct reaction between hydrogen and oxygen may form hot spots at the electrode due to gas permeation across the membrane, which can promote the agglomeration process of Pt particles [30].

Pt^{2+} dissolved at the cathode also moves towards the anode under the effect of concentration gradient [31], during which Pt^{2+} tends to be reduced to microcrystalline structures and deposited in proton exchange membranes or ionomers, which is known as Pt migration. After separation from the carbon support, these Pt deposits are unable to catalyse the oxygen reduction reaction (ORR) due to the lack of electrons. The

migration of Pt does not occur only in idling condition, but it is more pronounced as Pt tends to be more soluble in this condition [7]. Moreover, Pt migrates and then deposits into the membrane (Fig. 4), where it forms Pt bands [32,33], which can reduce the proton conductivity of the membrane and may also lead to electronic short circuits within the membrane [34].

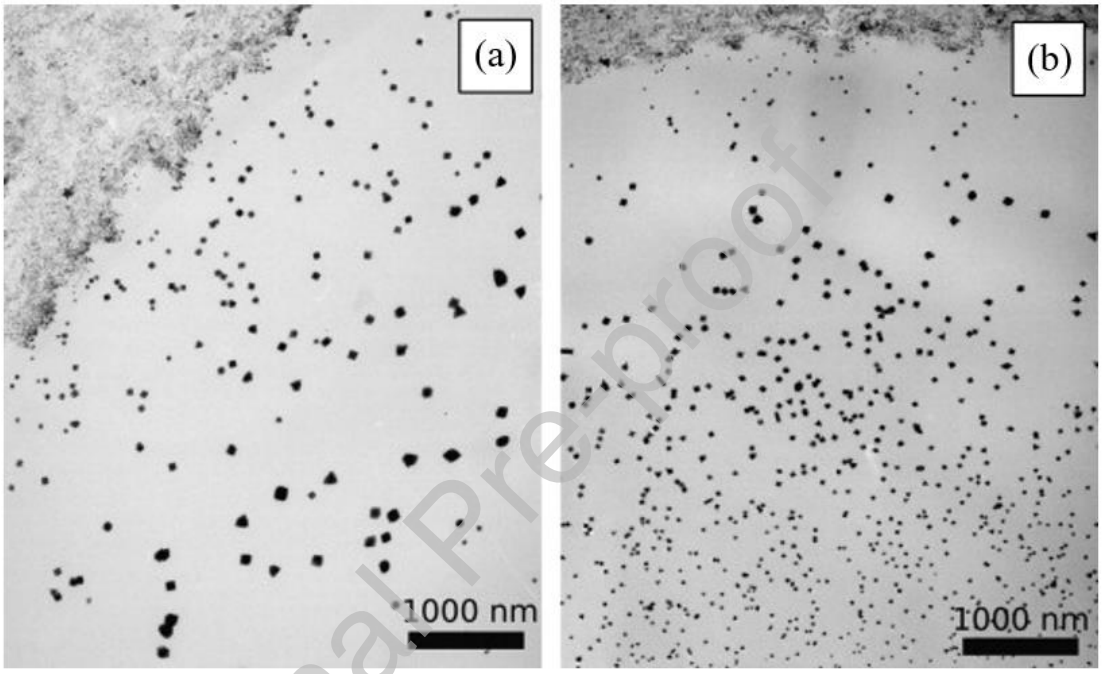

Fig. 4. TEM images of reprecipitated Pt crystallites. (a) PEMFC with more severe degradation; (b) PEMFC with more severe degradation [34]. Reprinted from Ref. [34] with permission of Elsevier.

However, the effect of Pt bands on the durability of PFSA membranes and their mechanism of action remain to be further investigated because the effect of Pt bands on the generation of H_2O_2 and free radicals is two-fold [35,36]. On the one hand, Pt bands have the role of catalysing the generation of H_2O_2 from hydrogen and oxygen, and some researchers have shown that Pt bands negatively affect the membrane

durability by measuring the fluorine emission rate and membrane thickness [37,38]; on the other hand, Pt bands also catalyse the generation of water from hydrogen and oxygen, and inhibit H_2O_2 and free radicals [39]. In other words, Pt deposition in membranes can catalyse the formation and quenching of H_2O_2 and free radicals simultaneously, and the Pt structural morphology and concentration distribution play an important role in the competition between the formation and quenching reactions [40,41]. If the relevant conditions when the quenching reaction dominates the reaction system can be derived, it can be attempted to artificially load a certain amount of Pt in PFSA membranes to improve the chemical stability and durability of the membranes.

2.2 Degradation analysis methods

Some researchers have conducted accelerated tests of proton exchange membrane durability by operating the PEMFC at open circuit voltage (OCV) without discharge [42]. In this condition, since there is no current generation and no consumption of reactant gas, its partial pressure in the electrode rises [11,43], which promotes gas permeation through the membrane [44,45]. Moreover, no water is produced in the OCV condition, which maintains the water content of the membrane and the partial pressure of water in the cathode at a low level. The insufficient expansion of the membrane increases its porosity, while the low partial pressure of water provides some space for oxygen in the cathode [46]; and the oxygen permeation process is not hindered by electroosmotic resistance [17]. Since the OCV condition can be regarded as what the idling condition can achieve at the limit, the performance degradation of the PEMFC under the OCV condition can be considered to be very close to the

conclusion of the idling condition. In addition, if the focus is on membrane durability, more severe conditions can be used, such as higher operating temperatures and lower humidity [7]; an increase in backpressure implies higher partial pressures of reactants, which enhances the permeation of gases through the membrane and accelerates the chemical decline of the membrane. Currently, numerous OCV operating conditions are available, and the differences are mainly in the temperature, relative humidity, and back pressure of each OCV operating condition [22,42,47].

Mitigation of PEMFC degradation under idling conditions requires both gas permeation and high cathode potential. Some reports suggest that cathode exhaust gas recirculation may be effective because it can dilute the cathode gas to a lower oxygen concentration level and can reduce the cathode potential during low load operation of the PEMFC [48,49]. However, the improvement effect of this method still needs to be confirmed by durability related tests.

3. Startup-shutdown

Under startup-shutdown conditions, a hydrogen-air interface at the anode of a PEMFC can cause a high interfacial potential difference at the cathode. This can lead to severe corrosion of the carbon material at the cathode, resulting in Pt catalyst particles falling off the carbon carrier, and possible aggregation and recombination of the ionomers. This can impede the mass transfer process between protons and water, reducing the ECSA and increasing the electrical resistance. These factors have a significant negative impact on the durability of the PEMFC.

3.1 Degradation mechanisms

3.1.1 Reverse current mechanism

During the startup-shutdown condition of PEMFC, some air exists at the anode, and when hydrogen enters the anode, a hydrogen-air interface is formed, which further leads to a high potential difference at the cathode (Fig. 5). This is the key factor of PEMFC degradation under startup-shutdown condition: the high potential difference at the cathode can result in severe corrosion of the carbon supports in CL, loss of Pt-catalyst detachment, and ECSA decreases, resulting in direct performance degradation.

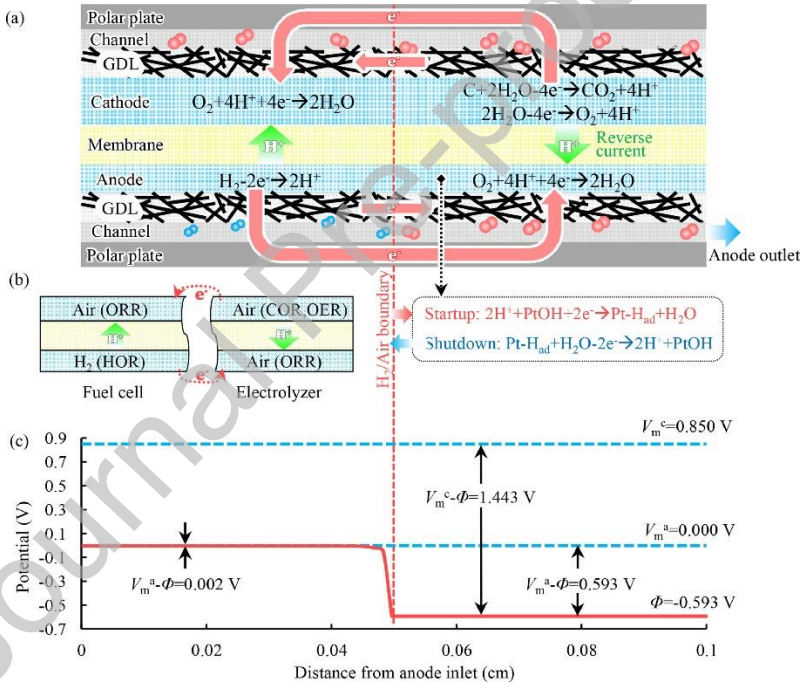

Fig. 5. Hydrogen-air interface effect on PEMFC [50]. Reprinted from Ref. [7] with permission of Elsevier. (a) Schematic diagram of reverse current formation mechanism. (b) Schematic diagram of dual-cell formation mechanism.(c) Potential distribution along the gas flow channel in PEMFC.

The simultaneous presence of air and hydrogen at the anode forms a hydrogen-air

interface as shown in Fig. 5(a) [50].When the PEMFC is started, the hydrogen-air interface moves towards the anode output side; whereas, when the PEMFC is stopped, the hydrogen-air interface moves away from the anode output side. Hydrogen-rich region (left side of the dashed line of the hydrogen-air interface shown in Fig. 5) and oxygen-rich region (right side of the dashed line of the hydrogen-air interface shown in Fig. 5) were formed on both sides of the hydrogen-air interface, respectively. Meanwhile, the anode and cathode can be considered to be equipotential due to the good electronic conductivity of the electrodes, gas diffusion layer (GDL) and bipolar plates, respectively. In the hydrogen-rich region on the left, the bipolar reaction of the cell occurs normally; while ORR occurring in the oxygen-rich region at the anode, the ionomer potential is further reduced. As a result, the potential difference in the cathode oxygen-enriched region increases significantly. This intensifies the carbon oxidation reaction (COR) and oxygen evolution reaction (OER) within the cathode. The carbon skeleton in the CL is destroyed due to oxidation, and protons generated by COR and OER are transferred from the cathode to the anode to generating a reverse current [50,51].

At this point, the PEMFC can be considered to consist of a cell (left side of the hydrogen-air interface) and an electrolytic cell (right side of the hydrogen-air interface), and the GDL for conducting electrons and the bipolar plate can be thought of as the external conductor. Tang et al. [52] performed dual-cell experiments, and currents were detected between the cells when anode gases were exchanged between the air and reformate gases. Eom et al. [53] found that when the anode Pt loadings

were low, the PEMFC degradation was mitigated. They attributed this to a decrease in the ORR rate, which led to a decrease in the reverse current, COR, and the rate of OER.

3.1.2 Carbon corrosion

During PEMFC operation, the possible COR and its corresponding standard potentials are shown in the following equations [54,55]:

$$C + 2H_2O \rightarrow CO_2 + 4H^+ + 4e^- \quad E^0_{\frac{C}{CO_2}} = 0.207V(vs.SHE)\#(9)$$

$$C + H_2O \rightarrow CO + 2H^+ + 2e^- \quad E^0_{\frac{C}{CO}} = 0.518V(vs.SHE)\#(10)$$

It can be seen that COR can occur at relatively low equilibrium potentials, although the kinetics of COR is slower in the regular potential range, the carbon corrosion situation can be neglected when the PEMFC operates normally [56]. However, in the startup-shutdown condition, excessive cathodic potential difference leads to a significant carbon corrosion condition. Researchers have concluded that potentials higher than 1.2 V lead to severe carbon corrosion [57]. The higher the cathodic potential [58] and the more cathodic Pt catalyst loaded [59], the more serious the carbon corrosion situation is.Yu et al. [60] found that the enhancement of carbon corrosion by Pt catalyst was mainly concentrated in the early stage, and the rate of carbon corrosion tended to a certain value with the passivation of the catalyst surface and the decrease of activity.

In addition, carbon corrosion in GDL is limited due to the absence of catalyst. It has been widely observed by scholars that CO_2 emission increases [56,61,62], the size of carbon particles decreases [63], and holes appear in the carbon skeleton [64], which

leads to a decrease in the strength of the cathode structure, and the CL may collapse under a certain pressure, allowing the cathode thickness to decrease [65,66]. As shown in the Fig. 6 below, (a)-(c) shows the appearance of holes in the carbon support [64], and (d)-(f) shows the thinning of the cathode [67].

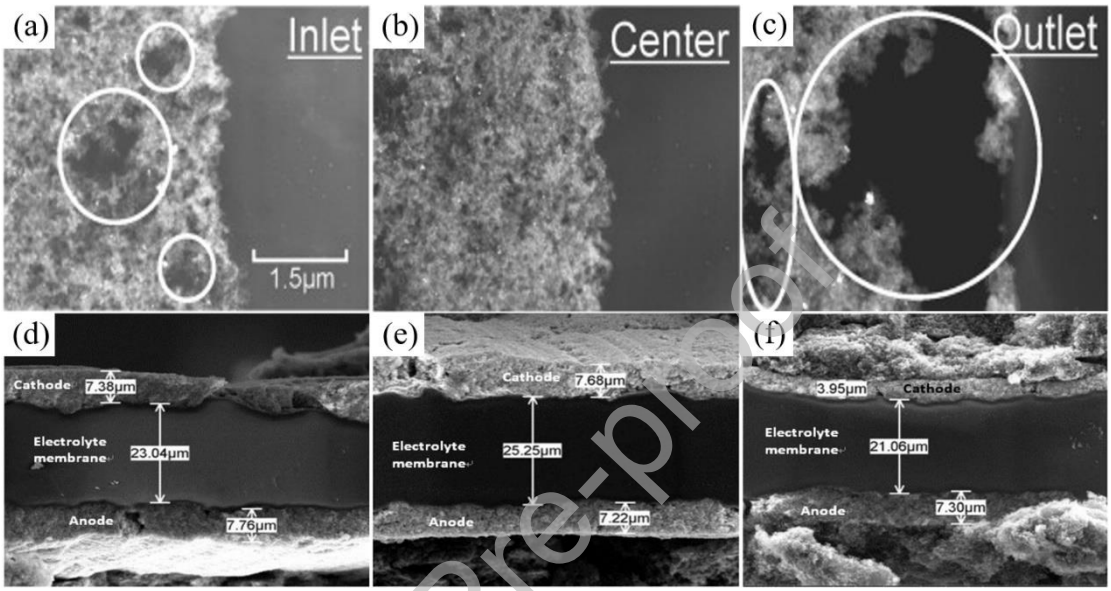

Fig. 6. STEM images at different locations of the anode after startup-shutdown condition acceleration experiments. 500 gas exchange cycles [64]: (a) anode inlet; (b) anode center; (c) anode outlet. Reprinted from Ref. [64] with permission of Elsevier. 1,800 startup-shutdown cycles [67]: (d): anode inlet; (e) anode center; (f) anode outlet. Reprinted from Ref. [67] with permission of Elsevier.

3.1.2.1 Non-uniform corrosion

Since the hydrogen-air interface is always moving with hydrogen injection, different locations of the PEMFC cathode are exposed to the oxygen-rich region for different periods of time and are subjected to different corrosion conditions. For example, if the anode outlet is always exposed to air, the corresponding cathode suffers the most

severe carbon corrosion. The anode inlet is exposed to air for a longer period of time if the anode is purged with air during shutdown. As a result, there are some differences in carbon corrosion at the anode inlet, center and outlet. Ishigami et al. [64] found that the inlet and outlet suffered from severe carbon corrosion as shown in the cathode carbon support holes in Fig. 6 (a)-(c) above. Lin et al. [67] accelerated fuel cell aging by simulating the actual start-up-stop-up process, and observed a similar phenomenon, as shown in Fig. 6 (d)-(f) above. The shrinkage of cathode thickness indicates that the localised cathodic corrosion facing the anode exit is the most severe region.

3.1.2.2 Effects on mass transfer

It is concluded that carbon corrosion alters the path of electron transfer, which causes an increase in ohmic and contact resistance [68]; the electrochemically active area is also reduced due to aggregation [69,70] and detachment [63,69]of the Pt catalyst, see Fig. 7. Carbon corrosion leads to significant changes in the composition and morphology of the cathodic CL, resulting in a redistribution of ionomer weights, a decrease in CL porosity [10], and an increase in hydrophilicity of the carbon support surface [20]. Ionomer redistribution creates partially un- and over-covered Pt particles, which not only reduces the electrochemically active area but also hinders mass transfer to the active surface of the covered Pt particles. It also weakens the water transport in the cathode, thus increasing the possibility of flooding [71]. As carbon corrosion makes the cathode structure unstable and more susceptible to collapse, cathode porosity is generally, but not absolutely, reduced, and is related to the

structural strength of the CL. Some authors have detected enlarged pores [64] and there are also reports claiming that the decrease in porosity is not necessarily uniform [65]. In general, the porosity decreases as the cathode thickness decreases, which again hinders the mass transfer process. Surface oxidation of carbon supports can produce a number of hydrophilic groups that attach to the carbon surface and reduce the surface hydrophobicity [72,73]. As a result, water transport becomes more difficult. In other words, water tends to accumulate in the declining cathode, leading to a thicker water film in the CL and hindering mass transfer.

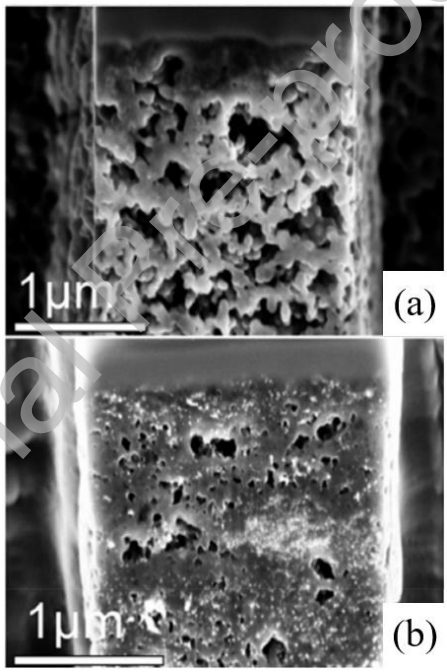

Fig. 7. Comparison of SEM images of CL at the cathode before (a) and after (b) 1,000 gas exchange cycles. Reprinted from Ref. [61] with permission of American Chemical Society.

3.1.2.3 Influencing factors and mitigation initiatives

The degree of carbon corrosion is also influenced by environmental conditions.

Higher gas humidity [74,75] and higher operating temperatures [76] have been reported to accelerate carbon corrosion. Furthermore, carbon corrosion can be controlled by optimising the startup-shutdown procedure [77,78]. The basic strategy is to reduce or eliminate the effect of the hydrogen-air interface. The following measures can be taken during shutdown. Rapid elimination of residual hydrogen in the anode reduces the residence time at the hydrogen-air interface and thus mitigates carbon corrosion; it can be achieved by blowing the anode [79] or introducing a virtual load to consume the residual hydrogen [80]. Elimination of residual air is also an approach, with some authors opting to cut off the air supply prior to hydrogen termination during shutdown [62]. In addition, virtual loads can be used to consume residual oxygen [80,81]. Researchers have also attempted to develop and utilise corrosion-resistant catalyst support materials such as graphite [68], carbon nanofibres [82], and carbon nanotubes [83,84].

3.2 Degradation analysis methods

For the aging of PEMFC under startup-shutdown condition, different accelerated testing methods have been adopted by different researchers. For example, the startup-shutdown process can be repeated rapidly, which is very close to the startup-shutdown condition in the actual working process of PEMFC [85,86]. This method has been used by researchers to evaluate the optimisation of human-set start-stop procedures [87], as well as the effects of condition parameters such as temperature, relative gas humidity, etc [74,88]. Other researchers have alternately transferred air and hydrogen to the anode to simulate the hydrogen-air boundary and

its movement in the anode [89]. In addition, because carbon corrosion is due to high cathodic potentials, high potentials applied to the cathode have also been used in tests to investigate the corrosion of the carbon skeleton in CL, the detachment of the Pt catalyst, etc [72,90].

4. Dynamic load

During the practical operation of the PEMFC, frequent output power changes are often required to meet the demands of vehicles in different situations. Under dynamic load conditions, the electrode potential, internal temperature, pressure and water state of the PEMFC undergo rapid fluctuations over a short period of time, generating a temperature/humidity cycle, which can significantly accelerate the mechanical degradation of the PEMFC components [91]. Moreover, the dynamic demand for gas supply may occur as gas starvation during loading, and the Pt catalyst will also decay under dynamic load conditions.

4.1 Degradation mechanisms

4.1.1 Mechanical degradation of PEMFC

At larger loadings, the electrochemical reaction rate is increased with a consequent rise in the rate of water production, which can lead to an increase in the water content of membranes and ionomers in the PEMFC. Conversely, smaller loads result in lower water content or even dehydration of the membrane and ionomer. The water absorption and dehydration of the membrane also cause it to expand and contract, respectively. Consequently, during repeated dynamic loading, the stresses generated by the cyclic changes in volume cause the membrane to undergo mechanical

degradation [92,93]. The membrane become thinner, pinholes and cracks may also appear in it [94,95]. Since CL contains certain ionomers, the change in its volume also causes structural changes and triggers mechanical recession [96,97]. Moreover, there is a difference in the degree of strain and deformation between the membrane and CL, and frequent dynamic loading can cause the residual stress and strain to crack and separate the membrane-CL junction [98,99] (Fig. 8). Similarly, delamination between CL and GDL has also been reported [99,100]. Delamination of components hinders the transport of protons (between membrane and CL) and electrons (between CL and GDL), and increases the contact resistance, which adversely affects the PEMFC output performance. To meet the required output power, the current density is increased in the regions adjacent to the delamination of the components. This results in increased water and heat production, which can affect the durability of the internals in these regions [98].

Furthermore, the humidity cycling-induced volume change of ionomers in CL may result in their aggregation and redistribution. This phenomenon has been observed by some researchers [96]. Under normal conditions, the ionomers in CL are highly dispersed but not very stable. Certain disturbances, such as changes in the structure of the CL or detachment and agglomeration of Pt catalyst particles, can cause the agglomeration and redistribution of the ionomers. The outcome is comparable to that outlined in the preceding section on the impact of carbon corrosion. It impedes the binding of protons to the Pt catalyst, thereby reducing the ECSA in disguise. Additionally, the over-covered ionomers increase the mass transfer resistance to some

extent.

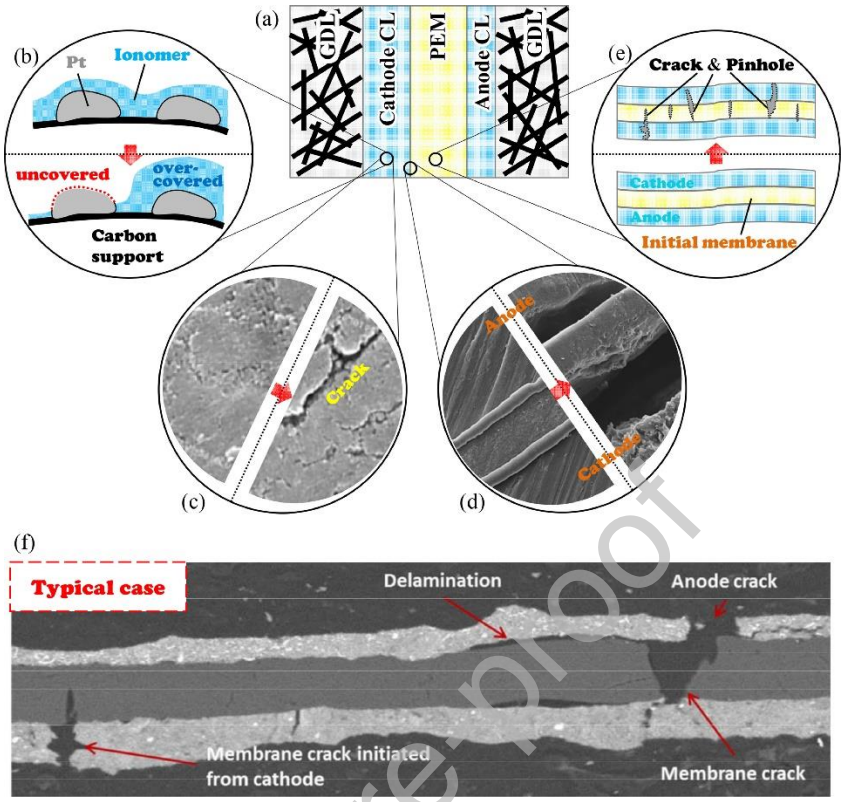

Fig. 8. Schematic diagram of mechanical degradation of PEMFC components under dynamic load conditions [7,95,99,100]. Reprinted from Ref. [7] with permission of Elsevier. (a) Brief schematic of membrane electrode assembly (MEA); (b) Agglomeration and redistribution of ionomers in CL; (c) Crack formation and extension in CL; (d) Delamination of CL with membrane; (e) Formation and extension of cracks and pinholes in the membrane; (f) Typical SEM image of the cross section after humidity cycling.

4.1.2 Gas starvation

During PEMFC loading, there is often a delay in gas supply relative to the increase in current. Rapid loading can lead to gas starvation [91,101] (Fig. 9). In addition, the distribution as well as the supply of gas in a PEMFC is not completely homogeneous,

with some non-uniformity among different locations in the cell stack [102], at the gas inlet and outlet [103], and between the ribs and channels [91]. Rapid loading may magnify the effects of such differences. Gas starvation is categorised into air starvation and fuel starvation, which have different mechanisms of action, but both can negatively affect the durability of the PEMFC.

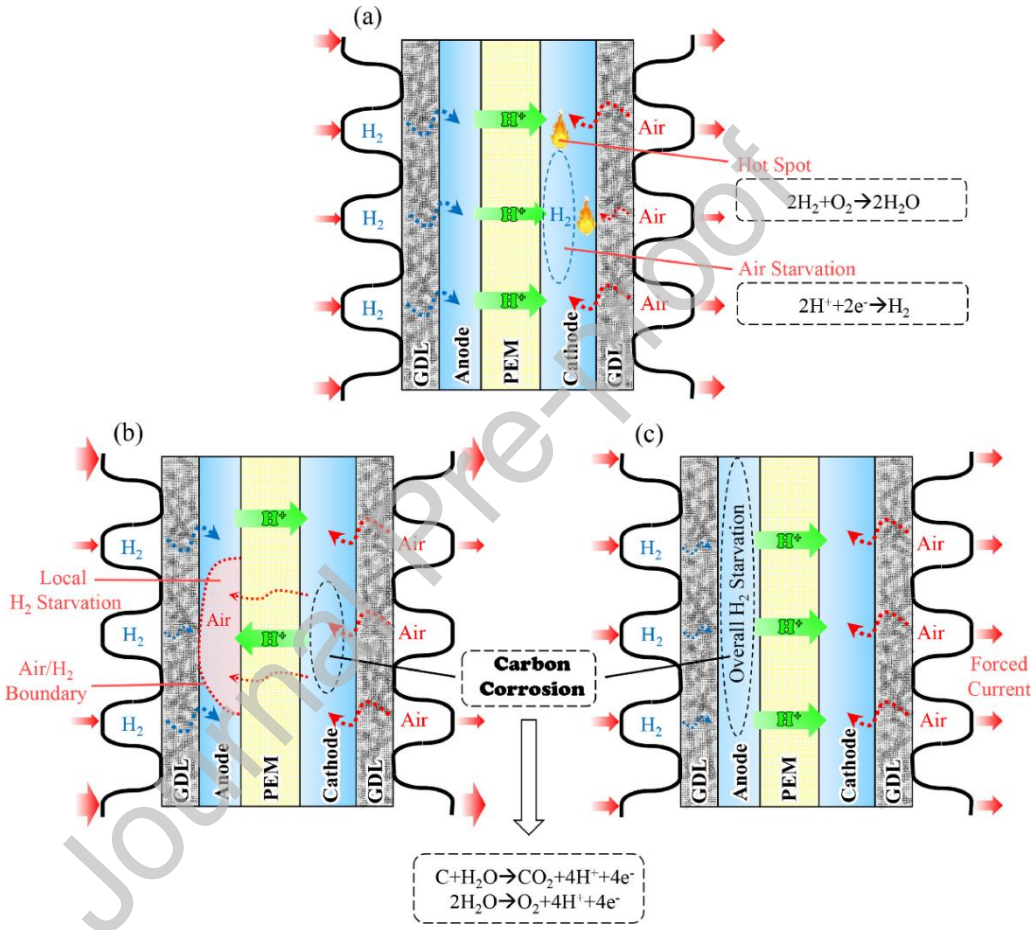

Fig. 9. Schematic diagram of PEMFC gas starvation under dynamic load conditions. Reprinted from Ref. [7]with permission of Elsevier. (a) Air starvation; (b) Localised fuel starvation; (c) Overall fuel starvation.

4.1.2.1 Air starvation

Air starvation occurs when the PEMFC is forced to produce the required current but

the air supply is insufficient. Due to the lack of oxygen, the excess protons passing from the anode to the cathode cannot participate in the ORR, then hydrogen evolution reaction (HER) takes place at the cathode. The presence of hydrogen in the exhaust gas emitted from the cathode when there is insufficient air has been reported in some literature [104,105]. These hydrogen gases at the cathode can directly react with oxygen in the neighbouring region, thus releasing a large amount of heat and generating hot spots. This is likely to lead to thermal degradation of the cathode membrane with growing sintering of the catalyst and a reduction in the electrochemical activation area [106,107].

4.1.2.2 Fuel starvation

As for the fuel starvation, it can be divided into two types: localised fuel starvation and overall fuel starvation, which have different mechanisms to affect the PEMFC durability. Localised fuel starvation occurs when there is a slight starvation of hydrogen supply, which leads to a decrease in the local pressure at the anode and an increase in the permeability of air to the membrane. When air infiltrates into the anode, a hydrogen-air interface is created, which leads to the same effect as the startup-shutdown condition on the PEMFC as described in the previous section [99,108]. Overall fuel starvation occurs when there is a severe starvation of hydrogen supply (stoichiometric ratio < 1), at which point the PEMFC cannot operate properly. Reverse polarity occurs if there is an external power source forcing the overall fuel starvation cell to maintain current [109]. In the test/practical workplace, both the potentiometer in constant-current operating mode and the normally operating PEMFC

in the same stack can be used as external power sources [110]. At this point, the antipodal PEMFC is more analogous to an electrolytic cell, as shown in Fig. 9(c) above, where COR and OER are performed in the anode to supply protons and maintain the load current. As a result, the anode potential increases rapidly while the cell voltage decreases. COR leads to shedding of Pt catalyst aggregates and a decrease in ECSA.

The damage caused by fuel starvation can be mitigated by optimising the gas supply and reactant dosage [111] the gas flow field [112], as well as the control of the loading rate during the actual loading process. In addition, there are some methods to add hydrogen storage layer at the anode outlet [113].

4.1.3 Loss and detachment of Pt catalysts

Pt catalysts also degrade under dynamic load conditions, and the reasons for this come from a variety of sources. As mentioned previously, the ionomers in the CL are deformed, which is likely to separate the Pt catalyst it covers from the carbon support [96]. During this period, the highly dispersed ionomers tend to aggregate, which can cause some Pt particles to lose the coverage of the ionomers, while some of the particles can be over-covered. The effect is similar to that of the redistribution of the ionomers due to carbon corrosion in the startup-shutdown condition: the uncovered Pt catalysts do not allow proton contact, while the overcovered portion increases the mass transfer resistance [71]. Since homogeneous, highly dispersed ionomers are inherently unstable in PEMFC, factors leading to changes in the structure of both Pt/C and CL can accelerate the redistribution of the ionomers [7]. Secondly, after cracks

are produced in CL, the Pt particles attached in and around the cracks are likely to be washed away by water as water will tend to flow towards the cracks [96]. The COR due to fuel starvation described previously is similar to the COR due to the hydrogen-air interface in the startup-shutdown condition, where the corrosion of the carbon support forces the Pt particles to separate.

4.2 Degradation analysis methods

To explore the degradation of PEMFC under dynamic load conditions, researchers typically test the cell using potential and humidity cycles. In potential cycling, considering the cathode potential range of PEMFCs, the applied potential is generally cycled from 0.6 V to 0.9 V - 1.0 V [114,115], which corresponds to the rated cell voltage and the cell voltage at OCV, respectively. Triangular [116], rectangular [114] and trapezoidal waveforms [116] are a few waveforms commonly used in cycling modes. When simulating membrane mechanical degradation caused by humidity cycling, it is important to carefully select the gas used. For example, cathode and anode gas supplies using N_2/H_2 [117], air/air [94] with N_2/N_2 [95] are used to eliminate the interference of cathode potential and membrane chemical recession on the results.

5. Cold start

At low temperatures, the product water in PEMFCs freezes, which can cause performance degradation and damage to components and even the overall structure.The cold start problem of PEMFCs has become a major impediment to their commercialisation in cold regions and scenarios [118]. Since cold start is a startup

situation of PEMFC under special conditions, the cold start period also involves PEMFC degradation under startup-shutdown condition as described in the previous section [7]. This section focuses on an overview of the degradation of the PEMFC caused by icing during cold start.

5.1 Degradation mechanisms

5.1.1 Consequences of frozen volume expansion

As water solidifies into ice, it increases in volume by about 9%. Since water is widely distributed in membranes and ionomers, icing leads to localised stress and even deformation of PEMFC components, similar to humidity cycling under variable load conditions, and freeze-thaw cycling can also lead to mechanical fatigue of PEMFC components, which in turn affects durability [119,120] (see Fig. 10). Ice at the interfaces of the components causes delamination of the membrane with CL and CL with GDL [121-123], leading to a significant increase in contact resistance [124,125]. For proton exchange membranes, most of the water in the membrane interacts with the polymer chains, making them somewhat immune to icing [126]. Once the water content in the membrane reaches saturation, the product water that continues to be produced will freeze if the internal temperature of the cell remains below freezing. This is likely to lead to delamination of the membrane with CL and the membrane surface becomes rougher or even ruptured and pinholed due to the presence of large ice crystals [127].

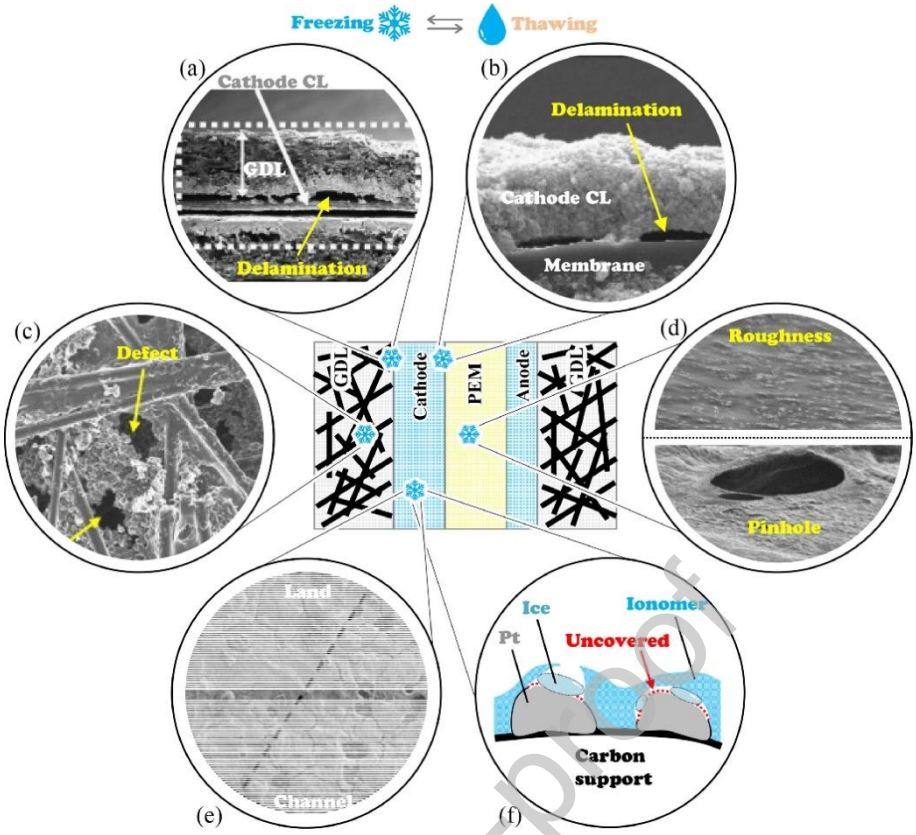

Fig. 10. Multidimensional PEMFC degradation due to freeze-thaw cycling. Reprinted from Ref. [7] with permission of Elsevier. (a) Delamination between GDL and CL [125]; (b) Delamination between CL and membrane [124]; (c) Defects in PTFE in the GDL [128]; (d) Roughening of the membrane surface and formation of pinholes [127]; (e) Crack formation and extension in CL [129]; (f) Ice-induced separation of ionomer and Pt catalyst [7].

5.1.2 Damage of PEMFC components during cold start

For CL, it has been proposed that although the initial water droplets formed on the surface of the cathode Pt catalyst do not freeze immediately due to the supercooling effect, they freeze more easily at freezing point when the small droplets agglomerate into larger ones [130]. Since water is mainly generated at the cathode, most of the ice is produced at the cathode CL and fills the pore structure of CL [131]. After repeated

icing, the characteristic pore size of the CL becomes larger and the number of larger pores increases, which is likely to lead to the creation of microcracks [123]. Water will tend to solidify at the cracks, which will accelerate the damage of the CL structure [129,132]. Additionally, for Pt catalysts in CL, ice at the interface separates the Pt particles from the ionomers, causing a decrease in ECSA [133,134]. Even after the ice melts, the coverage of the ionomers is not fully restored.

In the case of GDL, the ice in it disrupts the pore structure between the carbon fibers, separating the carbon fibers from the polytetrafluoroethylene (PTFE) coated on them. This reduces the hydrophobicity of the GDL, which in turn leads to a blockage of the mass-transfer process and an increased risk of flooding [127,128]. These conclusions have been reached by comparing the contact angle of water before and after cold start [128]. Furthermore, the expansion of volume during icing may also cause the carbon fibers themselves to fracture, which often results in some of the carbon fibers and hydrophobic coatings falling off as flakes [135].

For the microporous layer (MPL), damage can also occur during cold start due to the effects of icing [136,137]. Ozden et al. [123] found that the MPL was deformed after 60 freeze-thaw cycles. Large cracks formed on the surface, and flakes of the carbon fibres separated from the surface, resulting in a macroscopic increase in the pore volume and porosity. The damage to MEA by low temperature is shown in Fig. 11 below.

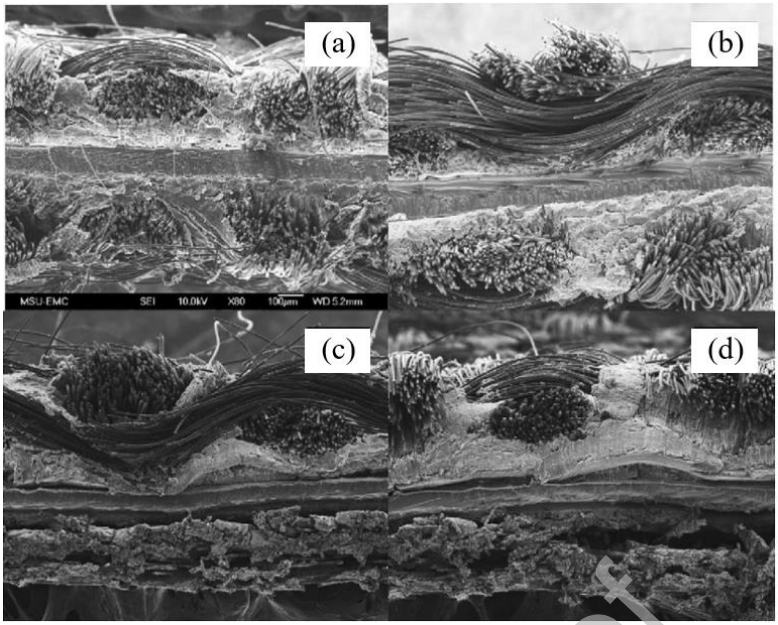

Fig. 11. Effect of low temperature on MEA. Reprinted from Ref. [127] with permission of Elsevier. (a) Fresh MEA; (b) MEA after room temperature operation; (c) MEA after -10°C operation; (d) MEA operation after -15°C operation.

5.2 Degradation analysis methods

Researchers have conducted accelerated aging tests for the cold-start process by controlling the temperature of the PEMFC and inducing frequent water-ice phase transitions. Currently, the lower temperature limit has been tested up to -40°C [122], while the upper temperature limit is generally the normal operating temperature of PEMFCs. In addition to freeze-thaw cycles, there are also reports for the cold-start process, including the effects of parameters such as initial humidity [130,138], current density [139], and so on. In addition, many scholars have designed cold-start strategies, such as the pre-start purge method [140,141] and the heating method [142,143] for the PEMFC, in an attempt to minimise or even eliminate the effect of icing.

6. Impurity contamination

The effects of impurities faced by the PEMFC during operation can be divided into two categories according to their source: impurities precipitated from the components of the PEMFC, such as the bipolar plates or sealing materials [144,145], which are usually metal cations, but also impurities carried by the purity limitations of the component manufacturing process, namely, the Pt catalysts may carry traces of chloride ion (Cl^-) [146]; the other type is impurities present in the reaction gas, which enter the PEMFC with gas transport and cause effects. As the PEMFC components will inevitably undergo a certain degree of aging after a certain period of operation, it is likely that metal cations will precipitate into the PEMFC; and a significant portion of the current source of hydrogen is the industrial side reaction [147], in which gases such as hydrogen sulfide (H_2S), ammonia (NH_3), and carbon monoxide (CO) are inevitably present, and there are also trace amounts of nitrogen oxides (NO_x), sulfur oxides (SO_x) and other gas impurities in the air. Therefore, it is very meaningful to study the effect of impurities on the durability of PEMFC.

6.1 Contamination by metal cations

Some transition metal cations can catalyse the decomposition of H_2O_2, producing an effect similar to the Fenton reaction, which results in a much higher rate of radical generation. The relevant mechanism is given by the following equations [148,149]:

$$M^{2+} + H_2O_2 \rightarrow M^{3+} + \cdot OH + OH^- \#(11)$$

$$M^{3+} + H_2O_2 \rightarrow M^{2+} + \cdot OOH + H^+ \#(12)$$

where M is a transition metal element such as Fe, Co, Cu, etc. It can be seen that

metal cations catalyse the generation of free radicals, thus accelerating the chemical degradation of the membrane. Furthermore, it has been shown that the sulfonic acid group in polytetrafluoroethylene (PTFE) membranes can be poisoned by metal cations, which adversely affects the proton conductivity of the membranes and causes damage [150,151] (see Fig. 12).

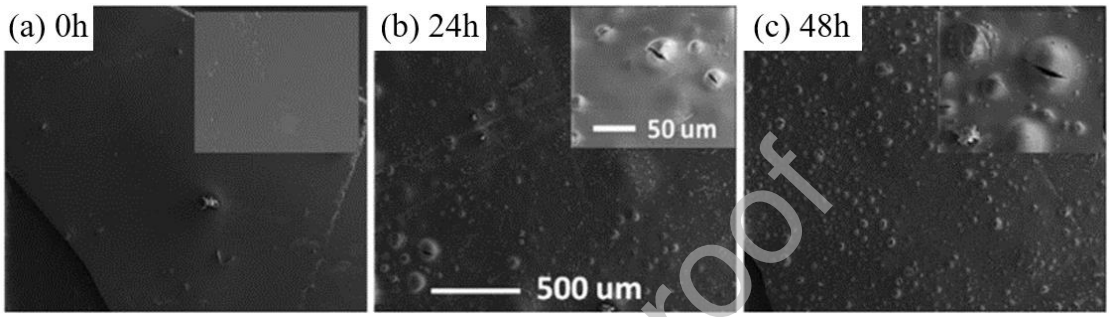

Fig. 12. Damage to Nafion membranes by Fenton's reagent at different exposure times. Reprinted from Ref. [151] with permission of Elsevier.

When conducting studies for cation contamination, two methods were usually used by researchers: the solution method and the exchange method [152]. The solution method involves immersing the membrane in a solution containing metal cations and H_2O_2, while the exchange method involves immersing the membrane in a solution of H_2O_2 with metal cations inside the proton exchange membrane. For the solution method, the cations, H_2O_2 and ionomers need to be in close enough proximity to each other for catalytic degradation to occur. In the case of the exchange method, the cations are always available in the membrane, which allows for moderate cation doping to initiate the chemical degradation of the membrane [15]. Healy et al. [153] compared the released composition of membranes submerged in Fenton's reagent (H_2O_2/Fe^{2+}) to that released from in-situ testing of PEMFC chemical degradation and found that the

compositions of the membranes were similar. For accelerated membrane decline, the comparison between solution and exchange methods has not yet shown a clear correlation, and it is important to explore degradation modes that more accurately reflect in-situ membrane degradation.

6.2 Contamination by Cl^-

6.2.1 Cl^- residue induced catalyst degradation

The precursor for the preparation of Pt catalysts is usually $H_2PtCl_6 \cdot 6H_2O$, in which Cl^- may have trace residues in the catalyst [154]. In addition, Cl^- carried by salt spray in the air may also be adsorbed on the Pt catalyst with the incoming air. A small amount of Cl^- can be very harmful to the performance of PEMFC [146]. Numerous studies have shown that the performance of the PEMFC decreases rapidly at the onset of Cl^- contamination, during which the Pt catalyst is subjected to a very high rate of corrosion and saturates after a period of time [155,156]. Subsequently, the corrosion process caused a slow decrease in PEMFC performance. Pt dissolved by corrosion can be redeposited on the catalyst surface, namely, the Cl^- induced decline is reversible to some extent. In addition, if the catalyst is a Pt-based alloy catalyst, Cl^- also poisons the catalyst active sites, and only a small amount of Cl^- is sufficient to dissolve and dealloy most of the non-precious metals in the alloy [157]. An increase in the concentration of Cl^- leads to a decrease in the Pt corrosion potential, thus accelerating corrosion [146].

6.2.2 Mechanism of Cl^- poisoning

Cl^- can form two types of complexes with dissolved Pt, $PtCl_4^{2-}$ and $PtCl_6^{2-}$, which

have the following chemical reaction formulae [146]:

$$Pt + 4Cl^- \rightarrow PtCl_4^{2-} + 2e^- \quad E^0 = 0.758V(vs.SHE)\#(13)$$

$$Pt + 6Cl^- \rightarrow PtCl_6^{2-} + 4e^- \quad E^0 = 0.742V(vs.SHE)\#(14)$$

At low potentials (0-0.4 V), Cl^- could move to the Pt surface. When the potential was in the range of 0.4-1.06 V, $Cl^- \cdot 3H_2O$ was continuously generated on the surface of the contaminated Pt catalyst. With increasing voltage, only oxide (PtO/PtO_2) was formed on the uncontaminated Pt surface with Cl^-, and the amount of oxide generated increased with the amount of dissolved Pt. PtO/PtO_2 acted as a protective oxide layer and slowed down the further dissolution of internal Pt. Finally, the contaminated Pt undergoes the reaction of the above chemical formulae. Pt^{n+} can be formed when the electrode potential is less than 1.2 V, while $PtCl_6^{2-}$ is formed when the potential is greater than 1.2 V [158].

6.2.3 Mitigation strategies of Cl^- poisoning

To prevent the toxic effect of Cl^- on PEMFC, one possible approach is to synthesise Pt using other Cl^--free precursors, such as $Pt(acac)_2$ [159], $Pt(NH_3)_2(NO_2)_2$ [160]. However, $Pt(acac)_2$ is costly and difficult to be applied on a large scale commercially, and $Pt(NH_3)_2(NO_2)_2$ is exothermic during the reduction process, which affects the performance of Pt catalysts [154]. Therefore, there is a great need to investigate methods to remove residual Cl^- from $H_2PtCl_6 \cdot 6H_2O$.

Modification of the catalyst itself can improve the ability to tolerate Cl^-. It has been found that making N-doped graphene and Pt-containing nanocomposites contain as many pyridine and pyrrole groups as possible is helpful for the improvement of the

catalyst's resistance to Cl^- corrosion [161].The degree of poisoning of Pt varies among the crystalline surfaces, in which Pt (110) is more severe than Pt (111), and thus it can be assumed that by controlling the movement of the crystalline surfaces of Pt to Pt (111), it is possible to inhibit the adsorption of Cl^- to Pt to some extent [162]. It also appears that the addition of a second atom type for the preparation of alloy catalysts in order to release the active sites from Cl^- can also play a role [154].

In addition, there are also reports related to the catalyst treatment process. One approach is to use post-treatment means, such as washing with large amounts of deionised water assisted by $AgNO_3$, which removes Cl^- residues [154]. In terms of dechlorination, both NH_3 and NaOH can be useful, with NaOH being non-toxic and cleaner with lower Cl^- residues compared to NH_3 [163]. Another approach is high temperature treatment, for instance, catalysts are prepared by strong electrostatic adsorption methods, where the gas atmosphere and the duration of the reduction process are varied in order to change the Cl^- content in the catalyst. The length of the reduction time needs to be ensured as high temperatures may vaporise the carbon support [164].

6.3 Contamination by carbon monoxide(CO)

For the impurity gases that may be present in the inlet gas, CO, H_2S, NH_3, and SO_2, which are some of the more common gases represented in this paper, are reviewed. After purification of hydrogen, which appears as an industrial by-product, the concentration of CO is typically on the order of 10 ppm, which is sufficient to cause a significant degradation in the performance of the PEMFC [165,166].

6.3.1 Mechanism of CO poisoning

At the anodic potential corresponding to the normal operation of the PEMFC, CO competes with H_2 for active sites on the Pt catalyst [167]. Since the heat of adsorption of CO on Pt is 134 kJ mol^{-1}, which is higher than the 87.9 kJ mol^{-1} corresponding to H_2 [165], CO is more readily adsorbed on the Pt surface than H_2, which results in the accumulation of CO on the Pt surface and a reduction in the available surface sites for hydrogen oxidation reaction (HOR) [148]. In addition, CO adsorbs on the Pt-H sites and hinders proton generation. The relevant reaction equations are shown below [166]:

$$CO + nPt \rightarrow Pt_n - CO_{ads} \#(15)$$

$$2CO + 2(Pt - H_{ads}) \rightarrow 2(Pt - CO_{ads}) + H_2 \#(16)$$

$$Pt - CO_{ads} + Pt - H_2O_{ads} \rightarrow 2Pt + CO_2 + 2H^+ + 2e^- \#(17)$$

The corner symbol "ads" indicates that the substance is in the adsorbed state.

6.3.2 Effects of CO poisoning on PEMFCs performance

At higher concentrations of CO (usually higher than 100 ppm), the polarisation curves show two different slopes at lower and higher current densities [168] (see Fig. 13). The former is caused by a combination of adsorption and oxidation of H_2 and CO at the anode, while the latter is caused by a gradual oxidation of CO in the adsorbed state to CO_2 and an increase in the rate of H_2 adsorption and HOR after a certain value of the anode potential is reached [169]. Temperature has a significant effect on CO contamination. With the increase of PEMFC operating temperature, CO desorption on the surface of Pt catalyst was fast and the degree of coverage decreased, which was

favourable for HOR [170]. The value of overpotential increase due to equal content of CO also varies at different current densities. Higher current densities accelerate the rate of H_2 consumption while CO is essentially unconverted, which results in higher CO content per unit time per unit area of the Pt catalyst surface and increased toxicity to HOR [170].

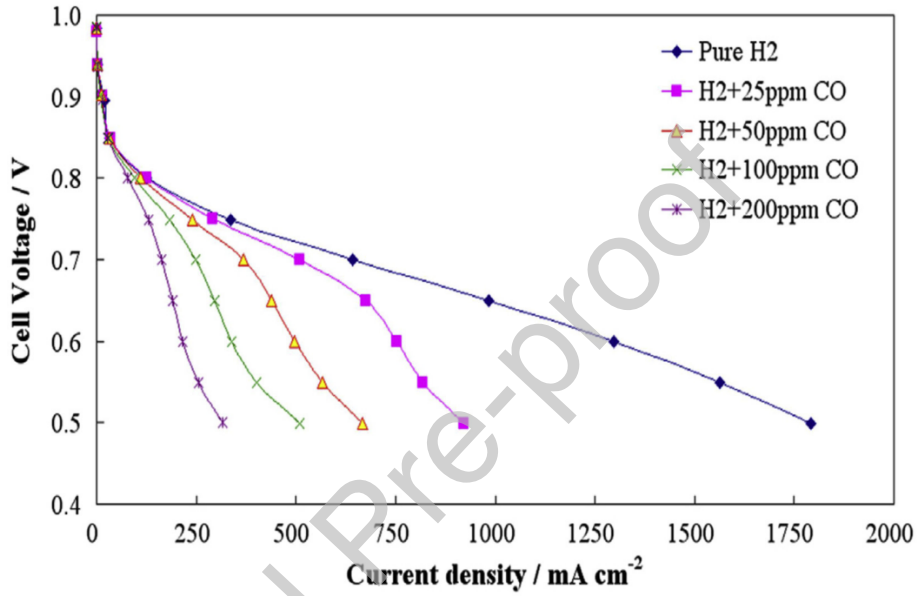

Fig. 13. PEMFC polarisation curves corresponding to different concentrations of CO. Reprinted from Ref. [168] with permission of Elsevier.

6.3.3 Mitigation strategies of CO poisoning

To mitigate the poisoning hazard of CO to PEMFC, it is necessary to promote the conversion of CO already adsorbed on the surface of Pt catalyst. Currently, there are two widely adopted strategies: one is to oxidise CO by doping some oxidants into the anode feed gas; the other is to develop catalysts resistant to CO poisoning.

6.3.3.1 Oxidants bleeding

In the anodic oxidation scheme, a certain amount of O_2 is generally passed to make

Pt-CO oxidised to form CO_2, releasing the catalyst active sites occupied by CO, which has low toxicity to HOR [171]. The mechanism can be expressed by the following equations [172]:

$$2Pt + O_2 \rightarrow 2(Pt - O)\#(18)$$

$$Pt - CO + Pt - O \rightarrow 2Pt + CO_2\#(19)$$

The disadvantage of this scheme is that O_2 also reacts with H_2, which will lose some of the reactant gas and O_2 that would have reacted with CO, as shown in the following equation [168]:

$$Pt - O + 2(Pt - H) \rightarrow H_2O + 3Pt\#(20)$$

Certainly, the weakening of the CO poisoning effect by means of anodic oxidation is obvious.A related study was carried out by Sung et al [173], who found that 50 ppm CO caused an 80% current loss, whereas the introduction of 5% air (1% O_2) restored the current density to 90% of the original maximum current density. Moreover, at a voltage of 0.5 V and a CO concentration of 25 ppm, the output current increased significantly from 920 mA cm^{-2} to 1,670 mA cm^{-2} after the introduction of 1% air in H_2. For 200 ppm CO, the output current increased from 315 mA cm^{-2} to 1,600 mA cm^{-2} by adding 5% air to the fuel, and the power density of the stack increased by 88%.

6.3.3.2 CO-tolerance catalysts

For catalysts against CO poisoning, Pt is generally used to form alloy catalysts with other metals such as Ru, Co, Ni, Sn, etc [174-176]. The mechanism of Pt-Ru, for example, is that Ru can preferentially adsorb H_2O at a lower potential and produce

Ru-OH clusters, which can rapidly oxidise the CO adsorbed on the surface of the catalyst, as shown in the following reaction formula [177]:

$$Pt - CO + Ru - OH \rightarrow Ru + Pt + CO_2 + H^+ + e^- \#(21)$$

It has been noted that alloying Pt with other metals can shift the d-band of Pt, by which alter its electronic structure and hinder CO adsorption [178]. Furthermore, alloyed catalysts can prevent the agglomeration of nanoscale particles to some extent through the synergistic effect among the components [179]. This improves the stability of the catalysts, prolongs the working time of the PEMFCs and enhances CO tolerance. In studies comparing the CO tolerance of various alloyed catalysts, Ru doping demonstrated the most significant effect [180-182], as shown in Fig. 14 below. Jin et al. [183] prepared catalysts with PtMo atom clusters and such type of catalysts achieved resistance to 1,000 ppm CO at a low Pt loading of 1.56 wt%. The improvement was mainly caused by the synergistic effect of PtMo-APs, Pt-SAs, and Mo-SAs in the clusters. Dong et al. [179] achieved even better CO tolerance than that of commercial Pt/C by combining alloying with the SMSI effect. They loaded a PtNiMo ternary alloy onto a Fe-N-C carrier, which exhibited excellent anti-CO performance. The catalyst retained over 80% of its current density even after being exposed to a concentration of 1,000 ppm CO for 2,000 seconds.

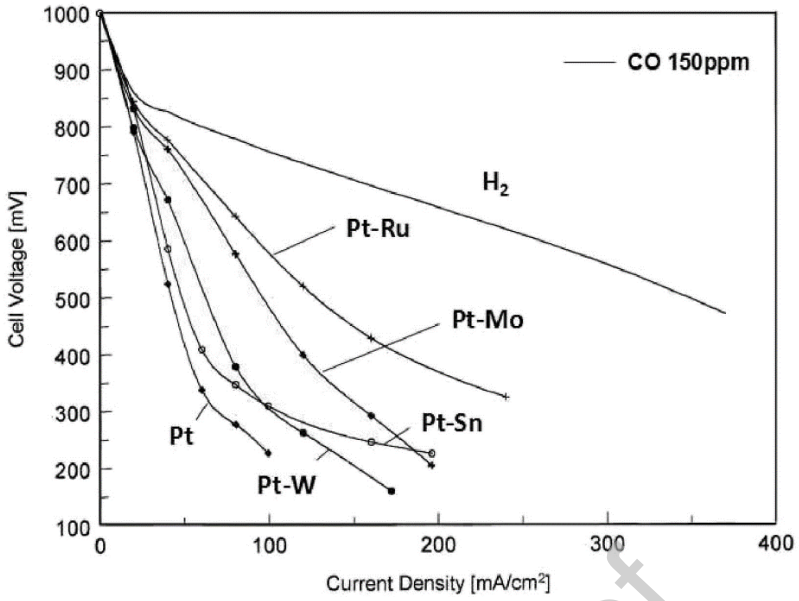

Fig. 14. Corresponding polarisation curves for different binary catalysts at H_2/CO (150 ppm), 75 °C. Reprinted from Ref. [168] with permission of Elsevier.

6.4 Contamination by H_2S

6.4.1 Mechanism of H_2S posioning

Similar to CO, H_2S has a high affinity for Pt catalysts. Its anodic reaction pathway in PEMFC is variable, and the exact poisoning mechanism is still controversial [184]. Some researchers have proposed the following poisoning mechanisms [185]:

$$H_2S + Pt \rightarrow Pt - S_{ads} + H_2 \#(22)$$

$$2H_2S + 2Pt - H_{ads} \rightarrow 2Pt - S_{ads} + 3H_2 \#(23)$$

That is, H_2S dissociates and adsorbs on the Pt surface to generate Pt-S_{ads}, and S has a stronger adsorption on the Pt surface, which can replace Pt-H_{ads} to generate Pt-S_{ads}, leading to a drastic reduction in the active sites available for HOR. It has also been shown that H_2S adsorption on the Pt surface to generate Pt-S_{ads} is also followed by an electro-oxidation reaction to generate H^+ [186]. Also, Pt-S_{2ads} is a possible form of

adsorption [187]. The expressions are as follows:

$$H_2S + Pt \rightarrow Pt - S_{ads} + 2H^+ + 2e^- \#(24)$$

$$H_2S + Pt - S_{ads} \rightarrow Pt - S_{2ads} + 2H^+ + 2e^- \#(25)$$

In addition, Pt-S_{ads} will react with water in the anode CL to produce sulfur oxides, which have some covering effect on the active sites on the Pt surface, as shown in the following expressions [186]:

$$Pt - S_{ads} + 3H_2O \rightarrow Pt + SO_3 + 6H^+ + 6e^- \#(26)$$

$$Pt - S_{ads} + 4H_2O \rightarrow Pt + SO_4^{2-} + 8H^+ + 6e^- \#(27)$$

6.4.2 Effects of H_2S poisoning on PEMFCs performance

At lower potentials, sulphur can be generated and accumulated on the surface of the Pt catalyst, destroying its surface activity. Uribe et al. [188] found that this toxic effect can be cumulative and has a considerable degree of irreversibility. Garzon et al. [189] reported that a low concentration of H_2S of 10 ppb resulted in a decrease of 32.8% in the current density of the PEMFC after anodic exposure of 1,000 h. When the concentration of H_2S rose to 1 ppm, the PEMFC performance had significantly decreased after 4 h, and was almost completely ineffective after 21 h. Subsequently, pure H_2 was used as the feed gas for several hours, and the performance still did not recover significantly (see Fig. 15). The effect of temperature has also been reported [190]: the adsorption of S-containing species on the surface of the Pt catalyst is more intense at low temperatures, whereas the adsorption reaction rate is accelerated at high temperatures.

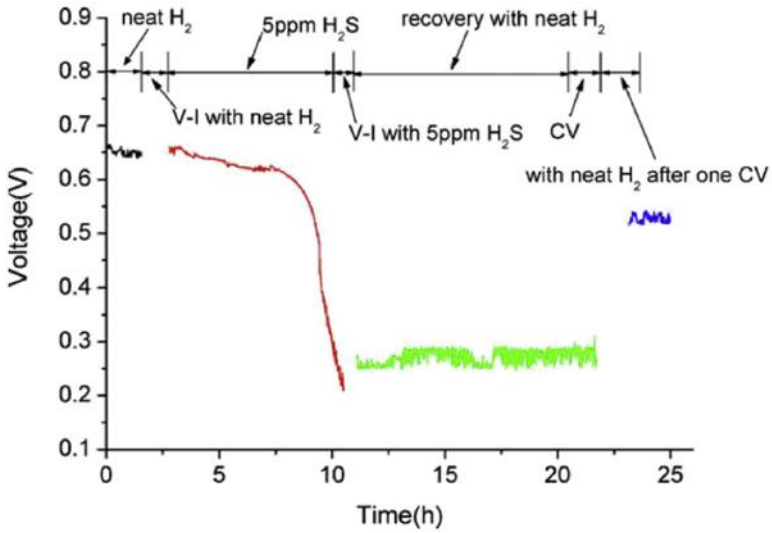

Fig. 15. Effect of 5 ppm H_2S on PEMFC output performance (70°C). Reprinted from Ref. [168] with permission of Elsevier.

6.4.3 Mitigation strategies of H_2S poisoning

Strategies that have been investigated for recovering the effects of H_2S contamination include the passage of pure hydrogen or ozone on the anode side, cyclic CV scanning, and the development of catalysts resistant to the toxic effects of H_2S. Feeding pure H_2 on the anode side partially restores PEMFC performance, although this may only be applicable at very low H_2S levels [186]. Kakati et al. [191] injected ozone at the anode and found that when the H_2S content was 100 ppm, the performance could be restored to about 95% of the initial value by continuous injection of 2% ozone for 600s. However, ozone itself leads to an accelerated degradation rate of the PEMFC components, again triggering irreversible decay [192].

The use of cyclic CV scanning is effective in terms of restoring PEMFC performance. Shi et al. [193] oxidised the chemiluminescent material of a Pt catalyst by means of a high voltage pulse (1.5 V), and then reduced the Pt oxide using a low pulse (0.2 V),

essentially restoring more than 90% of the performance, as shown in Fig. 16.

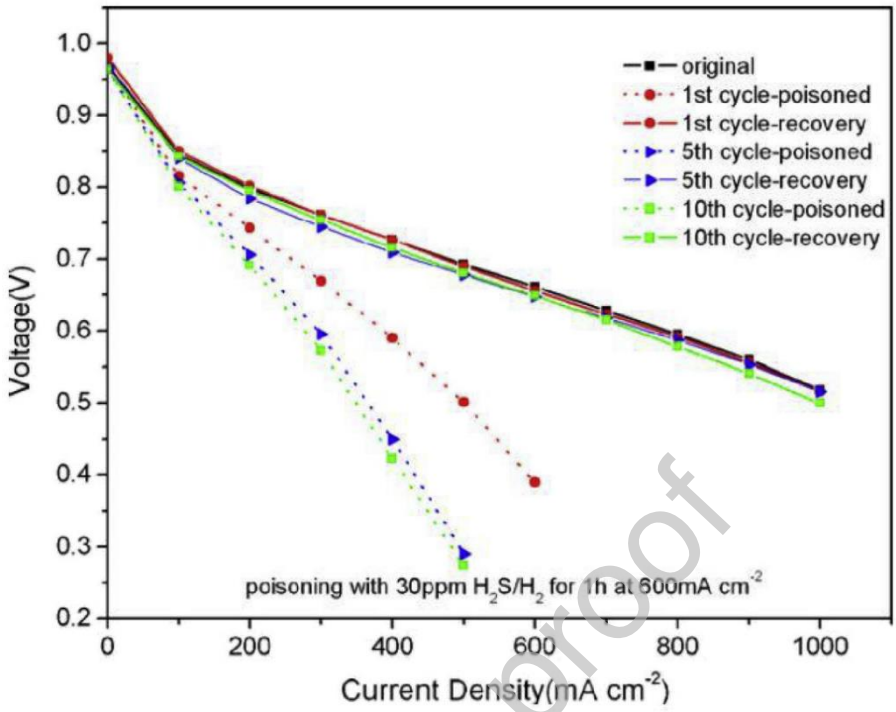

Fig. 16. PEMFC performance under H_2S poisoning-CV scan (0.2 V-1.5 V) cycle. Reprinted from Ref. [193] with permission of Elsevier.

Pd catalysts are superior to Pt in terms of resistance to H_2S poisoning effects. A Pd-Cu alloy catalyst was investigated, which had a higher H_2S tolerance and showed better performance in the presence of H_2S in the anode feed gas [193]. However, this catalyst could not achieve the performance of the Pt catalyst with pure H_2 feed gas.

6.5 Contamination by NH_3

6.5.1 Mechanism of NH_3 poisoning

NH_3 is also one of the typical anode contaminants for PEMFC, which has some residual amount in H_2 either as a reforming product or as a support of hydrogen, and its concentration can reach up to 150 ppm [168]. Some literature suggests that the toxicity mechanism of NH_3 is different from that of CO and H_2S. NH_3 does not have a

direct toxic effect on the Pt catalyst, but rather combines with H^+ to form NH^{4+}, which can hinder H^+ transport and reduce the proton conductivity of the membrane [194,195]. The reaction equations are as follows:

$$NH_3(g) \rightarrow NH_3(mem)\#(28)$$

$$NH_3(mem) + H^+ \rightarrow NH_4^+\#(29)$$

The NH^{4+} generated at the anode is transported through the membrane to the cathode, where the following reduction reaction occurs in the presence of a Pt catalyst at the cathode [168]:

$$2NH_4^+ \rightarrow N_2 + 8H^+ + 6e^-\#(30)$$

Rune et al. [195] showed that the transfer efficiency of NH^{4+} is about 20-25% of that of protons, and that NH^{4+} affects the ORR that is supposed to occur at the cathode, resulting in a degradation of the PEMFC performance.

6.5.2 Influcing factors of NH_3 poisoning

In terms of factors affecting ammonia contamination, the duration of contamination is one of the most important factors affecting the durability of PEMFC. Several studies have shown that short but higher concentrations of NH_3 contamination are less likely to affect membranes to the extent of irreversible degradation, while PEMFCs exposed to NH_3 for long periods of time tend to show irreversible decay [196]. Furthermore, the effect of ammonia on the catalyst can be mostly recovered, but contaminated membranes are more difficult to clean [197]. In addition, Hongsirikarn et al. [198] found that high relative humidity improves the tolerance of PEMFC to NH_3, with NH^{4+} decreasing the conductivity by a factor of about 3 when the relative humidity is

100%, and by a factor of about 55 when the relative humidity is 30%. They also found that high current densities attenuated the extent of membrane conductivity reduction caused by ammonia contamination, but promoted NH_3/NH^{4+} migration to the cathode. Temperature did not appear to have a significant effect on ammonia contamination.

6.5.3 Mitigation strategies of NH_3 poisoning

To mitigate the toxic effect of NH_3, prolonged injection of pure H_2 into the PEMFC is the most common scheme. Imamura et al. [199] exposes the PEMFC to 50 ppm NH_3 for 5 h and then injects pure H_2. The voltage is largely restored after about 10 h. However, with the elevated contamination duration of NH_3, a longer recovery time may be required even at lower concentrations [196], as illustrated in Fig. 17.

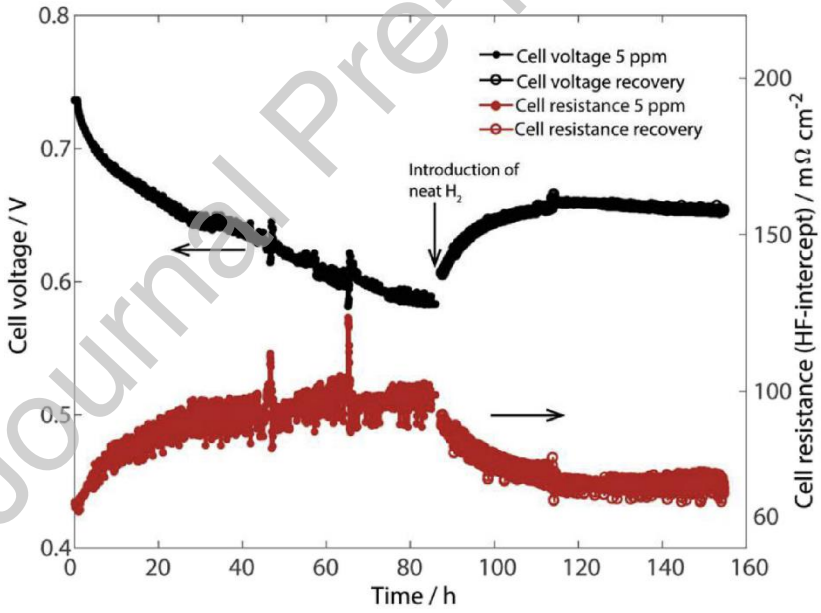

Fig. 17. PEMFC performance during 5ppm NH_3 contamination and pure hydrogen purification [196].

It has also been suggested that at higher potentials (usually >0.7 V), NH^{4+} generates N_2 via electrochemical reactions, and that expelling N_2 from the PEMFC can mitigate

the effect of NH^{4+} on performance [200]. In terms of catalyst, Au has a lower N adsorption energy than Pt, which helps to improve the poisoning of N-containing species on the catalyst surface. Therefore, Pt-Au may be an alloy catalyst resistant to NH_3 poisoning effect [201].

6.6 Contamination by SO_2

6.6.1 Mechanism of SO_2 poisoning

As an impurity present in the air, the effect of SO_2 on PEMFC has also received much attention.SO_2 can significantly affect the irreversible degradation of membranes and Pt catalysts. Many studies have shown that SO_2 causes a two-stage performance degradation in PEMFCs, where a sharp drop in voltage/current occurs before approaching the limiting voltage/current, followed by a second sharp drop [202]. Based on the observations, the current hypothesis is that at least two different S-containing species adsorb on Pt, one irreversibly adsorbed and the other reversibly adsorbed [203].

Jing et al. [204] proposed a mechanism for SO_2 poisoning as follows:

$$2Pt - SO_2 + O_2 + 4e^- \rightarrow 2Pt - SO_3 \#(31)$$

$$Pt - SO_3 + H_2O \rightarrow H_2SO_4 + Pt \#(32)$$

Mohtadi et al. [205] proposed an alternative mechanism of toxicisation as follows:

$$Pt + SO_2 \leftrightarrow Pt - SO_2 \quad \text{weak adsorption} \#(33)$$

$$Pt - SO_2 + Pt \rightarrow \underline{Pt - SO} + Pt - O \quad \text{strong adsorption} \#(34)$$

$$Pt - SO + Pt \rightarrow Pt - S + Pt - O \#(35)$$

SO_2 absorbed by the Pt catalyst cannot be completely desorbed during

electrochemical scanning, but remains in the catalyst active sites, which is the reason why the PEMFC performance is not fully recoverable [168].

6.6.2 Effects of SO_2 posioning

As shown in Fig. 18, Misz et al. [202] injected SO_2 at concentrations of 0.1 ppm, 1 ppm and 4 ppm into the cathode air in order to carry out performance tests of SO_2-toxicised PEMFCs. They found that the current continued to decrease with increasing SO_2 concentration. 0.1 ppm resulted in a performance loss of only about 2%, but 1 ppm and 4 ppm corresponded to performance losses of 62% and 85%, with rather limited recovery of the performance loss. It has also been reported that SO_2 degradation cannot be fully recovered by detecting the rate of F^- release in cathode drainage [206].

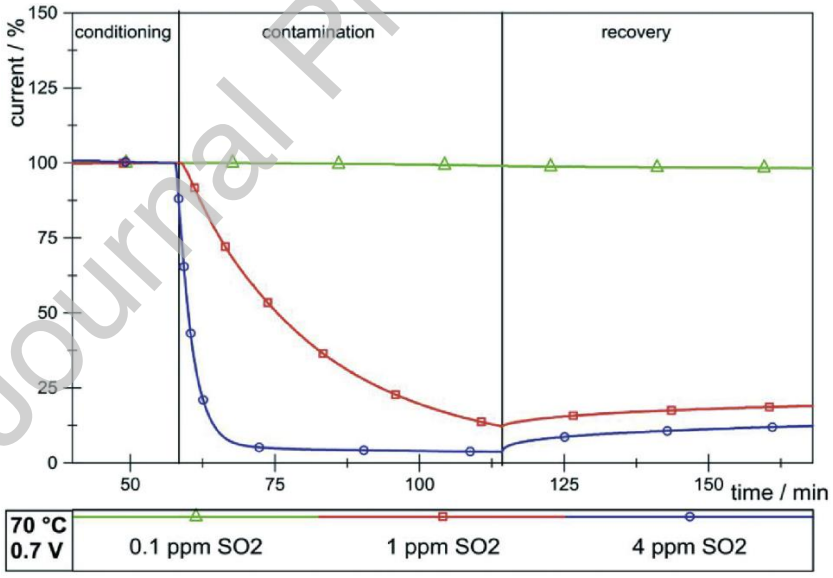

Fig. 18. Effect of pollution and recovery of different SO_2 concentrations on PEMFC current. Reprinted from Ref. [202] with permission of John Wiley and Sons.

6.6.3 Mitigation strategies of SO_2 poisoning

6.6.3.1 CV scanning

CV scanning removes irreversible SO_2 adsorption due to the fact that S-containing species adsorbed on Pt are oxidised to water-soluble sulphate at potentials higher than 0.8V. The performance can be restored to some extent as the sulphate is desorbed from the catalyst surface [207]. The wider the scanning potential, the more favourable the recovery of PEMFC performance [208]. As for the operating conditions, increasing humidity [209] and elevated temperature [168] could alleviate the degradation, the former due to the fact that SO_2 is easily soluble in water, and discharging the water could bring out some of the SO_2, and the latter may be because increasing the temperature would promote the desorption reaction of ORR and S-containing species.

6.6.3.2 SO_2-tolerance catalysts

In terms of catalyst development, the metal ligand in the alloy catalyst Pt-M can weaken the Pt-S bond, which can contribute to the oxidation of SO_2 at lower potentials [154]. SO_2 cannot be adsorbed on Ru, so Pt-Ru catalysts can be prepared to enhance the anti-SO_2 poisoning effect of PEMFC. It has been demonstrated that Ru can be used to reduce the adsorption energy of SO_2 by changing the electronic structure at the initial stage and accelerate the formation of SO_4^{2-} from SO_2 in the subsequent reaction [210]. In addition, other SO_2-resistant alloy catalysts have been reported, such as Pt_3Co [211], Pt_3Ni [212] and Pt-Mo [213].

7. Durability improvement measures

7.1 MEA materials

As mentioned above, the performance degradation of in-vehicle PEMFC is essentially

caused by material degradation. On the basis of cost control to find more stable materials to be applied to the corresponding components of PEMFC, it is important to achieve long-life stable operation of PEMFC and simplify the PEMFC system. Naturally, due to the PEMFC working process often occurs in high acidity, high temperature and other harsh operating environments, as well as in the automotive operating conditions appear in a variety of degradation mechanisms, which greatly improves the difficulty of finding suitable materials to improve the durability of the PEMFC in all aspects. Since the main part affecting the performance of PEMFC is MEA, many scholars have improved the durability of MEA by physically or chemically modifying the membrane, CL (catalyst and support), or even by using new materials.

7.1.1 PEM

As mentioned above, the main forms of PEM degradation under automotive operating conditions are physical recession due to cycling of the underlying operating conditions and chemical recession due to free radical attack. For the mitigation of physical recession, reinforced composite membranes can be used to enhance the mechanical strength of the membranes; for the mitigation of chemical recession, researchers have typically used two approaches: stabilisation of the polymer groups, and addition of free radical quenchers [214].

7.1.1.1 Reinforced composite membranes

Currently, the most commonly used PEMs for PEMFC are still PFSA-based sulfonic acid-based membranes [215] because of their excellent proton conductivity and better

physical/chemical stability [216]. However, their application in PEMFCs remains challenging, mainly due to their poor dimensional stability [217,218]. To maintain high proton conductivity, sulfonic acid-based membranes usually have a high density of sulfonic acid groups [219]. Under humidified conditions, the hydrophilic sulfonic acid groups absorb large amounts of water leading to swelling, which causes the molecular distances of the polymer chains to expand, thus facilitating reactive gas permeation, known as gas crossover [220]. As mentioned earlier, both mechanical fatigue due to volume changes in the membrane and free radicals generated by the gas crossover reaction can adversely affect the durability of PEMFCs. In order to reduce membrane swelling, researchers prepared reinforced composite membranes by chemically modifying and physically strengthening the polymer structure.

The use of mechanically stable matrices impregnated with PFSA to prepare reinforced composite membranes is a widely-used method. Matrices can be divided into organic and inorganic types. Organic matrices include porous PTFE [221], poly (vinylidene fluoride) nanofibres [222], and polyacrylonitrile nanofibres [223]; while inorganic matrices include carbon nanotubes [224], graphene oxide [225], metal-organic frameworks [226], and metal oxides [227]. Among them, the excellent mechanical strength of porous PTFE can significantly inhibit membrane swelling [216,228], and thus porous PTFE-based reinforcement strategies have been widely recognised by researchers.

In PTFE polymers, the carbon backbone, C-C/C-F bonds and the surrounding F electron cloud make the molecular structure highly stable [229,230] (Fig. 19(a)),

which is responsible for limiting membrane swelling and enhancing the dimensional stability of the membrane body. The surface morphologies of various porous PTFE films based on these different preparation methods are shown in Fig. 19(b)-(e) [231-234].

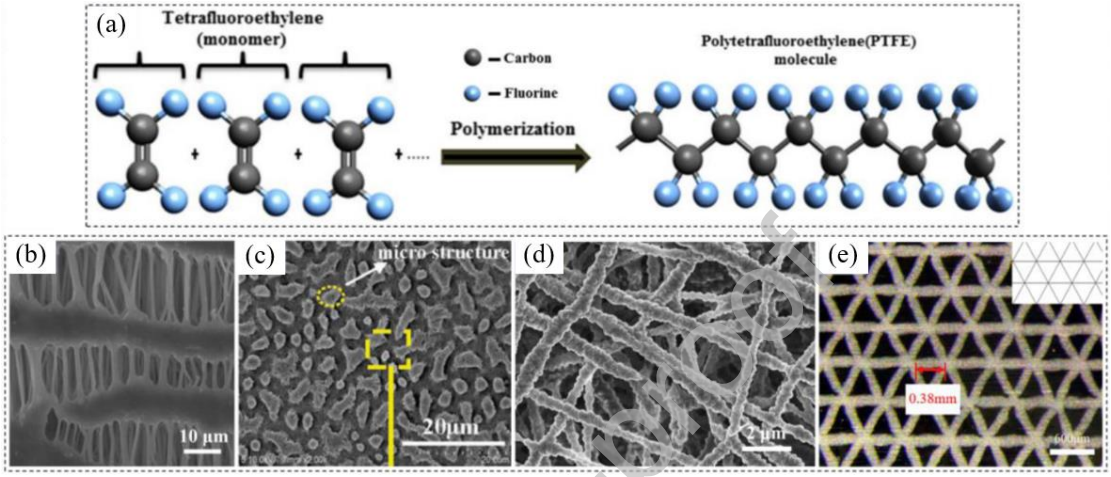

Fig. 19. (a) Molecular structure of PTFE polymer [230]; (b) paste extrusion-stretching [231]; (c) pore-forming agent assisted sintering [232]; (d) emulsion electrospinning [233]; (e) near field electrospinning [234]. Reprinted from Ref. [235] with permission of Elsevier.

Shi et al. [236] examined the dissolution rates of commercial Nafion 212 (no reinforcement) and Nafion XL (PTFE reinforcement) at 100% relative humidity with different temperatures. Nafion XL showed lower in-plane swelling and higher swelling in the thickness direction at either temperature tested. However, for membrane mechanical durability, the in-plane swelling rate was significantly more weighted than the thickness-direction swelling rate [237]. Tang et al. [238] simulated the in-plane stress changes in membranes with/without PTFE reinforcement under humidity cycling and showed significantly smaller stress fluctuations in the reinforced

membranes.

Several other studies have shown that the mechanical properties and dimensional stability of the membranes were enhanced by the introduction of porous PTFE reinforcement [239]. However, since PTFE itself has no proton conducting groups, it may lead to a slight decrease in membrane proton conductivity after reinforcing the membrane as a substrate [240]. This negative effect can be eliminated as much as possible by improving the interfacial compatibility through ultra-thin PTFE pads with high porosity or hydrophilic treatment of hydrophobic PTFE structures [241].

In addition to PTFE, there are also related reports on other matrices as raw materials for the preparation of reinforced composite membranes. He et al. [242] prepared sulfonated carbon nanotube/Nafion composite membranes by a self-assembled sol-gel process. The Su-CNTs significantly enhanced the ordering of the PFSA, which led to less curvature of the proton transporting water channel network. Addtionally, the reinforcement of the membranes by Su-CNTs limited the rearrangement of the Nafion backbone. This helps the membrane to maintain a high proton conductivity and increase the operating temperature and lifetime of the membrane. Some researchers also chose to find stable, inert materials in electrospun polymers as membrane reinforcement, such as sulfonated polyetherketones [243], poly (vinylidene fluoride-co-hexafluoropropylene) [244], etc. Liu et al. [245] modified the surface of PVDF-HFP nanofibres with polyelectrolytes and doped them into membranes, which improved the mechanical stability of the membranes while maintaining a proton conductivity of 106 mS cm^{-1} of proton conductivity. Cavaliere et al. [246] found that

the ionic cross-linking effect of PFSA and polybenzimidazole could form highly interconnected proton conducting surfaces, enhancing the stability of the composite membranes with some improvement. Thiele et al. [243] used the inkjet printing method to fill the Nafion with electrospun sulfonated polyetherketone to effectively reduce the resistance of the ionic membranes and enhance the power density. The test results of humidity cycling and OCV conditions showed no significant degradation in terms of H_2 permeation current.

7.1.1.2 Modification of molecular structure

Chemical degradation of membranes is mainly caused by the presence of reactive groups in their own chemical structure, so structural modification to eliminate reactive groups is an effective method. For instance, replacing H-containing end groups with inert groups or shortening the side chains by removing tertiary carbon bonds (-CF) and ether bonding carbon atoms (-O-CF_2) in the side chains can effectively reduce the degradation due to free radical attack [15]. Li et al. [247] investigated the effect of long-side-chain ionomer membranes (Nafion) and short-side-chain ionomer membranes (Aquivion) on the durability of the membrane. The results of accelerated aging tests showed that the maximum power drop of the short-side chain ionomer membranes was about 2%, while the maximum power drop of the short-side chain ionomer membranes was about 1.5 times. The results of the accelerated aging tests showed that the maximum power drop of the short side chain ionomer membrane was significantly less than that of the long side chain ionomer membrane.

DuPont used fluorine to treat fluoropolymers in order to convert unstable end groups

in the membranes to -CF_3 [248], and this method has also been used by several researchers for related studies [249]. Cheng et al. [250] pretreated the ionomers prior to membrane casting by hydrothermal decarboxylation, which significantly mitigated the chemical decline of the membranes while maintaining consistency with the pristine membrane equivalents and proton conductivities.

In addition, partial structural modification is also a more common means of membrane modification, such as grafting [251] and copolymerisation [252]. This usually changes the existing manufacturing process steps to some extent, often making the cost higher. The complex synthesis methods of PFSA ionomers also hinder more diverse molecular designs. The use of fluorine-free ionomers, such as aromatic ionomers, has been proposed to increase the flexibility of molecular design.Miyatake et al. [253] synthesised poly (phenylene) PEMs, which consisted of only phenylene and sulfonic acid groups, and exhibited high PEM conductivity and excellent oxidation resistance over a wide range of humidity due to the absence of heteroatom bonds. The proton conductivity and stability of its molecular structure and initial state were retained under Fenton's reagent and OCV working condition tests.

7.1.1.3 The use of free radical scavengers

Since the chemical degradation of membranes is essentially the result of a series of chemical reactions, and the reactants are free radicals and polymer ionomers. Therefore, removing free radicals to prevent them from reacting with the reactive groups in the membrane can likewise alleviate the chemical degradation of the membrane. Based on this idea, free radical scavengers (FRS) has been introduced into

PEM. Compared to membranes, FRS can preferentially react with free radicals, making polymers immune to chemical degradation. Generally, FRS is introduced during membrane casting without changing the manufacturing process, which is easier to achieve compared to modifying the reactive groups of the ionomer [248]. In conjunction with the PEMFC operating environment, FRS needs to meet the following requirements: (1) preferentially react with free radicals; (2) be able to be regenerated in a manner that allows for long term efficacy; and (3) be insoluble in acidic aqueous media.

FRS can be classified into organic and inorganic groups, with the former including L-ascorbic acid, terephthalic acid, α-tocopherol, and benzoquinone derivatives [254], whereas the latter contains Ce-based ionic or oxide states and metal compounds of Mn, Cr, and Co [255,256]. The Ce-based FRS, which is widely used in practical applications, is introduced here as an example. Ce-based oxides usually exist in the form of Ce_2O_3 and CeO_2, which correspond to Ce^{3+} and Ce^{4+}, respectively. The interconversion of Ce_2O_3 and CeO_2 makes Ce-based materials feasible to be used as a FRS. Ce^{4+} can oxidise certain components produced during PEMFC operation, such as H_2O_2,·OOH and H_2 (see Fig. 20), and the reduction product Ce^{3+} can be oxidised to Ce^{4+} by OH, thus establishing a regeneration cycle. Ce is usually added to ionomer dispersions in a certain ratio, and the introduction of FRS is achieved by mechanical mixing and subsequent casting [257]. Certain Ce salts can also be used as precursors for Ce-based oxides [258].

Most researchers have made Ce-based oxides in the form of nanocrystals randomly

dispersed in ionomers. The Ce-based oxide particles are mainly adjacent to the sulfonic acid group to improve the dispersion of the particles in the PEM. In addition, the ratio of Ce^{3+} to Ce^{4+} plays an important role in the free radical scavenging effect [259]. Ce^{3+} is often accompanied by oxygen vacancies, which provide reaction sites for scavenging free radicals, and an increase in this site significantly improves the free radical scavenging efficiency [260]. It has also been found that larger particles of Ce-based nanoparticles are more effective than smaller particles, which can be attributed to differences in particle surface activity [261].

Many studies have shown that appropriate levels of Ce-based oxide doping can significantly mitigate chemical degradation [257,262]. Wang et al. [258] concluded that too much or too little Ce-based oxides can lead to a decrease in chemical stability by analysing the SEM images of PEMs subjected to the action of free radicals. However, due to the fact that the actual working environment of PEMFC is more complex than that in Fenton's reagent, there are some differences between in-situ and ex-situ tests. This is due to the fact that in in-situ testing, even if the Ce-based oxide particles are fully leached, they can scavenge free radicals from the solution, but the leached Ce-based oxide particles in PEMFC will not act as FRS [263].

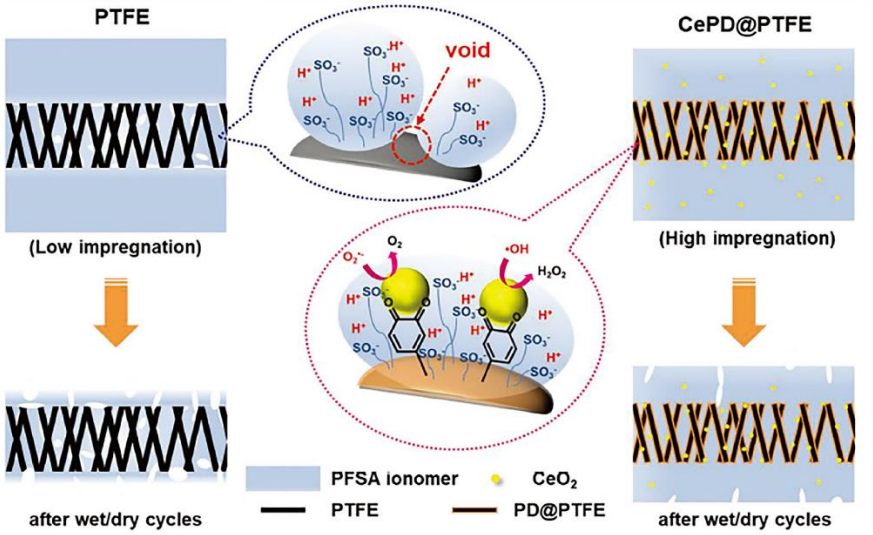

Fig. 20. Schematic diagram of e-PTFE reinforced PEM containing ceria as FRS. Reprinted from Ref. [263] with permission of John Wiley and Sons.

Ce-based oxides still have some shortcomings: the electric field may cause migration of Ce ions, which is toxic to the PEMFC; and the Ce particles may coordinate with the sulfonic acid group in the membrane, leading to a decrease in proton conductivity [264]. In order to obtain better FRS results, researchers have conducted numerous studies to improve the above mentioned deficiencies, and the migration of Ce-based oxides can be mitigated by immobilisation, such as the use of fillers with excellent mechanical properties as described previously, such as multi-walled carbon nanotubes [265], organosiloxane polymer mesh [264], and TiC [266], etc. The migration of Ce-based oxides can be mitigated by immobilisation. As for the decrease in proton conductivity caused by Ce-based oxides, it has been suggested that a potential solution exists by functionalising the surface of Ce-based oxide nanoparticles with proton conducting functional groups or polymers such as HPA, fluorophosphonic acid or silica supports grafted with sulfonic acid groups [267,268]. In addition, in order to

minimise the loss of performance due to the introduction of Ce-based oxides, it is necessary to improve their scavenging efficiency of free radicals in order to reduce the Ce-based oxide content in the membrane.

7.1.2 Catalysts

Due to the promising ORR performance, the preferred choice of catalysts for PEMFCs has so far been Pt-based materials. However, as previously reviewed, Pt catalysts under automotive operating conditions face a rather unstable operating environment, which can lead to the following forms of Pt degradation: electrochemical Ostwald ripening; Pt migration and deposition; Pt growth and agglomeration; corrosion due to contamination by impurities, and so on. Consequently, researchers have sought to further enhance the stability of PEMFC catalysts to achieve long-life operation. Currently, the following aspects have been reported: modification of the Pt particle structure; enhancement of the interaction between Pt particles and supports; and the use of corrosion-resistant supports. Research on corrosion-resistant supports is detailed in the review of carbon supports in the next section, and this section focuses on the first two.

7.1.2.1 Core-shell structure catalysts

One way of optimizing the structure is to use Pt-based core-shell catalysts, exploiting the synergistic interaction between the core and shell in order to improve the ORR activity and stability of the catalysts in complex reaction environments [269]. The Pt utilization of Pt-based core-shell catalysts is also higher due to the fact that only the atoms on the surface portion of the catalyst are in contact with the electrolyte and act

as catalysts in the ORR reaction [270]. Several studies have shown that this catalyst has shown better ORR activity and durability [271,272]. The Pt skin structure is a more stable structure due to the negative bias energy, and its growth-limiting behavior as well as the inhibition of surface oxide formation illustrate the stability of the Pt-based core-shell structure [273].

Some researchers have chosen to dope the nucleus with non-metallic elements to achieve high stability [274-276]. This is because the relatively high electronegativity of non-metallic elements gives them a strong affinity for Pt atoms, which helps to inhibit Pt dissolution [277]. It has been documented that the incorporation of non-metallic elements in Pt-based catalysts can weaken the performance degradation brought about by the Fenton reaction [278]. He et al. [279] prepared Pd-P interlayer core-shell Pt nanocrystals by deposition of a layer of Pt atoms on amorphous Pd-phosphide cores as a shell structure. The high corrosion resistance of the disordered a-Pd-P and the strong interaction between the Pt shell and the internal amorphous Pd-P significantly improved the durability of the catalyst. The catalyst achieves a mass activity of 4.08 A mg^{-1}_{Pt} and 1.37 A mg^{-1}_{Pd+Pt} at 0.9 V. Moreover, the loss of activity is only about 9% after 50,000 potential cycles, and the structural deformation that occurs is very subtle.

The use of a stable metal as the core is also a common approach. During the potential cycling of Pt-based core-shell catalysts, unstable nucleolytic dissolution usually occurs, leading to the destruction of the catalyst structure and greatly affecting its durability [280]. The introduction of a stable metal element as the core can effectively

alleviate this problem. Wang et al. [281] reported a catalyst by depositing Pt on the surface of Pd icosahedral crystal species. Its utilization of the interaction between the Pt shell and the Pd core resulted in an approximately fourfold increase in the mass activity of the catalyst at 0.9 V over commercial Pt/C even after 10,000 potential cycles. In another study by Wang et al. [282], it was also shown that the core-shell concave decahedral catalysts formed by Pd cores and Pt shells exhibited significantly higher mass activity than the pristine Pt/C catalysts after accelerated aging tests. Hu et al. [283] prepared Ti-Au@Pt/C catalysts, where protective TiO_2 and Au cores at the apex position of the edge cores suppressed the catalyst's potential cycling during dissolution and the loss of cell performance was negligible. Tao et al. [284] inserted atomic Pd interlayers into 1D Pd/Pt core/shell nanowires, resulting in a significant improvement in the catalytic stability of sub-nanometer Pt shells during ORR. The Pd/PdAu/Pt core/shell nanowires exhibited a degradation rate of only 7.80% in ORR mass-activity after 80,000 potentiostatic cycles. The Pd cores did not dissolve, preserving the overall sandwiched core/shell nanostructures intact. Other researchers have also made attempts to use Pt-based alloys as core materials, such as octahedral nanocrystals composed of face-centered tetragonal Pt-Co cores and ultrathin Pt shells, and after 30,000 accelerated aging tests, there was no significant change in the catalyst structure. The half-wave potentials and mass activities dropped by 11 mV and 21%, which indicated its good durability [285]. Some typical studies of core-shell catalysts are shown in Fig. 21.

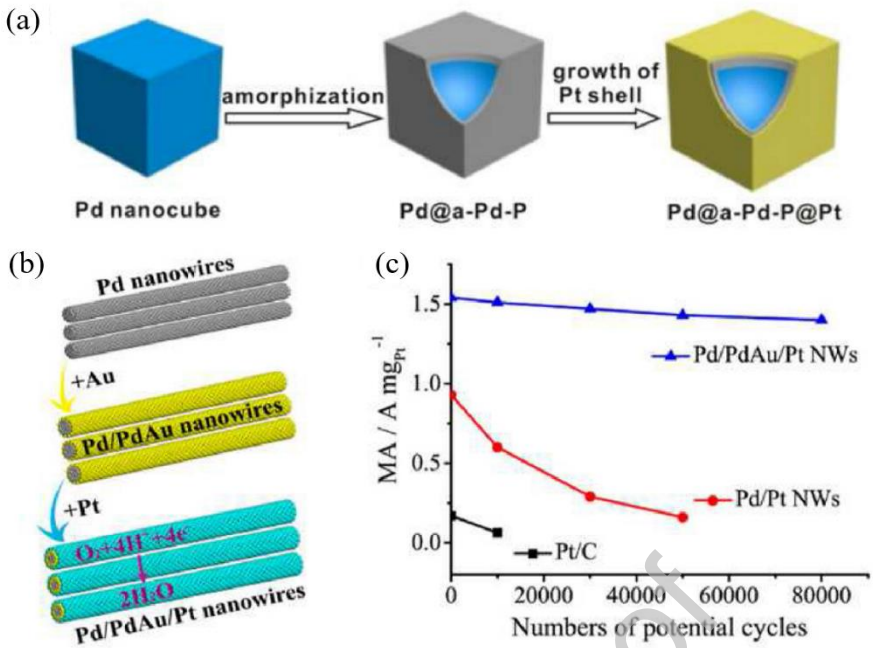

Fig. 21. (a) Typical synthesis of the amorphous-crystalline Pd@a-Pd-P@Pt. Reprinted from Ref. [279] with permission of American Chemical Society; (b) Synthesis schematic of Pd/PdAu/Pt NWs. Reprinted from Ref. [284] with permission of American Chemical Society; (c) Changes of MAs for electrocatalysts before and after different potential cycles. Reprinted from Ref. [284] with permission of American Chemical Society.

7.1.2.2 Highly-ordered alloy catalysts

Modification of Pt catalysts has also been carried out by alloying Pt with some transition metals. However, the prepared Pt-based alloys are usually disordered solid solutions due to the presence of diffusion barriers, which is detrimental to the stability of the catalysts in the PEMFC operating environment [286]. In recent years, researchers have developed alloy catalysts with fixed stoichiometric ratios and highly ordered atomic structures, in which the atoms of each constituent element are ordered in a specific crystallographic direction and their metal atoms interact through strong d

orbitals [287], which makes this class of catalysts more durable [288].

Yoo et al. [289] reported a catalyst prepared by direct thermal decomposition of carbon supports on [Fe $(bpy)_3$][$PtCl_6$] to synthesize nanoparticles with a Pt/Fe atomic ratio of 1:1. The high atomic ordering of this catalyst fully ensured that the Fe-Pt nanocrystals were not easy to agglomerate and dissolve during the ORR process, and the specific activity was almost unchanged after 20,000 potentiostatic cycles. Zhao et al. [290] synthesized N-doped ordered Pt-Ni cores with Pt shells by annealing in NH_3.The N-doped surfaces elevated the alternately stacked Ni_4-N portions along the [001] direction and the Pt layers for the formation of ordered structures, thus enhancing the long-term stability of the catalyst. In addition, doping of high melting point metals to modulate the local coordination environment has been shown to be an effective way to enhance the catalyst activity. Lin et al. [291] prepared Pt-Co-Mo catalysts, where Mo doping led to the optimization of the electronic structure of the catalyst surface, reducing the Co exudation during the potential cycling and enhancing the durability. Liang et al. [292] introduced a small amount of W, which also served to stabilize the ordered intermetallic structure to ensure that the catalyst maintains long-term stability during PEMFC operation.

Although some Pt-based alloy catalysts such as Pt-Fe, Pt-Co show favorable activity and stability, they are susceptible to the formation of Fenton reagents with H_2O_2, which can lead to the degradation of membranes and CL [293]. To avoid this problem, compounds can be formed using metal elements without Fenton activity. For example, nanocrystals of Pt-Zn have been prepared to inhibit the formation of reactive oxygen

species through the element Zn to suppress the Fenton reaction [294]. The introduction of rare earth elements, such as La, can also effectively alleviate the problems of catalyst dissolution and reactive radical generation [295]. In addition, Pt-based alloy catalysts usually require a fixed stoichiometric ratio, typically 3:1 or 1:1. changing the stoichiometric ratio of the nanoparticles usually destroys the ordered structure of the catalyst, which in turn reduces its stability. Sometimes a third metal element can be introduced to partially replace a certain amount of a metal in the alloy catalyst in order to safeguard the ordered structure [270].

7.1.2.3 Strong metal-support interaction (SMSI)

Weak interactions between metal nanoparticles and support materials are also an important reason for the poor stability of Pt-based alloy catalysts, so enhancing the interactions between Pt particles and supports is also a feasible way to improve the stability of catalysts. Strong metal-support interactions can promote the electron transfer between metal nanoparticles and supports, optimize the electronic structure on the surface of Pt nanoparticles, and effectively inhibit the dissolution, migration and aggregation of metal nanoparticles, thus improving the stability [296].

Heteroatom-doped carbon materials not only create more sites for the immobilization of metal nanoparticles. It also enhances the polarity and conductivity of the carbon supports, thus increasing the interaction between the supports and the metal nanoparticles. Boron atoms are similar in size to the carbon atoms and can easily replace the carbon atoms in the backbone [297]. Liu et al. [298] achieved mono-dispersity of Pt nanoparticles on supports by doping boron. The resulting

Pt/(BC)600 showed a 19.7% decrease in mass activity after 10,000 accelerated aging cycles, which was much better than that of commercial Pt/C (58.7% decrease). N-doped C also works well, as the lone electron pair of N alters the electronic properties of the carbon support, which facilitates the enhancement of the interactions between the support and the catalyst particles [297]. Lin et al. [299] used the N doped graphitic carbon nanosheets as supports to achieve uniform dispersion of Pt catalyst particles. The interaction also weakened Pt-O, which inhibited Pt dissolution and improved catalyst stability. Some researchers have also produced strong metal-support interactions by introducing metal oxides. Gao et al. [300] used highly dispersed Ta_2O_5 modified carbon nanotubes as supports to stabilize the Pt nanoparticles and enhance the metal-support interaction. The fabricated catalyst had a large ECSA of 78.4 m^2 g^{-1}_{Pt} at 0.9 V and a mass activity of 0.23 A mg^{-1}_{Pt}. The degradation of ECSA and half-wave potential was insignificant after 10,000 potential cycles.

In addition, the introduction of oxygen vacancies on the oxide support further modulates the Pt electronic configuration, which contributes to high durability. This is because oxygen vacancies modulate the energy band structure of metal oxides, increase their conductivity and facilitate electron transfer [301]. Meanwhile, appropriate levels of oxygen vacancies can further enhance the metal-support interactions, which in turn enable Pt nanoparticles to have higher migration energy barriers and inhibit their agglomeration [302]. Li et al. [302] prepared a series of CNT@SnO_2 as a support with precisely adjustable oxygen vacancy concentrations, and the strong metal-support interactions resulted in greater adsorption energy of the

Pt atoms, and the stability of the catalyst was very impressive. After 50,000 potential cycles, the negative half-wave shift of the Pt-CNT@SnO_2 sample was only 11 mV, and the mass activity and specific activity at 0.9 V only decreased by 20.5% and 10.3%, respectively. Fig. 22 shows additional attempts to enhance catalysts through SMSI [303-305].

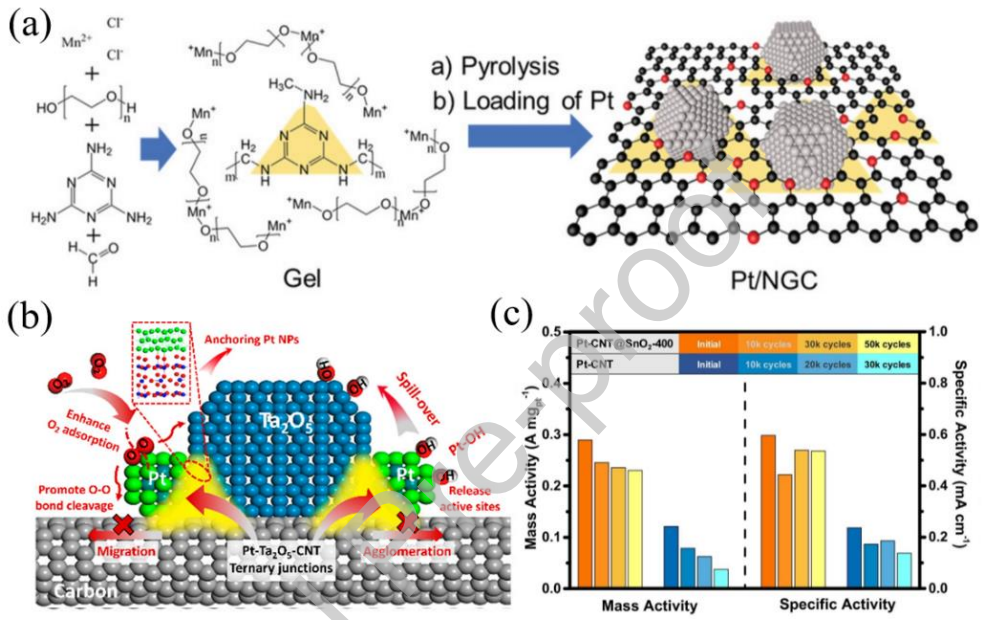

Fig. 22. (a) Schematic drawing of synthesizing highly graphitized NGC for loading Pt nanoparticles (Pt/NGC). Reprinted from Ref. [303] with permission of John Wiley and Sons; (b) Schematic diagram of Pt–Ta_2O_5-CNT nanoparticles. Reprinted from Ref. [304] with permission of American Chemical Society; (c) MAs and SAs of Pt-CNT@SnO_2-400 at 0.9 V during ADT. Reprinted from Ref. [305] with permission of Elsevier.

7.1.3 Catalyst support

Stable support materials are important for durable catalysts and even for improving the lifetime of PEMFCs. Carbon black (or Vulcan carbon) is still used as a support

material for most PEMFCs due to its good electrical conductivity and high specific surface area, which facilitates fast electron transport at the electrodes and good distribution of the Pt catalyst [306]. However, as mentioned earlier, the corrosion of the carbon support due to some of the working conditions has serious adverse effects on the stability of the catalyst, including Pt dissolution, migration and Ostwald ripening at the electrode surface. Combined with the working environment inside the PEMFC, the catalyst support should have good electrochemical stability, high specific surface area, high conductivity, excellent pore structure and strong anchoring effect with the catalyst particles. At present, there are two main methods to alleviate the carbon corrosion problem of PEMFC: (1) using novel carbon materials; (2) finding alternative materials.

7.1.3.1 Novel carbon materials

In terms of novel carbon materials, the study by Stonehart et al. [307] firstly established a link between carbon structure and ORR rate. They found that graphitic carbon with smaller grain spacing was more resistant to galvanic corrosion. It has been shown that increasing the degree of graphitization of carbon materials improves their resistance to sintering, which hinders the growth of Pt particles [308]. Therefore, highly graphitized carbon materials such as carbon nanotubes, carbon nanofibers and reduced graphene oxide may be promising carbon support materials for PEMFC [309,310]. Li et al. [311] found that a support made of carbon black mixed with reduced graphene oxide significantly improved the stability of Pt catalysts. After 20,000 potential cycles, the loss of ECSA was only about 5%, while the loss of

commercial Pt/C could reach almost 50%. Popov et al. [312] prepared N-doped mesoporous graphitic carbon supports by pyrolysis of M-chelates adsorbed on carbon black. Using this support, the maximum power density loss of the battery after 30,000 potential cycles was 26%, whereas the loss of the commercial Pt/C counterpart was 52%.

However, the hydrophobicity of the graphitic carbon particle surface is not conducive to Pt dispersion. More et al. [313] found that Pt particles tend to preferentially accumulate in the cleavage- and defect-rich edge sites of the graphitic carbon structure rather than nucleating on the highly graphitic and chemically inert surfaces, which results in susceptibility to agglomeration in the regions where Pt is not uniformly accumulated. To address this problem, graphitized carbon can be modified by non-covalent polyelectrolyte functionalization [314] and strong oxidation [315].

7.1.3.2 Alternative materials

For alternative materials used as catalyst supports, such as certain carbides, oxides and nitrides, which exhibit higher corrosion resistance and thermal stability than conventional carbon materials, they are considered as new candidate supports for Pt-based catalysts.

7.1.3.2.1 Carbides

For carbides, they are generally compounds containing C and elements with lower electronegativity. They have similar electron densities to Pt at the Fermi energy level and, therefore, can enhance catalytic activity through synergistic interactions [316]. WC serves as an attractive support material for supports due to its high chemical

stability and good electrical conductivity, and, furthermore, it also exhibits outstandingly strong metal-support interactions [317]. Bott-neto et al. [318] compared cubic suborbital (β-WC_{1-x}/C) and hexagonal (α-WC/C) types of W-C, with the former having a specific activity 3.6 times higher than that of commercial Pt/C, which stems from the increase in vacancies in the Pt 5d band, reducing the interactions of oxygen-containing species, and thus leading to rapid O-O bond breaking and slower adsorption rates. Yurtsever et al. [319] found that the mass-activity of WC nanorod support when the Pt nanoparticles were uniformly and completely covered, had superior mass activity to commercial Pt/C and almost no loss of ECSA after 3,000 cycle experiments.

Mo_2C has also received attention. when used as a Pt-supporting multi-walled nanotube material, showing superior mass activity of up to 150 mA mg^{-1}_{Pt}, followed by Pt/WC (127 mA mg^{-1}_{Pt}), and commercial Pt/C of (39.5 mA mg^{-1}_{Pt}) [320]. Nanocrystalline Mo2C is the commonly used structure in most studies [306,321]. Elbaz et al. [322] used a one-pot synthesis of Mo_2C with a Pt precursor resulting in a unique catalyst structure in the form of nano rafts. The catalyst exhibited only a 10% loss of ECSA after 5,000 cycles in an accelerated stress test program. The electronic interactions in the nano-rafts arise from the stronger binding of Pt atoms to the Mo_2C surface through the formation of Pt-C. The Pt/Mo_2C catalyst prepared by Saha et al. [323] achieved a power density 111% higher than that of Pt/C after 30,000 AST cycles. For other carbides, such as TiC, ZrC, NbC, etc., only a few researchers have carried out relevant studies on them.

7.1.3.2.2 Oxides

In the application of oxides, Ti-based oxides have better CO resistance and durability, which has brought them to the attention of many researchers. Doping of Ti-based oxides with other elements such as Nb, Ta, Ru, etc. is a common way to enhance the durability of the support as the doped metals lead to changes in the chemical state, crystal structure, and electrical properties, which can be used to mitigate the deficiency of the other elements to some extent [324,325]. After doping, many studies have confirmed the reduction of ECSA loss after AST cycling. For example, it has been reported that the ECSA loss of Pt/Ta-TiO_2 is claimed to be only 51% of that of commercial Pt/C [326]. Choi et al. [327] investigated Nb-doped TiO_2 supports for Pt catalysts, and excellent stability was observed on optimized samples with 4 mol% Nb in the support, with only a 15% ECSA loss compared to 55% loss of commercial Pt/C after 25,000 AST cycles, with only 15% loss of ECSA. excellent performance can be further observed by single cell durability testing at 10,000 cycles. Where Pt/Ti-Nb4 exhibits only 20% current degradation at 0.6 V compared to 85% loss for the Pt/C sample.

The use of doping with other elements to improve the properties of the original support material is a more common approach, which has been used by several researchers to investigate SnO_2 as a PEMFC support material using doping elements such as Sb [328], Nb [329], Ta [330], F [331], etc., in order to improve the performance and durability. Mohanta et al. [332] found excellent stability of Pt/ATO. After 70,000 AST cycles, the loss of ECSA was only 14%, whereas the catalyst

TK-20, which used carbon black as support, lost 50% of its ECSA. They attributed the stability of the catalyst to the "electrochemical transistor effect" in the high potential region due to the reduced surface conductivity, which prevents the dissolution of the Pt particles.

For the doping of other elements, some way of performance tuning is also required. For example, the poor electronic conductivity of Pt/Nb-SnO_2 leads to a lower electrochemical activity than Pt/ATO [329]. A study aimed to overcome this problem through a network of fused aggregates between Nb and SnO_2 nanoparticles by partial necking [333]. Meanwhile, a study demonstrated the melt aggregation structure of Ta-doped SnO_2 with a conductivity about 40 times that of Nb-$SnO_{2-\delta}$. The durability of Pt/Ta-$SnO_{2-\delta}$ was superior to that of commercial Pt/C after 1,000 h of MEA testing with only 0.016% dissolution of SnO_2 [330]. Other researchers have conducted Ta-doping studies and showed that Pt/Ta-SnO_2 retained 81% of ECSA after 6,000 cycles, had higher electrical conductivity than its Nb-SnO_2 counterpart, and possessed superior durability than its ATO counterpart in MEA tests, and could be used as a promising metal dopant for carbon-free Pt supports [334].

7.1.3.2.3 Nitrides

In contrast to carbide and oxide materials, most nitride materials have not been investigated as catalyst support in PEMFC, with the exception of TiN, which is highly resistant to corrosion in acidic and oxidizing environments and interacts with the catalyst. Contrary to oxides, TiN does not suffer from surface passivation due to the formation of oxide layers [335]. In addition, NB is also a new Pt support material and

some studies have shown that it shows good performance and durability [336]. With a larger ECSA compared to Pt/C [337], Pt/TiN has less ECSA loss and no significant change in its double layer capacitance, indicating that this catalyst has better stability in the PEMFC operating environment [338]. Nanostructured TiN has been widely used as a Pt catalyst support to achieve higher ECSA. Pan et al. [338] used TiN multi-hollow nanotubes as a support for Pt catalysts and maintained up to 77% ECSA after 12,000 cycles of AST test, while the ECSA of Pt/C catalysts was reduced to 45% of the initial value after just 4,000 cycles. Perego et al. [339] used graded TiN thin film MEA as a Pt support with mesoporous structure by pulsed laser deposition and successfully achieved only 13% reduction in ECSA after 15,000 AST cycles.

Other researchers have doped TiN with different elements such as O [340], Co [341] and Ni [337]. O was introduced with the aim of overcoming the instability of TiN at high oxidation potentials. Chin et al. [342] demonstrated that ALD-assisted TiO_xN_{1-x} samples have good resistance to degradation. Whereas, the introduction of ORR active elements such as Co and Ni helps to increase the value of the half-wave potential [341], and, XPS analyses yielded an increase in Pt (0) species and a decrease in Pt (II) species upon the introduction of Co or Ni as well as a negative shift in the binding energy of Pt 4f, which suggests that the TiN alloys with transition metals can provide more electrons to the Pt atoms [337], making the affinity between Pt and intermediate oxide species weakened and ORR activity increased [343]. Moreover, OH species can be adsorbed on TiN or $Ti_{0.9}Co_{0.1}N$ supports, which reduces the OH coverage on Pt catalysts and increases the number of vacant sites for O_2 adsorption,

resulting in improved ORR activity and durability [344]. Researchers have also observed that the SMSI and synergistic effects between Pt nanoparticles and transition metal alloyed TiN inhibit the aggregation or segregation of Pt nanoparticles, leading to improved stability [345]. Jiang et al. [346] prepared an advanced catalyst support based on vertically aligned titanium nitride nanorod arrays (TiN NRs) (see Fig. 23), and a thin film PtPdCo catalyst with a Pt loading of 66.9 μm cm^{-2} was supported onto TiN NRs to serve as the cell cathode. The results of the 2,000 potential cycles accelerated degradation test indicate that the PtPdCo-TiN electrode is more stable than the commercial gas diffusion electrode.

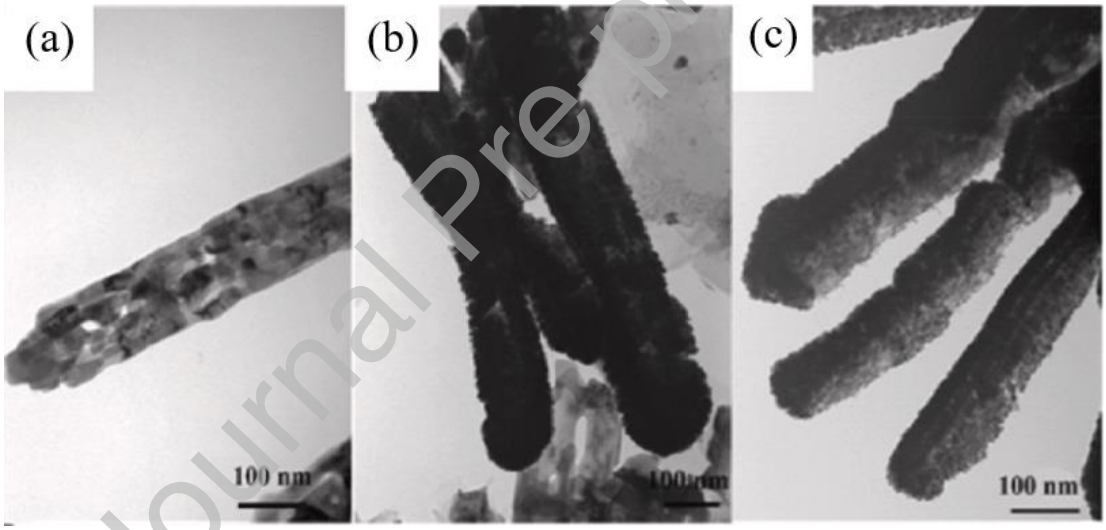

Fig. 23. (a) TiN NRs; (b) Fresh PtPdCo–TiN NRs; (c) PtPdCo-TiN NRs after annealing at 400°C. Reprinted from Ref. [346] with permission of John Wiley and Sons.

Porous boron nitride is an ultrafine Pt nanoparticle support that has attracted the attention of researchers in recent years. Electron-rich nitrogen atoms and electron-deficient boron atoms facilitate the electron-feedback process, which has a

strong anchoring effect on Pt nanoparticles [336]. The excellent durability of Pt/p-BN catalysts has also been observed, with a minimum ECSA drop of only 0.62% after 10,000 AST cycles. This was attributed to the strong catalyst-support interaction and the high tolerance of p-BN to the acidic operating environment in PEMFC [347]. Even though not many studies on p-BN have been conducted so far, Pt/p-BN is expected to reveal advances in highly active and durable PEMFC catalysts.

7.2 Bipolar plates and flow fields design

The bipolar plate is an incredibly important component of a PEMFC stack, where its design significantly affects the output performance, weight, and cost of the PEMFC. Since the bipolar plate connects single cells to form a stack as well as collects and transfers the generated current from one cell to the next, its durability, electrical conductivity and thermal conductivity are required. Furthermore, the bipolar plate should ensure the uniformity of gas distribution on the electrode surface with the effectiveness of removing exhaust gases and product water, the former to avoid the occurrence of hotspot formation that leads to localized high current density, which in turn makes the cell less durable, and the latter to avoid the possibility of flooding that hinders mass transfer [348].

7.2.1 Metallic bipolar plate optimization

Common materials used for bipolar plates are graphite, polymer materials and metals. While graphite is widely used and has excellent hydrophobicity and corrosion resistance, its brittleness and low strength limit it in the application scenario of automotive power sources. In addition, machining flow channels on graphite is more

expensive [349]. Polymer materials, such as thermoplastic or thermoset plastics, have limited use due to the low electrical conductivity [350]. Metallic bipolar plates are preferred as the material for automotive PEMFCs due to the ease of fabrication, mechanical properties, excellent electrical and thermal conduct ability [351]. This section analyses the use of metallic bipolar plates.

7.2.1.1 Degradation of Metallic bipolar plate

While metal bipolar plates are suitable for automotive applications, they are prone to degradation. The acidic environment, high operating temperatures, and harsh conditions such as dynamic loads, start-up and shutdown, and idling during in-vehicle operation cause high voltages on the bipolar plates and lead to corrosion [352,353]. Chapter 6 describes how the metal detaches from the bipolar plate as the corresponding cation; such procedure contaminates the membrane/CL and accelerates the degradation of the PEMFC. Additionally, an oxide film forms on the metal bipolar plate, increasing the contact resistance and reducing the efficiency and performance of the PEMFC [354]. Therefore, improving the corrosion resistance of the metal bipolar plate is crucial for achieving long-term operation of automotive PEMFCs.

Stainless steel is currently the most widely used material for metal bipolar plates due to the abundant varieties, low cost, and certain degree of chemical stability [355]. However, it is limited by the susceptibility to corrosion. Multiple studies conducted by combining various types of stainless steel with different elemental components to achieve corrosion resistance. Certain transition metals, including Cr, Mo, and Ni, can improve the corrosion resistance of stainless steel by forming an oxide layer on the

surface of the bipolar plate [356,357]. However, this oxide layer can negatively impact electrical conductivity due to the high resistance, resulting in a significant decrease in the output power. The use of a simple metal oxide layer alone is insufficient in achieving a satisfactory stainless steel bipolar plate [358].

7.2.1.2 Coating materials

At present, the best way to improve corrosion resistance and reduce contact resistance is the applications of coatings to the stainless steel surfaces. The most commonly used coating materials are carbon and metallic substances [359,360].

7.2.1.2.1 Carbon materials

Carbon material is commonly used as a coating material for metal bipolar plates due to the excellent corrosion resistance and high electrical conductivity [359]. A single layer of amorphous carbon used as a film coating provides durability and low contact resistance, which helps protect the bipolar plate from corrosion. This issue has been investigated by several scholars. Li et al. [361] investigated the effect of different frequencies of pulsed DC sputtering power on the generation of graphite nanoclusters in carbon coatings. They observed a stronger tendency for graphite nanoclusters generated at medium frequencies. These graphite nanoclusters form micro primary cells with the coating and the solution, leading to the depletion of the clusters and protecting the carbon coating. As a result, the coating durability is significantly improved. In addition, the coating results in a low interfacial contact resistance between the bipolar plate and the GDL. Yi et al. [362] demonstrated that the thickness of the a-C coatings significantly affects the durability. Thick coatings often have

multiple vacancy defects due to stress relaxation, which reduce the densification and durability. Thin coatings may not provide satisfactory corrosion resistance due to the amorphous transition layer present underneath them.

However, the durability of this coating in harsh environments does not yet meet the corresponding durability requirements for PEMFCs in vehicle applications [350]. Additionally, the low deposition rate and the possibility of peeling also limit its further commercialization. Scholars have used two main approaches to improve the performance of coatings: deposition of multilayer carbon coating materials and doping of metallic elements. The adhesion of the multilayer coating on stainless steel is stronger than that of the single-layer coating. This can effectively improve the corrosion resistance of the stainless steel bipolar plate and maintain the electrical performance [363]. Doping certain metal elements can release residual stress within the coating and increase atomic diffusion rate, improving adhesion and overall carbon coating performance [364].

7.2.1.2.2 Metal materials

7.2.1.2.2.1 Transition metals

Metal coatings can be mainly classified into two types: transition metal coatings and inert metal coatings. Transition metals have better electrical properties and corrosion resistance compared to carbon materials. Stainless steel contains a certain amount of transition metals, which results in better adhesion of transition metal coatings on stainless steel bipolar plates [365]. Li et al. [366] prepared tantalum-modified coatings on the surface of 316L SS; test results indicated that the bipolar plates achieved a

higher self-corrosion potential compared to the bare substrate. The corrosion current densities were 1.95 μA cm^{-2} and 0.14 μA cm^{-2} under simulated cathodic and anodic conditions, respectively. Additionally, the Ta coatings improved the hydrophobicity and electrical conductivity of the bipolar plates. Dong et al. [367] prepared a chromium-rich coating on the surface of stainless steel using an encapsulated chromium penetration process. Kinetic potential polarization tests revealed that the bipolar plates with the coating had ultra-low corrosion current densities of 0.264 and 0.222 μA cm^{-2} under simulated anodic and cathodic conditions, respectively. This was attributed to the excellent protective effect of the formed chromium carbide and passivation films.

Transition metal carbides have been used as coating materials to improve the performance of stainless steel bipolar plates. In a study by Wang et al. [368], molybdenum carbide coatings were deposited on 316L stainless steel surfaces using magnetron sputtering, resulting in a uniform and dense surface. It was found that thicker coatings improved corrosion resistance. The best corrosion current densities of 0.23 μA cm^{-2} were achieved by using a thin chromium transition layer and a molybdenum carbide coating with a thickness of approximately 1,052 nm. This thickness was about three orders of magnitude lower than that of uncoated stainless steel. Li et al. [369] modified titanium carbide coatings using tantalum and titanium carbide. During the growth process of the coating, Ta atoms thermally diffuse in the columnar TiC and react with carbon atoms. The obtained TaC, along with the rest of the cover layer, effectively inhibited the corrosion of the bipolar plate. The corrosion

current density decreased significantly from 84.016 μA cm^{-2} to 0.092 μA cm^{-2} when compared with uncoated stainless steel.

Transition metal nitrides have also been studied as coating materials to enhance the performance of stainless steel bipolar plates [370]. However, although they have excellent corrosion resistance, the poor electrical properties are the main limited factors [371]. In fact, some studies have shown that the interfacial contact resistance of stainless steel bipolar plates with such coatings does not meet the DOE requirements (<10 mΩ cm^{-2}) [372,373]. Auxiliary modification may be necessary to reduce contact resistance.

7.2.1.2.2.2 Inert metals

Inert metals typically exhibit excellent electrical and corrosion resistance properties. Researchers have utilized this to prepare coatings on stainless steel bipolar plates [374,375]. Currently, the primary materials used for inert metal coatings are gold and silver. Huang et al. [374] utilized silver-plated 316 SS bipolar plates treated with a chemical passivation technique. The passivation process successfully reduced the occurrence of pinhole defects in the coatings and significantly enhanced the corrosion resistance of the bipolar plates. The polarization current density of the silver-plated SS 316L bipolar plates was approximately two orders of magnitude lower than that of the uncoated bipolar plates in both cathodic and anodic environments. Kumar et al. [376] conducted correlation tests on 10 nm gold-plated SS 316L and demonstrated that the corrosion current density under simulated cathodic conditions was less than 1 μA cm^{-2}. They also concluded that nanometer-thick gold-plated coatings could meet

the cost targets for bipolar plates required for commercialization. However, it has been argued that the corrosion resistance of gold plating depends on the thickness of the coating. Thin inert metal coatings may not meet the established requirements for corrosion resistance [377]. Therefore, balancing the cost of expensive inert metals with the required corrosion resistance of bipolar plates is a main challenge that must be addressed.

7.2.2 Flow fields design and optimization

During PEMFC operation, the reactants/coolants flow through the flow channel and generally form a laminar flow that hinders mass transfer [378]. The structural design of the flow field can change the distribution of reactant gases and liquid water discharge, which considerably determines the water-gas transport capacity. In turn, the water-gas transport capacity has a significant impact on the electrochemical reaction rate, which in turn affects the performance, lifetime and energy consumption of the PEMFC [379]. However, the homogeneity of the fuel gas, maximizing the reaction area, minimizing resistance, transporting the right amount of water and large-scale simple fabrication make the optimization of the flow field design quite challenging. Scholars have conducted a lot of research on the flow field structure and its optimization by considering the above factors and combining them with specific application scenarios.

7.2.2.1 Basic flow fields

Typical types of flow fields are summarized in Fig. 24. In general, there are conventional flow fields such as parallel, serpentine and interdigitated flow fields

[380].

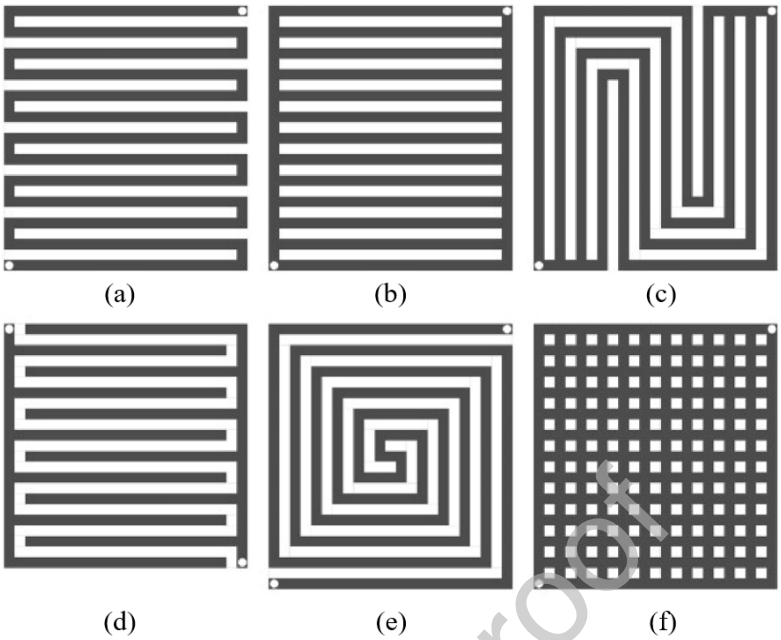

Fig. 24. Schematic diagram of the typical flow fields: (a) Serpentine; (b) Parallel; (c) Multi-serpentine; (d) Interdigitated; (e) Spiral; (f) Mesh flow fields. Reprinted from Ref. [380] with permission of Elsevier.

The parallel flow fields have lower pressure drop and less dependence on external blowers [381], however, the overall performance is not impressive due to the low flow rate of the fluid, non-uniform distribution, and poor water removal [382].

The serpentine flow field is the more commonly used flow field option. The structure enables the forced flow of reactive gas to the whole active region, which improves the coverage of reactive gas in the CL with better gas distribution, and the high flow rate of the fluid in the flow field allows the product water to be discharged quickly. It can be said that this flow field has better water-gas transport characteristics [383,384]. However, the disadvantage is that the excessively long flow path produces a large pressure drop and parasitic losses increase. Multiple serpentine flow fields can

alleviate the problem of large pressure drop in single serpentine flow fields [385]. It has been shown that 4-channel serpentine flow field has better gas distribution and current density uniformity than single-channel and dual-channel serpentine flow fields [386]. Besides, there is a corresponding critical length value for the performance of the serpentine flow field, and if the length is too long, the pressure drop in the flow field will rise sharply, which is obviously unfavorable to the PEMFC performance [387]. Therefore, when choosing a serpentine flow field, it should be ensured that the length of the flow field is less than the critical value.

The interdigitated flow field has a dead-end channel structure and an under-ribbed GDL transport path, which results in an accelerated longitudinal transport of the reactant gas and contributes to the removal of liquid water. However, the gas flow resistance through the porous GDL is high, and the flow field also requires precise control of the clamping pressure under the ribs in the PEMFC stacks to maintain reasonably high porosity of the GDL [388].

7.2.2.2 Novel flow fields

In order to achieve higher current and power densities in PEMFC, the flow field design is improved towards lower pressure drop, more uniform gas distribution, more efficient water management, and lower processing, fabrication difficulty and cost. Optimization and innovation of the original basic flow field to obtain a new type of flow field with more commercialization potential has become a hot research topic. Design methods for novel flow fields can be generally classified into three categories: geometry optimization, built-in baffle optimization and bionic optimization.

7.2.2.2.1 Geometry optimization

The geometry of the flow channel has a great influence on its water-air transport capacity, and the improvement of the geometry including the length, width, and height of the channel, especially the selection of the channel-rib width ratio has been widely investigated [389,390]. Yoon et al. [391] concluded from single-cell experiments that smaller rib widths contribute to the mass transfer and can improve the performance of the PEMFC. Yang et al. [392] concluded from two-dimensional simulations that the optimum channel-rib width ratio for 2.8:0.5 and 4.2:0.3 corresponded to the best performance in forward and reverse alignment, respectively. Varghese et al. [393] found that the best performance was achieved with a rib width ratio of about 1:1 when there was no assembly pressure; this value became 0.25:1 in the presence of an assembly pressure. In the different studies, the used research methods and operating conditions varied, which led to inconsistencies in the resulting optimum rib-width ratios. It is necessary to consider the effects of gas, water, heat, electricity, and force on the performance of the PEMFC when selecting the optimum channel-rib width ratio. Kerkoub et al. [394] designed three types of flow fields, including serpentine, interdigitated and parallel, with six channels to rib width ratios defined as η (channel width/rib width) have been analyzed (see Fig. 25). They found that at high operating voltages, the geometric design and channel-to-rib width ratio have minimal impact on cell performance. However, at low operating voltages, they have a significant effect. Additionally, improving cell performance can be achieved by decreasing the channel width and increasing the rib width.

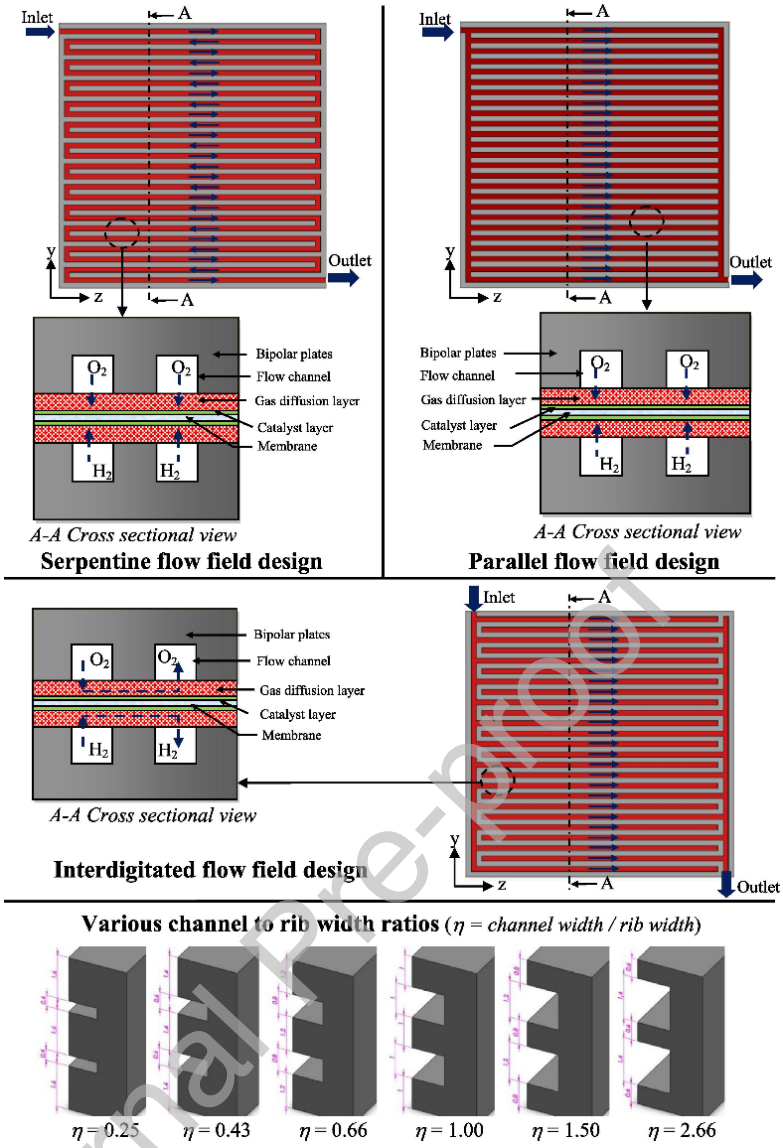

Fig. 25. Schematic of PEM fuel cell with various flow field designs and channel to rib width ratios. Reprinted from Ref. [394] with permission of Elsevier.

The study of cross-sectional shape is an important part of flow field structure design, which can significantly affect the reactant distribution and liquid water transport [395,396].Ahmed et al. [397] used numerical simulation studies to analyze the effect of different runner cross-sectional shapes on the performance of PEMFC in the region of high current density, and the results showed that rectangular runner cross-section had the best performance, while trapezoidal runner cross-section was favorable for

convective mass transfer. Zhu et al. [398] found that the inverted trapezoidal runner had the largest liquid water saturation coverage, while the rectangular runner with an aspect ratio of 0.1 had the smallest liquid water saturation coverage. Based on this, Mohammedi et al. [399] selected a total of 30 cross-sectional shapes and it was shown that trapezoidal and semi-elliptical base shapes of the runner cross-section have greater power density than rectangular while inverted trapezoidal and inverted semi-elliptical have poorer performance. It can be concluded that along the vertical direction of the runner, the PEMFC performance is better when the edge length of the cross-section near the GDL side is less than the length of the cross-section on the principle GDL side. That is because the reactive gas in this cross-section enters the GDL by forced flow and reaches the reactive sites on the CL quickly to accelerate the electrochemical reaction and improve the cell performance [400].

Moreover, there have been studies on structural optimization in the horizontal and vertical directions for the flow field [401]. Fig. 26 shows some of these designs. Horizontal structural optimization focuses on wave structures [402] and throat structures [403], in which periodic perturbations are generated by continuously changing the cross-section of the flow channel, thereby increasing the oxygen concentration gradient. In addition, the increase in localized flow velocity accelerates the discharge of liquid water. Vertical structural designs include conical structures [404], stepped structures [405], and wave structures [406]. Such structures can significantly improve the vertical transport of oxygen and accelerate electrochemical reactions.

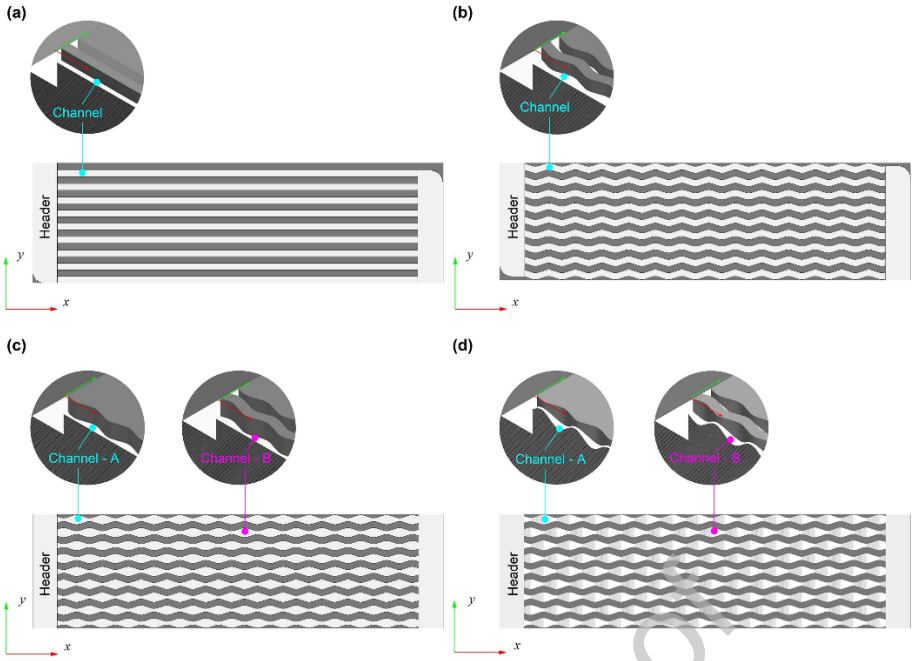

Fig. 26. Schematic of the four flow channel designs: (a) straight; (b) wavy; (c) 2D-Nozzle; (d) 3D-Nozzle. Reprinted from Ref. [401] with permission of Elsevier.

7.2.2.2.2 Built-in baffle optimization

Adding baffles in the flow channel can change the gas flow direction and velocity to effectively enhance convective mass transfer, force the reactive gas to distribute rapidly and uniformly on the catalyst surface, and accelerate the electrochemical reaction. The shape, arrangement, size, and structural parameters of the baffle have a great influence on the performance of PEMFC. Researchers have also conducted a lot of studies on this. In terms of baffle shape, Ghanbarian et al. [407] analytically investigated the effect of square, semicircular and trapezoidal baffles on a conventional DC channel using 3D numerical simulation (see Fig. 27). In their analysis, the baffles increased the oxygen concentration in the CL and effectively mitigated the concentration loss in the high current density region due to the synergistic effect induced by diffusion and advection mechanisms. Among them, the

trapezoidal baffle has the most significant optimization effect. Whereas, Ebrahimzadeh et al. [408] combined numerical simulations and experimental methods and found that triangular baffles provided the maximum performance enhancement in a double serpentine flow field. The mechanism by which the shape of the baffle affects the performance of the PEMFC is similar to the shape of the cross-section, that is, by accelerating the transport process of the reaction gas to the CL.

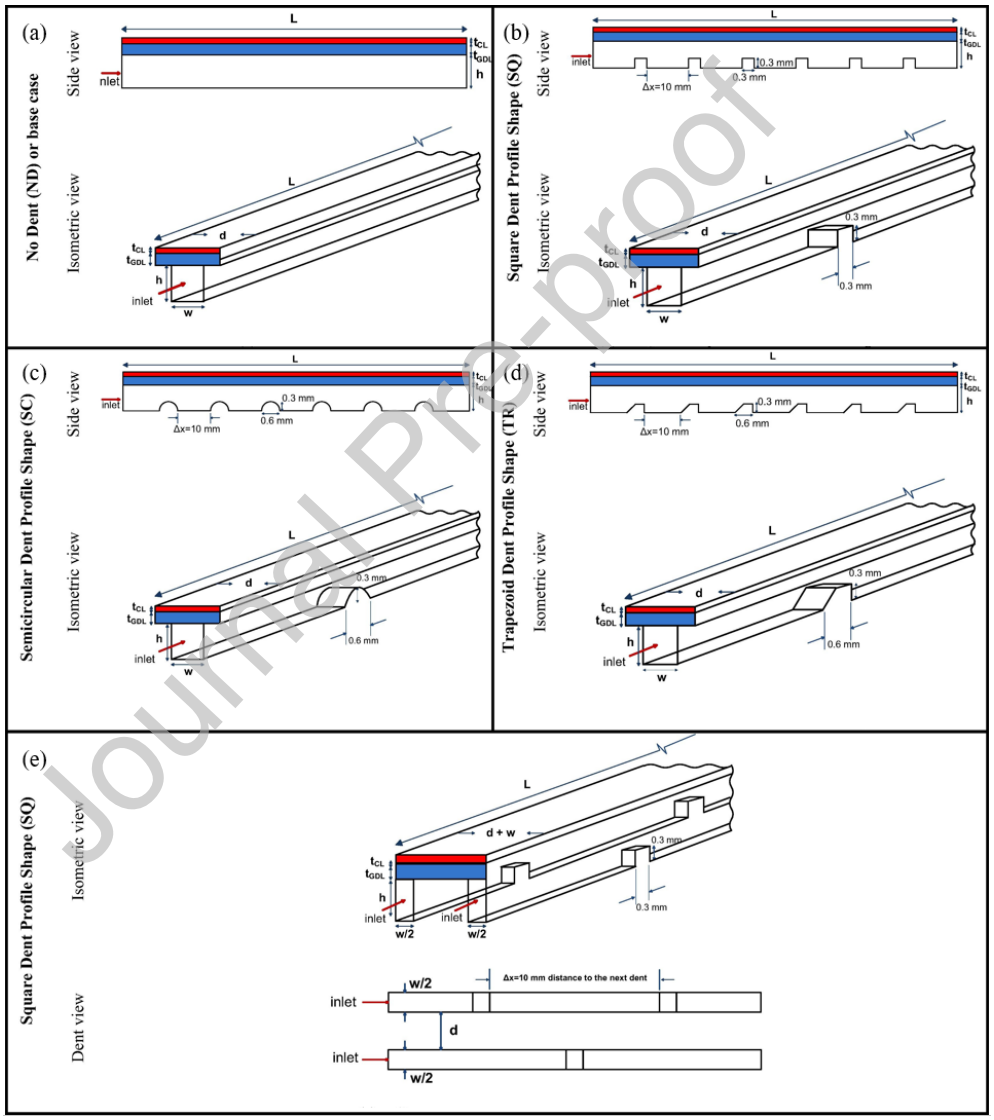

Fig. 27. Schematic of the geometries for the: (a) base case; (b) square dent; (c) semicircular dent; (d) trapezoid dent; (e) square dents with zigzag arrangement. Six

dents were embedded in all the dented cases along the channel. Reprinted from Ref. [407] with permission of Elsevier.

The arrangement of baffles has an impact on the synergistic effect of mass transfer. Staggered baffles allow for the enhancement of convective mass transfer by exploiting the pressure drop between neighboring flow paths, which also results in more liquid water being retained in the flow paths, contributing to an increase in the membrane water content, thereby enhancing the proton conductivity [409]. Heidary et al. [410] discovered through numerical simulations that a staggered baffle arrangement in a parallel flow field resulted in a 7% increase in the maximum performance as compared to a parallel arrangement, and a reduction in the pressure drop of 1.6 kPa. Wang et al. [411] conducted a comprehensive evaluation of baffles with different numbers, heights and arrangements and found that the non-uniformly arranged flow field resulted in a more uniform distribution of the PEMFC current density compared to the uniformly arranged one, and the stability of the output performance was improved.

Regarding the baffle structural parameters, Perng et al. [412] inserted baffles of different heights and spacings into conical flow channels with different taper ratios and gap ratios and performed a projected finite element analysis, concluding that high reactant velocities can effectively improve the concentration polarization and enhance the performance of the PEMFC at high current densities. Additionally, Chen et al. [413] found that increasing the return air length of the baffle can effectively reduce the pressure drop. Changing the size and structural parameters of the baffle can

improve the PEMFC performance with little increase in cost. Yin et al. [414] analyzed the trapezoidal baffle by three-dimensional numerical simulation and concluded that the mass transfer capacity as well as the performance of the PEMFC is optimal when both the forward and backward inclination angles of the trapezoidal baffle are 45°. The enhancement of the PEMFC performance by the structural parameters barely affects the cost, which is the main advantage of this optimization method over other optimization methods [413]. However, there is a limitation that the variation of structural parameters may have less impact on the overall PEMFC performance.

7.2.2.2.3 Bio-inspired optimization

PEMFC flow fields have the function of distributing reaction gases, exhaust gases and liquid water. Biomimetic structures with similar functions are also found in nature. Several academics have developed bionic structured flow fields to optimize PEMFC mass transfer and water-gas management capabilities. The main bionic flow fields include leaf-shaped, lung-shaped and tree-shaped flow fields.

Leaf-shaped flow fields were first proposed by Kloess et al. [415]. Using computational fluid dynamics (CFD) simulations and experimental methods, they observed that the pressure loss in a leaf-shaped flow field was reduced by 59.8% and 47.4% compared to a serpentine and an interdigitated flow field, respectively, while the peak power density increased by 30%. Roshandel et al. [416] indicated that the uniformity of the reactant distribution was better in a leaf-shaped flow field. Liu et al. [417] concluded that a vertically-placed asymmetric leaf-shaped flow field results in better PEMFC performance compared to a symmetric leaf-shaped flow field. Ginkgo

biloba-shaped flow field [418] and leaf-shaped interdigitated flow field [419] (see Fig. 28) have also been reported, which have better performance in terms of velocity distribution, reactant distribution and water removal capability.

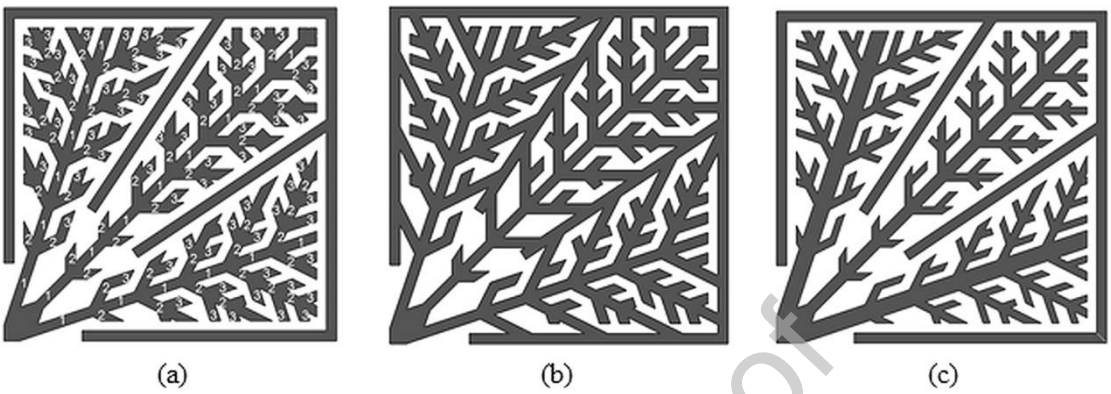

Fig. 28. Bio-inspired flow field designs with three generations of channels: (a) Interdigitated flow field design with constant channel width; (b) Non-interdigitated bio-inspired design with constant channel width; (c) Interdigitated design with varying channel width determined by Murray's law. Reprinted from Ref. [419] with permission of Elsevier.

Besides the leaf-shaped flow field, the lung-shaped flow field was also investigated by Kloess et al. [415]. The results showed that the uniformity of pressure drop and reactant distribution in the lung-shaped flow field was superior to that of the basic flow field. Kjelstrup et al. [420] found that the lung-shaped flow field was effective in mitigating the concentration polarization as well as improving the PEMFC performance by 10-20% while reducing the amounts of catalysts used. A numerical study by Asadzade et al. [421] obtained a more uniform velocity distribution. Cho et al. [422] presented a finite-element model of a PEMFC with fractal branching, lung-inspired flow field (Fig. 29). They found that when the effect of the number of

branching generations N = 6, a platinum utilization of approximately 36 kW g^{-1}_{Pt} is achieved, and the volumetric power density of fuel cell stacks can be increased by over 80%.

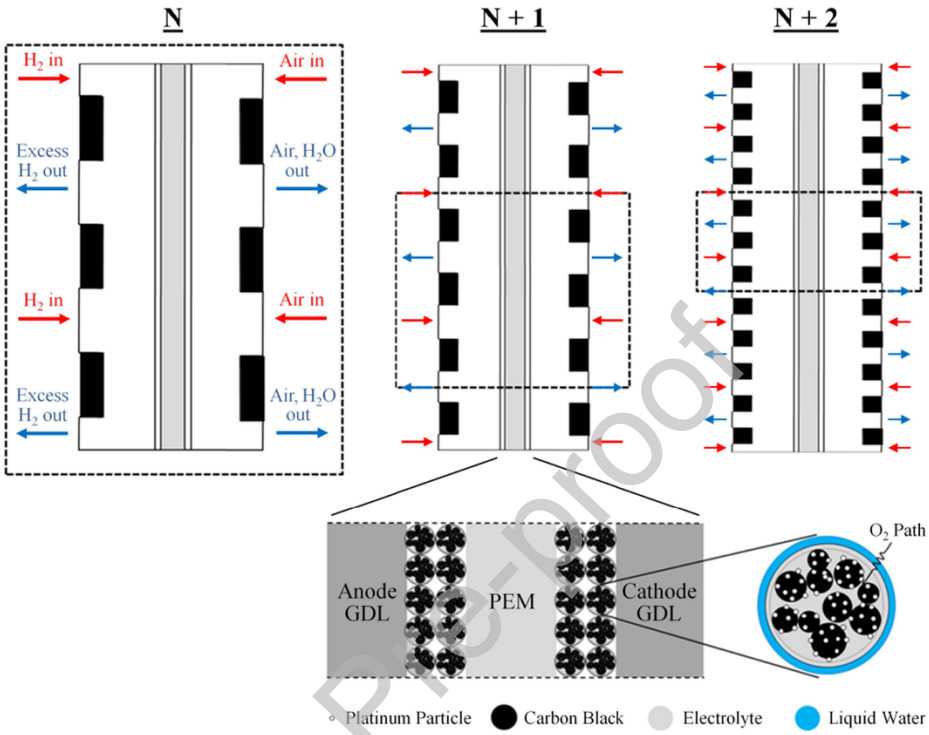

Fig. 29. Schematic of the modeling domain of the lung-inspired flow-field based PEMFC at various generations. Reprinted from Ref. [422] with permission of Elsevier.

The tree structure consists of a trunk and branches, which utilize the fractal principle to reduce the pressure loss in the flow field [423]. The bifurcation level of the branches is one of the main research topics in tree flow fields. Daniel et al. [424] discovered through CFD simulations that an increase in the level of bifurcation leads to better PEMFC performance. Damian et al. [425] found that an increase in the number of bifurcations improves the homogeneity of the reactant gas distribution as well as obtains a more homogeneous distribution of the current density, and that a

bifurcation configuration of 37° is more conducive to the liquid water emission. Sauermoser et al. [426] experimentally investigated the effect of width scaling factor on the performance of PEMFC and showed that the PEMFC has the maximum peak power when the width scaling factor of the inlet and outlet are 0.917 and 0.925, respectively. Meanwhile, the increase of width proportionality factor can effectively reduce the pressure drop, decrease the pump power, and increase the net power of PEMFC.

In addition, new bionic flow fields such as honeycomb-shaped flow field [427], fishbone-shaped flow field [428], and lotus-shaped flow field [429] are included in the future study of PEMFC flow fields. While different bionic flow fields have their own advantages, the complicated processing technology and high fabrication cost have become the main factors restricting their development. However, with the continuous progress of processing technology and breakthroughs in the field of materials, it is believed that bionic flow fields will become one of the choices for high-performance flow fields in the near future.

7.2.3 Flow uniformity

The uniformity of flow inside the PEMFC is crucial for its durability and performance. Flow uniformity can be categorized into two levels [430]: the first level pertains to the uniformity of flow within a single cell, while the second level pertains to the uniformity of flow between different single cells in the stack. Section 7.2.2 provides an overview of the basic flow field and the optimized designs proposed by researchers in recent years. One of the main goals of these designs is to improve the uniformity of

flow within the cells. Thus, this section will present the second level of uniformity, i.e. cell-to-cell flow.

7.2.3.1 Issues of non-uniformity flow

To achieve higher power output, automotive PEMFCs require a large number of individual cells connected in series. Ideally, the stack power should be equal to the sum of the output power of the individual cells. The durability of the stack depends on the weakest cell in the stack or its structure [430]. However, in reality, the durability of the entire stack does not reach the ideal state described above. Achieving an absolutely uniform flow distribution between individual cells is difficult due to factors such as friction losses in the stack [431]. The non-uniformity of the flow distribution is one of the most significant obstacles to the ideal state [432]. Uneven flow distribution results in uneven electrochemical reactions, which can cause problems or even failures in the thermal or water management inside the stack [433]. Excessive water can cause flooding, hindering mass transfer and reducing cell output [111]. Excessive dryness or hot spots from high temperatures can accelerate the degradation of cell components [216]. Uneven temperature distribution can also generate thermal stresses, negatively affecting the durability of the seals of the stack [434].

7.2.3.2 Manifolds for flow distributions

The manifold of a PEMFC stack is responsible for distributing the flow into each individual cell and collecting the unreacted gas, transporting it to the outlet of the stack [435]. Manifolds can generally be divided into bifurcation and consecutive types [436]. Liu et al. [437] proposed a flow distributor with cascaded runner bifurcation to

enhance the flow uniformity inside the stack. According to their argument, the bifurcated distributor should prioritize the ratio of flow channels diameters between neighboring levels and the ratio of channel lengths between bifurcated levels to minimize any significant gap between the two sub-flows after the bifurcation. However, it is important to note that this type of distributor requires precise manufacturing and may not be suitable for all inlet flow conditions. In automotive applications, high power stacks may experience an increase in bifurcations as the number and complexity of flow channels rise. This can cause a rapid increase in pressure drop, which negatively impacts the stack's stable operation over time [430]. To address this issue, many scholars selected a consecutive type manifold with simple structure and low pressure drop. Nevertheless, if there is a difference in the flow resistance of each parallel path, the distribution of reactants may become inhomogeneous [438]. The parallel paths can be divided into four categories: dividing, combining, U-type, and Z-type.

Selecting appropriate combinations among the stack's structure and dimensions is a significant challenge in the stack design. Various flow characteristics may also result from multiple operating environments [439]. To achieve uniform flow across the stack, it is necessary to design optimal flow field and manifold distribution based on numerical and empirical findings. Additionally, because of the small size (typically on the millimeter scale) of the flow path and the complexity of the stack structure, accurate visualization and measurement of the flow inside the PEMFC stack is

challenging [440]. As a result, researchers commonly use theoretical model to calculate and optimize flow uniformity.

7.2.3.3 Introduction to manifold flow theory development

The assessment and prediction of flow effects in PEMFC stacks require more generalized theories due to the variety of flow conditions, feature sizes and manifold structures. Bernoulli's theorem is widely used in pipeline design and flow studies. Early research on flow distribution in PEMFCs focused on this theorem or its variants [441,442]. Based on the linear relationship between pressure drop and flow rate, the flow field can be analogized to an electric circuit using Kirchoff's law to calculate current at the junction [443]. However, in practice, fluids differ significantly from electric currents. One key difference is that fluids exhibit inertia, resulting high flow rates, sub-flows formed at pipe bifurcations in a manifold flowing may not flow at the same rates. Studies have shown that branched streams have high pressures, indicating that ignoring inertial effects in circuit analogies can lead to significant errors in the analysis of high-velocity flows or flows with high Reynolds numbers [436]. Some models disregard inertial effects, limiting their ability to describe flows with high Reynolds numbers [382,441]. Additionally, friction effects are also present in the flow, and models that neglect them can only be applied to short manifolds [444,445].

Acrivos et al. [446] considered inertia, proposing a model that became the basis for studying manifold flow [447]. Recently, models have begun to include the effects of electrochemical reactions and liquid water on flow resistance [448]. Wang has conducted theoretical research on manifold flow and achieved promising results. He

combined the effects of friction and momentum to create a unified theoretical framework; the generalized governing equations were used for flow distribution in manifold systems [436,449]. The theory is comprehensive, establishing a direct quantitative relationship among flow distribution, flow conditions, and structure. It has been successfully applied to the design of PEMFC stack manifolds. Methods proposed by other researchers are derived from Bernoulli's equation or overall energy balance. Midoux et al. [450,451] analyzed various models of manifold flow distribution and performed comprehensive analyses of friction coefficients, momentum coefficients, and channel flow resistance coefficients, which partially verified Wang's generalized governing equations. Pan et al. [452] proposed a novel criterion for the flow uniformity of the stack by considering two dimensionless configuration parameters that reflect the flow distribution. They established a quantitative relationship between the coefficient of variation and these configuration parameters. The proposed criterion was also verified by simulation results.

7.2.3.4 Flow uniformity optimization

As the commercialization process of PEMFC gradually develops, the demand for its durability increases. Scholars have recognized the significance of uniform flow in the stacks and have conducted relevant research on the optimization measures.

Experimental methods for large PEMFC power stacks can be complex and expensive. Therefore, many researchers use simulation method to study and optimize flow distribution. Chen et al. [453] simulated a two-dimensional stacking model by CFD method. They found that both large channel resistance and wide manifold benefited

the flow uniformity. However, for the practical application of PEMFC, a large pressure drop is unfavorable. Therefore, they advocated to increase the manifold width only. Huang et al. [431] combined a CFD model with an empirical model to establish a model that considers the airflow distribution inside the manifold and verified it through experiments. The results indicate that the mass distribution and pressure drop of the U-type stack are better than those of the Z-type configuration. Furthermore, the non-uniformity of flow increases proportionally with the current density. In their following study [454], it was also found that the fluid distribution in the manifold is strongly affected by the inlet geometry. By optimizing the intermediate zone, inlet tube diameter, and diffuser length, the vortex size can be adjusted to promote a uniform flow distribution in PEMFC stacks. Su et al. [440] investigated the impact of vortices in the feed header on flow distribution. They found that the distribution uniformity decreases significantly with the generation of vortices. The flow characteristics, including the number, location, and intensity of vortices, are highly correlated with the size and shape of the feed header. Lu et al. [455] proposed a distribution zone with a partially dotted matrix for optimization. Placing the matrix close to the air inlet effectively improves flow uniformity. The size of the matrix should be appropriately designed to balance the accuracy and the manufacturing cost. Pan et al. [456] emphasized the importance of proper generation and distribution of transverse flow in achieving flow uniformity. They optimally designed the distribution zone by combining central horizontal meshes and transverse vertical meshes based on

the mechanism of transverse flow control; and the porosities of these two types of mesh are quantified for optimal flow distribution.

Although commercial CFD software makes it easy to obtain information from the model, it is inconvenient for preliminary design and structural optimization of large-scale fuel cell stacks due to its time-consuming and expensive nature. Therefore, several researchers have used analytical models for design and optimization studies of flows in large-scale stacks. For example, Qin et al. [457] modelled a PEMFC stack using a flow network method. This allowed them to determine the pressure and mass distributions of the reactant gas and coolant by combining the cross-flow effect and the minor losses in the flow process. The design of cathode flow channels and cooling channels for the stack was also optimized. Huang et al. [448] developed an analytical model by considering multiple factors, such as local pressure losses, pressure recovery phenomenon, electrochemical reactions, and the presence of liquid water in a single cell. To improve flow distribution in both U-shape and Z-shape PEMFC stacks, it is recommended to increase flow resistance in the unit cell and decrease flow resistance in the manifold. To optimize the flow resistance arrangement in U- and Z-shaped stacks, a differentiated assembly strategy can be employed, which is capable of achieving a more uniform flow distribution in the manifold.

7.3 Stack assembly

Since a single PEMFC cannot provide enough power and voltage for automotive applications, multiple single PEMFCs are connected in series and assembled as a PEMFC stack. Large stacks can have hundreds of components, including end plates,

collectors, clamping bolts or straps, a variety of sensors, and components in a single cell. While the design of a single PEMFC is relatively simple, the design process of a large power stack may have many problems that can never be encountered by a single PEMFC, such as thermal stress/strain, system vibration, seal leakage, structural failure, etc [428]. In automotive operating conditions, large power reactors also face complex operating conditions as described above, and it is challenging to achieve long-life operation and improve the durability of power reactors, which still requires a large number of technical issues to be solved in terms of structural design and analysis.

7.3.1 Endplates and clamping methods

Hundreds of components in a large PEMFC stack are compressed together by two end plates, applying a huge clamping force by tightening bolts. Another clamping method is the steel belt clamping technique. The end plates are the most important components supporting the stack as they are usually fixed in the position where the stack is to be used. End plates should have the following properties: sufficient mechanical strength and stiffness to withstand tightening pressures, stack gravity, vibration and shock, and other loads to which they may be subjected; high modulus of elasticity and high yield stress limits to ensure that the stack can be restored to its initial state when external forces are removed; the smallest possible mass/volume to increase the stack's power density; high bending stiffness to achieve uniform contact pressure inside the stack; and good corrosion resistance, ease of fabrication, low cost, etc.

7.3.1.1 Materials of endplates

One of the most widely used metal alloys for end plates is aluminum alloy because of its low mass density, as well as good strength and stiffness, stainless steel is also an option due to its good mechanical properties and corrosion resistance. It has been suggested that if the application scenario of the power stack requires the end plates to be as lightweight as possible, then aluminum alloys will have a higher priority, and if a small size of the stack needs to be achieved, then stainless steel will be a better choice due to its better overall mechanical properties [388]. In addition, to improve the insulation and corrosion resistance of metal endplates, a common approach is to use for instance aluminum oxide films or epoxy surface coatings [458].

In addition to metals, polymeric materials such as phenolic plastics, polyethylene, and phenolic resins are considered as a promising endplate material because of their light weight, low cost, good corrosion resistance, and low thermal conductivity. However, in practice, the mechanical strength of polymers is not sufficient and their nonlinear stress-strain relationship at high stresses and certain viscoelasticity at high temperatures make them more susceptible to performance degradation [459]. The use of composites and optimized structures are viable means of improving the mechanical properties of endplates [460,461].

7.3.1.2 Geometry and clamping methods optimization

7.3.1.2.1 Clamped with tightening bolts

Besides the choice of material, the geometry, dimensions and clamping methods of the end plates need to be carefully considered. Rectangular endplates are the most common shape for large PEMFC stack designs, and tightening bolts is one of the most

traditional and simple methods of clamping. For ideally rigid materials, the compression of the end plates caused by tightening the bolts can be used to achieve a uniform distribution of pressure within the stack. However, the absence of rigid materials means that applying a tightening torque to the bolts can cause the end plates to deform in both bending and compression, thus creating uneven pressure within the stack (see Fig. 30). A simple way to increase the stiffness of the endplate is to increase the thickness of the plate, however, the weight and volume of the stack will increase accordingly, resulting in a decrease in power density. Therefore, the optimal thickness of the endplate should consider the pressure distribution inside the stack and the weight/volume of the stack.

In order to reconcile the contradiction between the weight and stiffness design of the endplate, there are some researches around this. Evertz et al. [462] proposed the concept of endplate shape design, namely ribbed structure, D-shaped bow structure, square and bomb shape, etc. It is concluded that solid endplates have the worst performance, while endplates with D-bow structure have the best performance. They also envisaged the possibility of pre-curved endplate surfaces or thin layers with curved thicknesses in order to make the pressure inside the stack more uniform. Later, other scholars worked on specific designs based on this idea. Yu et al. [460] used composite sandwich endplates, where the uniformity of the internal pressure was ensured by using pre-generated curvature of the endplates of the stack, and a pressure distributor was used to enhance insulation and uniformity of the pressure distribution. Others have focused on the multi-objective optimization of endplates, namely

topology optimization, weight reduction optimization and bolt arrangement optimization.

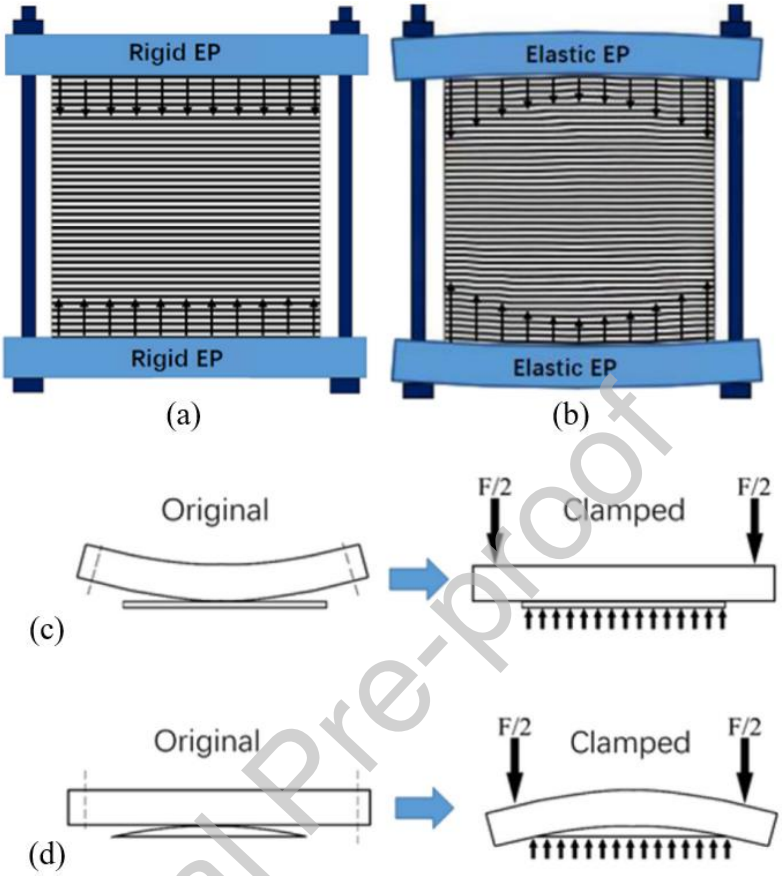

Fig. 30. Schematic to improve the pressure distribution inside PEMFC stack: (a) ideal rigid end plate (EP)s; (b) real elastic EPs; (c) pre-curved surface of EP; (d) a thin layer with curved thickness. Reprinted from Ref. [388] with permission of Elsevier.

7.3.1.2.2 Clamped with steel belts

As mentioned above, PEMFC stacks can be clamped together using bolt clamping methods. However, a strong uneven distribution of pressure can occur if the width of the end plates is significantly larger than the stack. In addition, the bolt-clamping method usually occupies a larger space because the dimensions of the endplates must be larger than the dimensions of the bipolar plates in terms of length and width.

Researchers have proposed a more compact method, namely, the steel belt clamping method.

Liu et al. [463] performed a cross-section optimization design of steel belt clamped end plates to obtain a uniform pressure distribution in the stack. They found that the optimal shape of the solid aluminum end plate was similar to a semicircle, and in further optimization, a 39.5% reduction in the weight of the end plate and a 41% reduction in the standard deviation of the normal deformation displacement within the stack were achieved. This is, of course, based on the results of 2D design theory. For practical applications, the 3D design theory has higher accuracy. In the 3D design, the standard deviations of normal displacement and normal pressure of MEA were reduced by 9.16% and 11.5%, respectively. Wu et al. [464] showed that an equidistant arrangement of clamping bands would make the internal contact pressure distribution usually more inhomogeneous than an unequal arrangement (see Fig. 31). The use of an unequal clamp load arrangement combined with an equidistant arrangement of clamping belts results in a more uniform contact pressure.

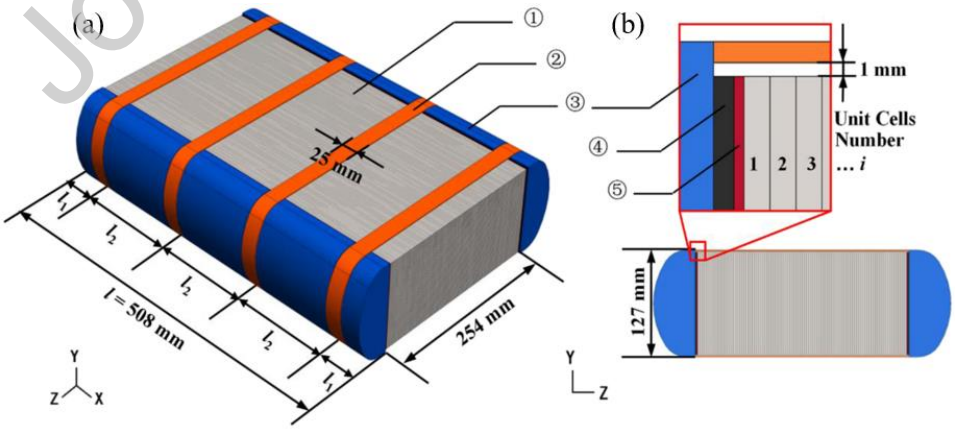

Fig. 31. The stack size and belt arrangement: (a) 3D view and (b) side view.

① 100 cells; ② clamping belt; ③ EP; ④ insulating layer; ⑤ current collector. Reprinted from Ref. [464] with permission of John Wiley and Sons.

7.3.2 Sealing methods

As an automotive power source, sealing failure between individual cells in a PEMFC stack is also one of the main problems affecting the durability of the stack. A well-designed seal can effectively isolate the reaction gas, coolant, and external environment from each other to ensure the safe and stable operation of the system; in contrast, the sealing failure may lead to the leakage of hydrogen, or even the mixing of hydrogen with air at the cathode, which not only has a serious negative impact on the lifetime of the PEMFC reactor, but also jeopardizes the safety of the PEMFC system [465]. Hence, it is necessary to design and manufacture high-performance, durable sealing materials, optimize the sealing structure, and improve the mechanical strength to improve the sealing durability of PEMFC reactors. Seal materials with good durability have the following characteristics: all elastomeric sealing materials should be able to resist hydrogen, oxygen, water, and heat well, and have sufficient chemical resistance and resistance to mechanical stresses in PEMFC power stacks.

7.3.2.1 Classification of sealing methods

Sealing materials can generally be divided into two categories: solid-state gaskets and liquid sealants. Solid-state gaskets are the traditional type of sealing and can be obtained by cutting, stamping, and molding silicone and fluor elastomers [465]. Solid gaskets are easy to assemble and remove, but the major disadvantage is that the gasket and the bonding surface do not easily close tightly, resulting in interfacial leakage.

Liquid sealants can flow into complex surface structures and have excellent sealing performance, which can effectively prevent cell interface leakage [466]. Liquid sealants can be mainly classified into in-situ molded gaskets and in-situ cured gaskets [467]. The former is a liquid sealant applied to the sealing surface before cell assembly, and when the cell is assembled, the sealant is cured to achieve the sealing effect. This sealant can be crosslinked at room temperature and does not require a high precision sealing surface due to the free flow of fluid [467]. The latter needs to be cured in some way after application to the sealing surface, such as by heat or UV radiation, and then assembled to provide a sealing effect. Cured-in-place gaskets allow for complex sealing geometries and usually do not require a mold, but rather a membrane gasket [467].

7.3.2.2 Sealing material degradation

7.3.2.2.1 Chemical degradation

The durability and stability of sealing materials are of great significance to the long-life operation of PEMFC stacks, and here it is necessary to briefly explain the forms of sealing material degradation.

Sealing materials will undergo chemical degradation over time due to exposure to acidic and humid environments [468]. To date, several scholars have reported studies on the chemical degradation of sealing materials under different operating conditions. As an example, Lin et al. [469] used copolymer resins, liquid silicone rubber, fluor-silicone rubber, EPDM rubber, and fluor elastomer copolymers as gasket materials under simulated and accelerated conditions at 80 °C for testing, and found

that chemical degradation of these seals could be up to 63 weeks. Li et al. [470] discovered that the chemical degradation of silicone rubber was largely affected by the concentration of the exposure medium. The degradation begins with an increase in surface roughness until the exposed portion ruptures. This is due to the change in chemical properties of the silicone rubber surface in the test environment. Wu et al. [471] investigated silicone rubber gaskets by subjecting them to a weak acidic solution with temperatures ranging from 20 °C to 90 °C cycling through air. The results showed that the loss of weight and the hardness of the silicone rubber increased with the number of temperature-cycling cycles and the concentration of the acid solution, which was caused by the loss of the fillers in the silicone rubber. Feng et al. [472] investigated degradation of silicone rubbers with different hardness in various aqueous solutions (see Fig. 32). It was discovered that silicone rubbers degrade significantly in strong acid solutions due to the catalytic effect of protons on the decomposition of Si-C and Si-O-Si bonds. This degradation can even result in the formation of large cracks and voids on the surface.

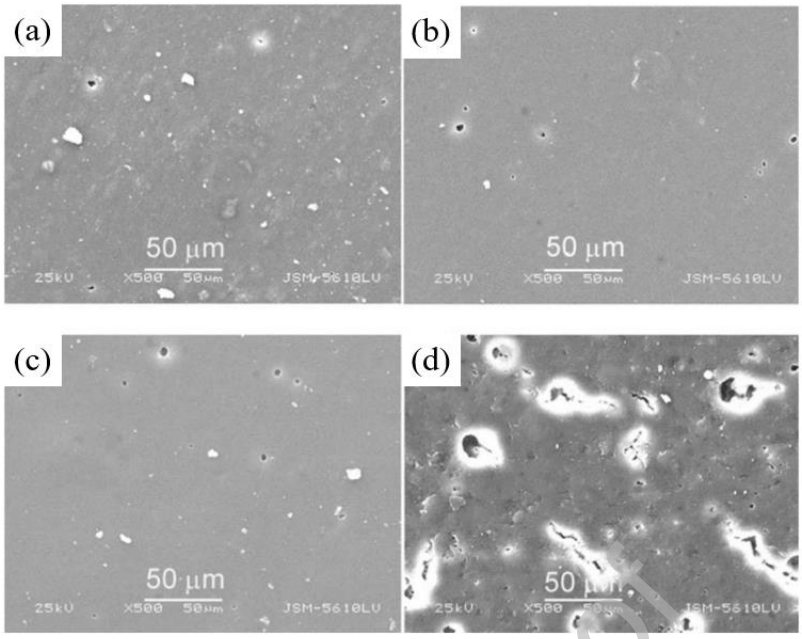

Fig. 32. SEM images of silicone rubber surface after exposure to different solutions: (a) in de-ionized water; (b) in acetic acid; (c) in simulated solution; (d) in strong acid aqueous solution. Reprinted from Ref. [472] with permission of Elsevier.

7.3.2.2.2 Mechanical degradation

The mechanical properties of sealing materials play an important role in sealing stability, and their mechanical properties after prolonged use have not been fully investigated [465]. Currently, rubber is widely used due to its good heat resistance and chemical stability. Meanwhile, its sealing ability is mainly determined by its mechanical properties [473]. It is necessary to study the mechanical properties of sealing materials. Currently, studies on the degradation of mechanical properties of rubber seals for PEMFC power stacks have been reported. Qiu et al. [473] investigated the effects of temperature and compression ratio on the mechanical properties of four rubber gaskets. The results showed that the compression ratio has a significant effect on the mechanical properties of the sealant, while the increase in

temperature decreases the modulus of the sealing gasket. Zhang et al. [474] discovered that the deformation of the rubber seals intensifies with the increase in compression ratio and sealing ring dimensions, and the von Mises stress increases for better sealing performance; the high stress region of the rubber seals concentrates in the inner part of the cross-section, which makes them susceptible to material relaxation.

7.3.2.3 Sealing structure design

It is also necessary to study the sealing structure of PEMFC stacks. It has been analyzed that the sealing structures of PEMFC stacks can be classified into four categories [475], as shown in Fig. 33: the direct sealing structure is simple and can be easily reassembled and removed, but when the sealing gaskets are clamped on the PEM, the PEM may be damaged or broken due to the shear and tearing forces at the edge of the gaskets. The frame sealing structure wrapped around the PEM is an integrated structure, which is helpful for assembly and mass production; however, there are problems in the connection between the sealing structure and the GDL are problematic in terms of connection, as well as some adhesive materials may stick the bipolar plates together while wrapping the PEM, making disassembly difficult. The MEA-wrapped frame sealing structure has more advantages than the two sealing structures mentioned above because it is easy to assemble and has a low cost. The rigid protection structure is also an ideal sealing structure. Its main feature is that one or more rigid layers are arranged in the inactive region at the edge of the membrane to withstand the compression force generated by the bipolar plates during the assembly

process, with the aim of preventing damage to the reaction region of the MEA.

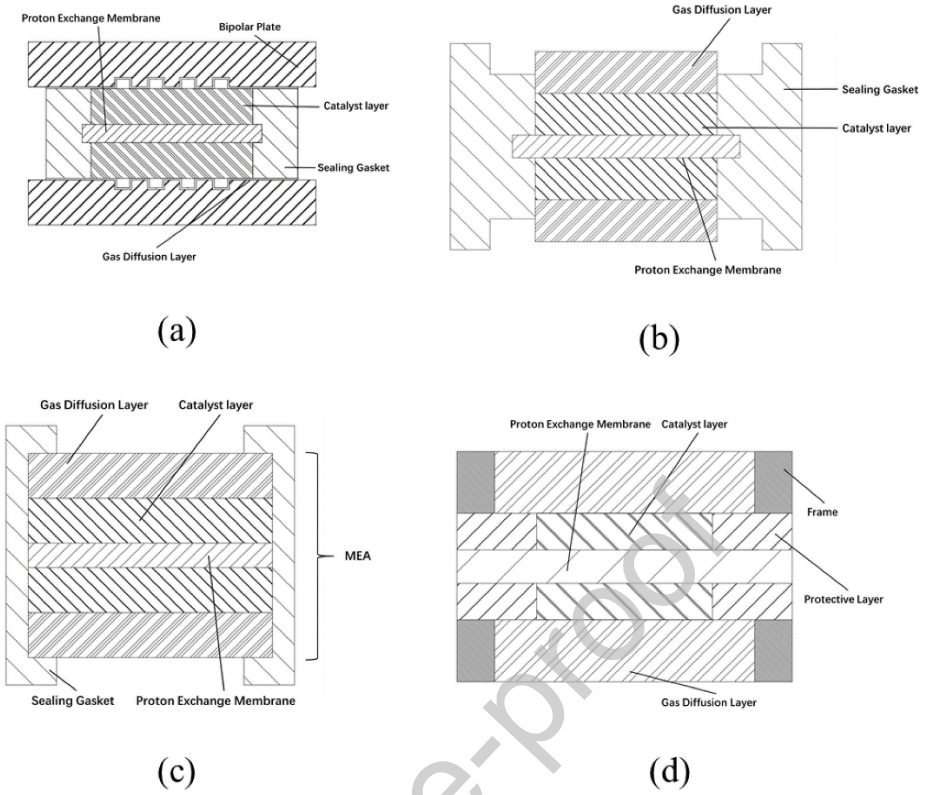

Fig. 33. The MEA structures: (a) PEM direct sealing structure; (b) PEM-wrapped frame sealing structure; (c) MEA-wrapped frame sealing structure; (d) Rigid protective frame sealing structure. Reprinted from Ref. [475] with permission of Elsevier.

The frame sealing structure built to enclose the MEA in the non-reactive region of the MEA is usually formed by injection molding, which has been designed and studied in detail by many scholars. For example, James et al. [476] used an adhesive to bond the edges of the MEA and the sealing region of the flow field plate to form the first part of the seal; the second part of the seal was formed by placing a manifold sealing material around the MEA. For the frame seal structure wrapped around the MEA, the more common process is to position the non-reactive region of the membrane

electrode in a membrane fixture and inject the sealing material into the fixture via injection molding to form the sealing portion. Barton et al. [477] fabricated a sealing frame around the MEA, which was injection molded to form an integrated MEA structure. The cross section of the sealing frame was designed in various configurations to improve the sealing performance of the structure.

7.4 Control strategies

Automotive PEMFC systems are characterized by uncertainty, great hysteresis, strong coupling, time-varying behavior as well as nonlinearity, and there are problems such as modelling difficulty and large computational effort. Scholars have studied the control strategy of the automotive PEMFC system based on the trade-off between the error and the computational quantity in order to improve the PEMFC durability.

7.4.1 Hydrogen supply system

7.4.1.1 Structure and considerations of hydrogen supply system

For PEMFC, there are three main operating modes for the hydrogen supply system: hydrogen direct discharge mode, dead-end mode and recirculation mode. Since the direct discharge mode and the dead-end mode have the problems of poor hydrogen utilization, safety hazards and water accumulation prone to performance degradation and CL carbon corrosion, respectively, the most widely used mode in PEMFC vehicles is the hydrogen recirculation mode [478]. This method uses a recirculation device to transfer the unreacted hydrogen from the anode outlet to the anode inlet again, and simultaneously completes the humidification of hydrogen, which not only improves the utilization rate of hydrogen and thus the fuel economy, but also helps to

improve the uniformity of the distribution of hydrogen and water inside the PEMFC stack, so as to enhance the durability of the PEMFC stack [479].

The hydrogen supply system should be able to provide fuel gas at appropriate pressure and flow rate for the normal operation of the PEMFC stack. It has been shown that a better balance between efficiency and durability of PEMFC can be achieved when the stoichiometric ratio is 1.1-1.5 [480]. When the stoichiometric ratio is low, insufficient gas supply will cause fuel starvation, while too high a stoichiometric ratio will increase the gas flow rate, and the discharged gas will carry a considerable portion of the moisture inside the stack, which is prone to membrane drying. Meanwhile, the stoichiometric ratio needs to maintain a certain degree of stability, otherwise the voltage and humidity of the PEMFC are susceptible to more drastic time variations, which is not conducive to the long-life operation of the PEMFC. In addition, the pressure difference between the cathode and anode is also a factor to be considered; high-pressure pulses and fluctuations can damage the MEA if the pressure difference is unstable [481].

7.4.1.2 Optimization of control strategies for hydrogen supply system

For the purpose of achieving better performance and longer lifetime operation of the PEMFC, many researchers have proposed and optimized the control strategy of the hydrogen system. Lee et al. [482] installed dual valves on the recirculation loop to enable the anode to operate in four modes (Fig. 34), namely dead-end, recirculation, compression, and purge, with switching of the operating modes according to the current density, and the results showed that the loop structure and this control strategy

can effectively prolong the PEMFC operating time. Liu et al. [483] proposed an anode purging solution based on the observation of nitrogen impurities in the system, which determines the purging interval and duration according to the nitrogen concentration of the anode. This solution can increase the hydrogen utilization to 99% and enhance the durability of the PEMFC. Yuan et al. [484] presented a fuzzy logic proportional-integral (PI) controller with feed-forward to control the hydrogen pressure. Such controller significantly improves the dynamic performance of hydrogen pressure and further reduces the overshoot caused by perturbations compared to the conventional PI controller.

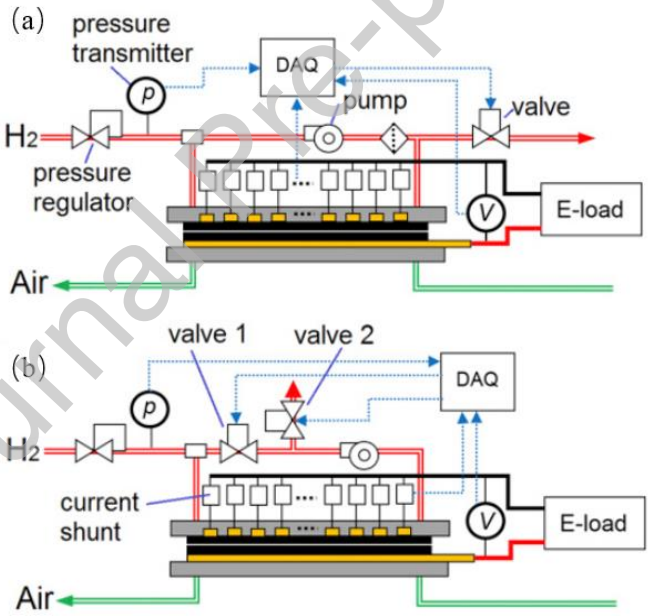

Fig. 34. (a) Traditional configuration for anode recirculation; (b) Novel configuration of the anode employing two valves. Reprinted from Ref. [482] with permission of Elsevier.

He et al. [485] suggested a switching model predictive control (MPC) strategy based

on the hydrogen recirculation pump model to regulate the hydrogen cycle of the PEMFC stack. It predicts the return manifold pressure and the angular velocity of the pump, which provides fast response speed and tracking accuracy despite load variations, mitigates the degradation of the anode components, and achieves efficient and stable operation of the PEMFC. Quan et al. [486] introduced an enhanced MPC based on perturbation prediction. They predicted the speed of the vehicle in real time by an exponential smoothing-based Markov model, and then obtained the speed of the vehicle through the vehicle dynamics and PEMFC models to obtain a current prediction sequence with stochasticity as a perturbation of the hydrogen control system, which is input into the prediction model. This enhanced MPC effectively reduces the effect of step-change current and improves hydrogen utilization to avoid fuel starvation.

7.4.2 Air supply system

7.4.2.1 Structure and considerations for air supply system

The air supply system plays a key role in the overall PEMFC system. The major tasks include purifying, pressurizing as well as humidifying the air [487]. As mentioned above, airborne contaminants can cause damage to the catalysts and membranes within the PEMFC, reducing the performance and durability of the PEMFC. Therefore, the incoming air has to be cleaned in an air filter before entering the stack. The mass flow rate of the air supply directly affects the concentration of oxygen inside the reactor, which requires the air supply system to provide enough oxygen for the continued and stable operation of the PEMFC reactor and prevent oxygen

starvation. The performance of the PEMFC increases with the increase of the reactant pressure, with the optimal pressure being 150-250 kPa [488], and the membranes need to be kept in a fully hydrated state to obtain the best performance. Air filters, air compressors, and humidifiers are the components in a typical air supply system to meet the above objectives.

The control of an air supply system is similar to the control of a hydrogen supply system in that both require control of the pressure and stoichiometric ratio of the gas. However, while hydrogen is supplied through high-pressure hydrogen tanks with pressures and flow rates that can meet the PEMFC stack requirements [489], air relies on the air supply system to draw from the environment, which is difficult to control due to the slow mechanical correspondence [490]. Meanwhile, the air supply system is a typical high-degree nonlinear two-input-two-output coupled control system, where the two coupled control variables, that is, the mass flow rate and the pressure, are affected by both the air compressor speed and the backpressure valve opening, which means that a change in either of the mass flow rate and the pressure will disturb the other one, and the coordinated control of the actuators is difficult to implement [491]. Consequently, there is a great need to adopt suitable control strategies to achieve optimal coordinated control of the mass flow and pressure of the air supply in order to provide the PEMFC system with good steady state and transient characteristics so as to enhance its lifetime.

7.4.2.2 Optimization of control strategies for air supply system

Researchers have made considerable work. Zhao et al. [492] proposed an

observer-based fractional order proportional-integral-derivative (PID) controller to control the oxygen excess ratio and cathode pressure simultaneously. Both its steady state and transient performances are more favorable compared to the conventional PID control strategy. Liu et al. [490] proposed a dual closed-loop fuzzy PID controller based on a feedforward decoupled controller, enabling independent control of the flow rate and the pressure, thus exhibiting better dynamic response performance and stability, as well as decreasing the possibility of gas outage and improving the durability of the PEMFC stacks (see Fig. 35). Tian et al. [493] suggested a hybrid MPC and PID control strategy to control the air compressor voltage and the backpressure valve opening concurrently. The MPC is used for the coordinated control of both, while the PID removes the steady-state error when the system is in the steady state under the MPC, which makes the hybrid control strategy more effective compared to the MPC and PI alone. In addition, the MPC-PID hybrid control strategy also has good passive and active fault-tolerant control effects in the event of a system fault. Ou et al. [494], on the other hand, combined the fuzzy control strategy with the traditional PID control strategy to develop a feed-forward fuzzy PID control strategy to achieve the control of the oxygen excess coefficient. The controller can effectively regulate the oxygen excess coefficient when the PEMFC output current changes abruptly and reduce the parasitic power consumption of the air compressor to avoid the occurrence of oxygen starvation, which improves the efficiency of the PEMFC system and prolongs its lifespan in the meantime.

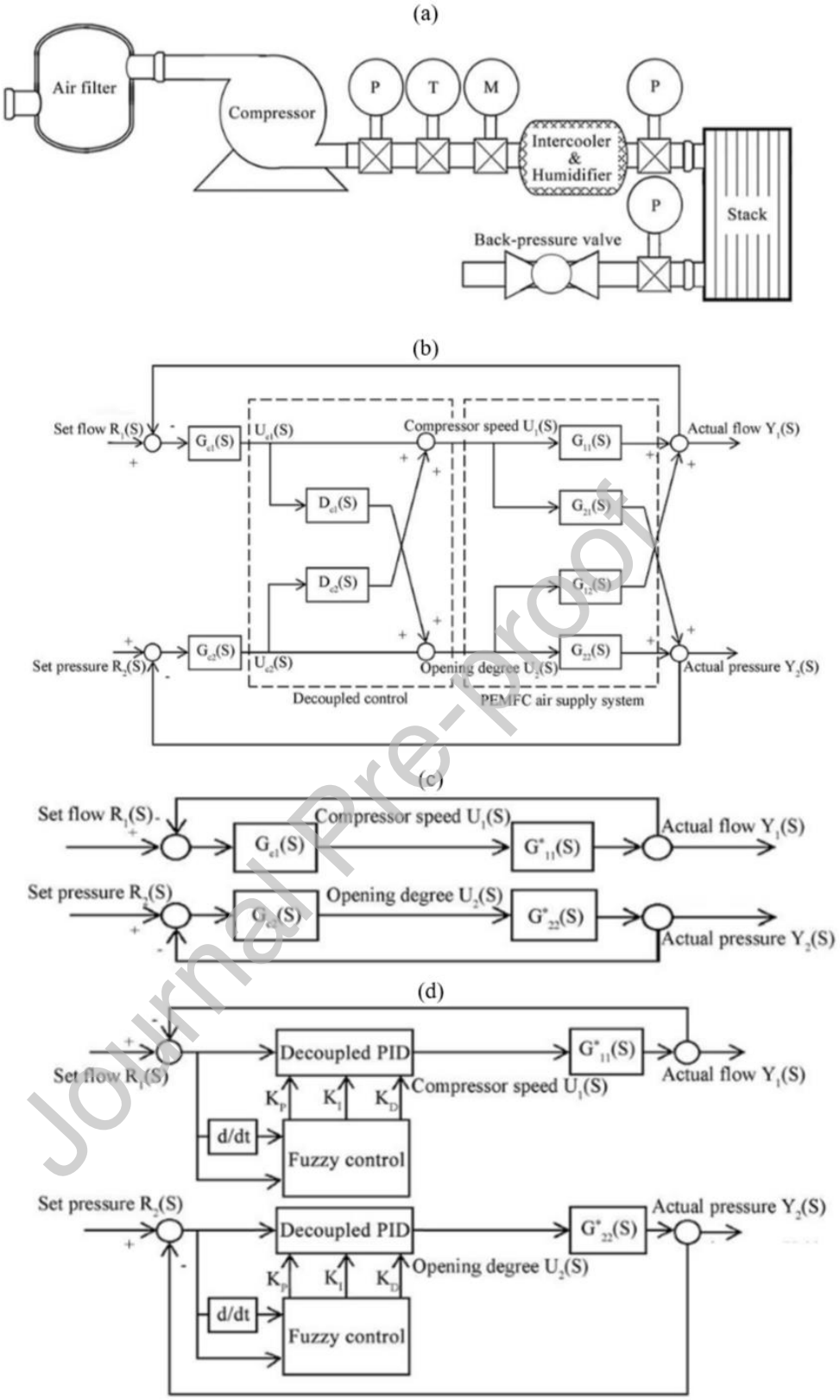

Fig. 35. Structure diagram of the test bench and controller. (a) Topology diagram of test bench; (b) Feedforward decoupled controller; (c) Equivalent control system after

feedforward decoupling; (d) Decoupling double closed-loop fuzzy-PID controller. Reprinted from Ref. [490] with permission of Elsevier.

7.4.3 Water-thermal management system

7.4.3.1 Structure and considerations for water-thermal management system

Control of temperature will have an important impact on the gas humidity, catalyst activity, membrane performance, electrochemical rate, and so on, inside the PEMFC. Various cooling methods are available for the PEMFC, including air cooling, phase change cooling, and liquid cooling [495]. Liquid cooling is the most appropriate cooling method in the application scenario of automotive power sources due to its high specific heat coolant and ease of integration [496,497]. Only a small portion of the heat generated during the operation of a PEMFC can be carried away by the internal gas flow, which means that the coolant undertakes most of the heat-carrying responsibilities [498]. Whereas the operating temperature of the PEMFC is relatively low, the temperature difference between the coolant and the environment is not significant, making heat dissipation difficult [499]. Proper water management can ensure the normal operation of PEMFC and improve its efficiency. Many scholars have extensively studied PEMFC water management, which mainly includes means such as changing the flow field or MEA microstructure, applying control strategies to provide optimal working conditions, and changing the flow path or MEA materials [500]. This section introduces the control strategy aspect.

Temperature management is an important safeguard for the smooth operation of PEMFC vehicles, which directly affects the output performance and longevity of the

PEMFC. Higher temperatures can exacerbate the evaporation of liquid water, leading to membrane dehydration and voltage drop; while lower temperatures can cause "flooding" of the flow paths, hindering mass transfer, as well as triggering a number of cold-starting problems such as those mentioned above when the temperature is below freezing point. As the heat generated by the PEMFC is difficult to be discharged in time, it may accumulate and cause the temperature of the stack to rise sharply above its normal operating temperature range; while during start-up, the temperature of the stack is often lower than its normal operating temperature range, and the catalyst activity at this time is not satisfactory, which affects the kinetic performance of the PEMFC. In the meantime, the uneven internal temperature distribution of the stack will also reduce the durability and stability of the cell. Proper water management is also necessary to keep the PEMFC water balance in an optimal state. The accumulation of liquid water can lead to problems such as impeded mass transfer process, flooding of catalyst active sites, and decreased membrane conductivity. The measures are mainly to humidify the interior of the PEMFC stack and to drain the excess liquid water in a timely manner to avoid membrane drying and flooding. The humidification methods can be divided into three types: external humidification, internal humidification and self-humidification [501], while the drainage methods are static drainage and dynamic drainage [502].

7.4.3.2 Optimization of control strategies for water-thermal management system

The inherent nonlinearity of the PEMFC system and the uncertainty of the model parameters make it difficult to control the water/thermal management system. Li et al.

[503] presented a machine-learning based PID control strategy, which allows for real-time change of the PID controller parameters to enable a more accurate control of the temperature by adjusting the cooling water flow in the pump. A single threshold control only for the water pump or radiator can lead to a strong coupling between the inlet temperature and the temperature difference between the inlet and outlet. To address this problem, Su et al. [504] proposed a decoupling control strategy, namely to establish a water pump flow controller and a fuzzy PID blower controller to stabilize the temperature difference between the inlet and outlet of the power reactor under variable load conditions while ensuring the inlet temperature is close to the target temperature value. However, there are also interactions between the water pump and the radiator. Li et al. [505] replace the independent controllers of the water pump and radiator in the traditional control framework by an integrated control strategy based on distributed deep reinforcement learning, thus taking the interactions between the water pump and radiator into account. Fu et al. [506] propose a water-thermal management strategy based on the Xgboost algorithm to control the temperature while keeping the membrane water content at a reasonable level. Under the mixed driving cycle, the control strategy based on the Xgboost algorithm that they developed has the best control performance compared to other strategies based on machine learning and fuzzy logic control, with a reduction in the maximum deviation of the temperature of the PEMFC stack and the variation of the membrane water content.

7.4.4 Energy management system

7.4.4.1 Structure and considerations for energy management system

PEMFC requires a specific electrochemical reaction time to complete the energy conversion, whose dynamic response is slow, and can hardly meet the power output demand under complex and variable automotive operating conditions if driven directly as an automotive power source [507]. As a result, an automotive PEMFC system usually consists of a PEMFC and a lithium-ion battery or supercapacitor used as an energy buffer [508]. Also, an integrated DC/DC converter is needed to generate the current and voltage required by the motor and provide a power output that meets the usage requirements [509]. This approach allows the PEMFC to output a stable, high-quality current, which serves to improve the durability of the PEMFC. Considering the cost and efficiency of the system, the complexity of the structure, and the difficulty of control, the most common structure in the current automotive PEMFC system is the PEMFC + battery structure. With the continuous development of PEMFC technology, the future is expected to form a high-power PEMFC + low-power lithium-ion battery structure composition. The former is used to meet the vehicle power demand, and the latter is used to recover braking energy [479].

When using lithium-ion batteries or supercapacitors as auxiliary energy sources for the PEMFC system, the power distribution among energy sources will have a direct impact on the fuel economy, while severe power fluctuations will affect the durability of the PEMFC system, so it is crucial to coordinate the energy flow among energy sources [510]. For different automotive operating conditions, energy distribution and power control are achieved through the energy management system, as well as the

regulation and optimization of the control strategy to reduce the unfavorable operating conditions of the PEMFC, reduce the impact of the loads on the PEMFC, improve the overall response speed of the vehicle, and meanwhile, cooperate with the recovery of the braking energy to improve the energy utilization rate.

7.4.4.2 Optimization of control strategies for energy management system

To mitigate the impact of power fluctuation on PEMFC durability, a frequency-separated energy allocation strategy can distribute power demand among power sources; that is, the low-frequency power is allocated to the PEMFC, and the medium- and high-frequency power is distributed to the supercapacitor and lithium battery. This hierarchical optimized energy management strategy can achieve PEMFC power following control based on motor power demand, charge state, and so on, which reduces the number of times of PEMFC loading and switching, and ensures the durability of PEMFC [511]. Fu et al. [510] presented a frequency decoupling strategy based on fuzzy control according to this allocation method (see Fig. 36). Both simulation and experimental results show that this strategy can effectively reduce hydrogen energy consumption, limit the PEMFC power fluctuation, and help to extend the PEMFC lifetime. Considering the impact of energy management on the aging degradation of PEMFC, Tang et al. [512] proposed a deep reinforcement learning-based energy management strategy. It incorporates the PEMFC system degradation into the objective function by adjusting the weights of both degradation and hydrogen consumption to achieve a balance between the fuel economy and the PEMFC system degradation. Zhou et al. [513] considered the system cost, fuel

consumption and PEMFC recession on the PEMFC system, a self-optimizing power matching strategy is proposed based on a deep deterministic strategy gradient, which can achieve long-life PEMFC operation based on low-energy operation. Jia et al. [514] proposed an energy management strategy based on real-time adaptive model predictive control, where, at each control interval, the linear variable parameter prediction model is updated online to adapt to the changes in the battery state of charge, and then a constrained optimization problem is formulated to achieve the desired trade-off between four performance metrics: hydrogen consumption, PEMFC current fluctuation, battery power loss, and battery state of charge. The results show that the strategy behaves well in reducing hydrogen consumption and PEMFC current fluctuation.

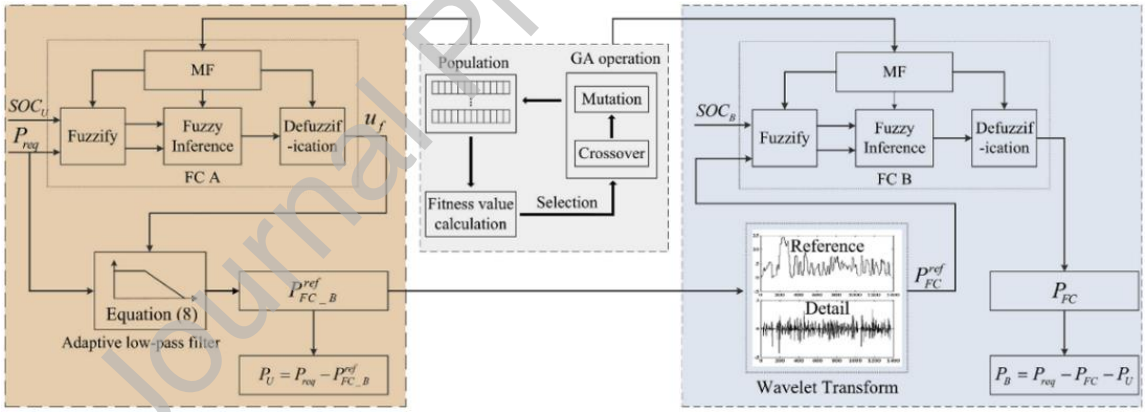

Fig. 36. Optimized frequency decoupling strategy based on fuzzy control. Reprinted from Ref. [510] with permission of Elsevier.

8. Conclusions and prospects

In practical automotive operating conditions, PEMFCs may encounter various types of degradation. This paper presents an overview of the degradation mechanisms and manifestations of PEMFCs under typical automotive operating conditions. The toxic

effects of impurities on catalysts and membranes for PEMFC degradation and corresponding mitigation strategies are also discussed. Possible solutions have been proposed to address the durability issue of PEMFCs. The main findings are summarized as follows.

Main degradation mechanisms under typical automotive operating conditions are membrane chemical degradation and Pt catalyst agglomeration/migration under idling conditions, carbon corrosion under start-stop conditions, mechanical degradation of PEMFC components and gas starvation under dynamic load conditions, damage to components due to expansion of water freezing in cold-starting. For each typical operating condition, there are corresponding AST methods for facilitating cost-effective research by summarizing degradation manifestations and concluding relevant mechanisms.

Impurity contamination is also a significant factor in the degradation of PEMFC. Metal cations produced by the breakdown of bipolar plates, chloride ions carried by Pt catalysts, and impurities such as CO, H_2S, SO_2, and NH_3 present in the reaction gas have negative effects on the durability of PEMFCs. Impurities usually alter the electrochemical reaction paths through their chemical properties, causing catalysts to fail. Since the cause of the degradation is focused on the material properties of the catalyst, the most common and essential mitigation strategy is developing the high impurity-tolerance catalyst.

Currently, efforts to enhance the endurance of PEMFCs under automotive operating conditions focus on four main areas: MEA materials, bipolar plates and flow fields

design, stack assembly, and control strategies. Refreshing the membranes, catalysts, and supports with novel materials can extend the operational lifespan of PEMFCs while maintaining their output performance. Optimizing the stack design, specifically the end plates, sealing, and bipolar plates, can provide effective solutions to issues expected to occur during the operation of the PEMFC stack. Improvements to the control strategy have the potential to enhance PEMFC durability quickly. However, further research is required to explore control strategies with rapid dynamic response and high stability.

The main challenges of improving the durability of automotive PEMFC are listed below.

First, lots of research on improving the durability and operating conditions of fuel cells for vehicles still focuses on studying a single cell, even a half-cell. However, since fuel cells for vehicles usually have multiple individual cells, it is crucial to investigate the durability of these individual components in large-scale fuel cell systems, as well as the impact of consistency between the cells.

Second, although there exists a comprehensive and profound understanding of the degradation mechanism in PEMFCs, there is currently no general model for researching the stability of components. This is due to the variation in experimental conditions among researchers, making it difficult to form a convincing theory. In order to make a valid assessment of degradation studies on different conditions, it is necessary to develop general criteria and theory.

Third, in practice, balancing low cost and high durability for commercializing

PEMFCs is difficult. Some components and designs that promote long-term operation of PEMFCs are often unavailable for large-scale applications due to their high cost. Some measures only state that they can meet durability requirements, but it remains unclear whether they could meet the cost requirements for PEMFC with the corresponding increase of cost. Costing in relation to the actual production process may be necessary.

CRediT author statement

Zikuo Liu: Conceptualization, Visualization, Writing-Original draft preparation. **Shanshan Cai**: Writing - Review & Editing, Supervision. **Zhengkai Tu:** Conceptualization, Supervision. **Siew Hua Chen:** Resources.

Acknowledgments

The authors thank the National Key Research and Development Program of China (Grant No. 2022YFB4003705) for funding and supporting this work.

References

[1] P. Pei, Q. Chang, T. Tang, A quick evaluating method for automotive fuel cell lifetime, Int. J. Hydrogen Energy, 33 (2008) 3829-3836.

[2] T. da Silva Veras, T.S. Mozer, D. da Costa Rubim Messeder dos Santos, et al., Hydrogen: Trends, production and characterization of the main process worldwide, Int. J. Hydrogen Energy, 42 (2017) 2018-2033.

[3] K. Jiao, J. Xuan, Q. Du, et al., Designing the next generation of proton-exchange membrane fuel cells, Nature, 595 (2021) 361-369.

[4] X. Chen, C. Yang, Y. Sun, et al., Water management and structure optimization study of

nickel metal foam as flow distributors in proton exchange membrane fuel cell, Appl. Energy, 309 (2022) 118448.

[5] J. Wang, System integration, durability and reliability of fuel cells: Challenges and solutions, Appl. Energy, 189 (2017) 460-479.

[6] Z. Liu, H. Chen, T. Zhang, Review on system mitigation strategies for start-stop degradation of automotive proton exchange membrane fuel cell, Appl. Energy, 327 (2022) 120058.

[7] P. Ren, P. Pei, Y. Li, et al., Degradation mechanisms of proton exchange membrane fuel cell under typical automotive operating conditions, Progr. Energy Combust. Sci., 80 (2020).

[8] P. Pei, H. Chen, Main factors affecting the lifetime of Proton Exchange Membrane fuel cells in vehicle applications: A review, Appl. Energy, 125 (2014) 60-75.

[9] N. Yousfi-Steiner, P. Moçotéguy, D. Candusso, et al., A review on polymer electrolyte membrane fuel cell catalyst degradation and starvation issues: Causes, consequences and diagnostic for mitigation, J. Power Sources, 194 (2009) 130-145.

[10] X.-Z. Yuan, H. Li, S. Zhang, et al., A review of polymer electrolyte membrane fuel cell durability test protocols, J. Power Sources, 196 (2011) 9107-9116.

[11] Y. Nosaka, K. Ohtaka, N. Ohguri, et al., Detection of OH Radicals Generated in Polymer Electrolyte Membranes of Fuel Cells, J. Electrochem. Soc., 158 (2011) B430.

[12] L. Ghassemzadeh, S. Holdcroft, Quantifying the Structural Changes of Perfluorosulfonated Acid Ionomer upon Reaction with Hydroxyl Radicals, J. Am. Chem. Soc., 135 (2013) 8181-8184.

[13] J. Zhang, B.A. Litteer, F.D. Coms, et al., Recoverable Performance Loss Due to

Membrane Chemical Degradation in PEM Fuel Cells, J. Electrochem. Soc., 159 (2012) F287.

[14] A. Collier, H. Wang, X. Zi Yuan, et al., Degradation of polymer electrolyte membranes, Int. J. Hydrogen Energy, 31 (2006) 1838-1854.

[15] P.C. Okonkwo, I. Ben Belgacem, W. Emori, et al., Nafion degradation mechanisms in proton exchange membrane fuel cell (PEMFC) system: A review, Int. J. Hydrogen Energy, 46 (2021) 27956-27973.

[16] M. Zaton, J. Rozière, D. Jones, Current Understanding of Chemical Degradation Mechanisms of Perfluorosulfonic Acid Membranes and their Mitigation Strategies: A Review, Sustainable Energy Fuels, 1 (2017).

[17] L. Ghassemzadeh, K.-D. Kreuer, J. Maier, et al., Chemical Degradation of Nafion Membranes under Mimic Fuel Cell Conditions as Investigated by Solid-State NMR Spectroscopy, The Journal of Physical Chemistry C, 114 (2010) 14635-14645.

[18] S.v. Venkatesan, C. Lim, S. Holdcroft, et al., Progression in the Morphology of Fuel Cell Membranes upon Conjoint Chemical and Mechanical Degradation, J. Electrochem. Soc., 163 (2016) F637.

[19] L. Ghassemzadeh, T.J. Peckham, T. Weissbach, et al., Selective Formation of Hydrogen and Hydroxyl Radicals by Electron Beam Irradiation and Their Reactivity with Perfluorosulfonated Acid Ionomer, J. Am. Chem. Soc., 135 (2013) 15923-15932.

[20] M.B. Blanco, I. Bejan, I. Barnes, et al., Atmospheric Photooxidation of Fluoroacetates as a Source of Fluorocarboxylic Acids, Environ. Sci. Technol., 44 (2010) 2354-2359.

[21] C. Chen, T.F. Fuller, The effect of humidity on the degradation of Nafion® membrane, Polym. Degrad. Stab., 94 (2009) 1436-1447.

[22] M. Inaba, T. Kinumoto, M. Kiriake, et al., Gas crossover and membrane degradation in polymer electrolyte fuel cells, Electrochim. Acta, 51 (2006) 5746-5753.

[23] M.P. Rodgers, B.P. Pearman, L.J. Bonville, et al., Evaluation of the Effect of Impregnated Platinum on PFSA Degradation for PEM Fuel Cells, J. Electrochem. Soc., 160 (2013) F1123.

[24] S. Kundu, M. Fowler, L.C. Simon, et al., Reversible and irreversible degradation in fuel cells during Open Circuit Voltage durability testing, J. Power Sources, 182 (2008) 254-258.

[25] C.G. Chung, L. Kim, Y.W. Sung, et al., Degradation mechanism of electrocatalyst during long-term operation of PEMFC, Int. J. Hydrogen Energy, 34 (2009) 8974-8981.

[26] R.M. Darling, J.P. Meyers, Kinetic Model of Platinum Dissolution in PEMFCs, J. Electrochem. Soc., 150 (2003) A1523.

[27] S. Cherevko, N. Kulyk, K.J.J. Mayrhofer, Durability of platinum-based fuel cell electrocatalysts: Dissolution of bulk and nanoscale platinum, Nano Energy, 29 (2016) 275-298.

[28] T. Ioroi, Z. Siroma, S.-i. Yamazaki, et al., Electrocatalysts for PEM Fuel Cells, Advanced Energy Materials, 9 (2019) 1801284.

[29] B.T. Sneed, D.A. Cullen, K.S. Reeves, et al., 3D Analysis of Fuel Cell Electrocatalyst Degradation on Alternate Carbon Supports, ACS Appl. Mater. Interfaces, 9 (2017) 29839-29848.

[30] M. Zhao, W. Shi, B. Wu, et al., Influence of Membrane Thickness on Membrane Degradation and Platinum Agglomeration under Long-term Open Circuit Voltage Conditions, Electrochim. Acta, 153 (2015) 254-262.

[31] W. Bi, T.F. Fuller, Modeling of PEM fuel cell Pt/C catalyst degradation, J. Power Sources,

178 (2008) 188-196.

[32] J. Péron, Y. Nedellec, D.J. Jones, et al., The effect of dissolution, migration and precipitation of platinum in Nafion®-based membrane electrode assemblies during fuel cell operation at high potential, J. Power Sources, 185 (2008) 1209-1217.

[33] E.F. Holby, W. Sheng, Y. Shao-Horn, et al., Pt nanoparticle stability in PEM fuel cells: influence of particle size distribution and crossover hydrogen, Energy & Environmental Science, 2 (2009) 865-871.

[34] F. Ettingshausen, J. Kleemann, M. Michel, et al., Spatially resolved degradation effects in membrane-electrode-assemblies of vehicle aged polymer electrolyte membrane fuel cell stacks, J. Power Sources, 194 (2009) 899-907.

[35] N. Ohguri, A.Y. Nosaka, Y. Nosaka, Detection of OH radicals as the effect of Pt particles in the membrane of polymer electrolyte fuel cells, J. Power Sources, 195 (2010) 4647-4652.

[36] D. Zhao, B.L. Yi, H.M. Zhang, et al., The effect of platinum in a Nafion membrane on the durability of the membrane under fuel cell conditions, J. Power Sources, 195 (2010) 4606-4612.

[37] W. Yoon, X. Huang, Study of Polymer Electrolyte Membrane Degradation under OCV Hold Using Bilayer MEAs, J. Electrochem. Soc., 157 (2010) B599.

[38] A. Ohma, S. Suga, S. Yamamoto, et al., Membrane Degradation Behavior during Open-Circuit Voltage Hold Test, J. Electrochem. Soc., 154 (2007) B757.

[39] N. Macauley, L. Ghassemzadeh, C. Lim, et al., Pt Band Formation Enhances the Stability of Fuel Cell Membranes, ECS Electrochemistry Letters, 2 (2013) F33.

[40] C. Kim, J.-G. Oh, Y.-T. Kim, et al., Platinum dendrites with controlled sizes for oxygen

reduction reaction, Electrochem. Commun., 12 (2010) 1596-1599.

[41] M. Inaba, H. Yamada, J. Tokunaga, et al., Effect of Agglomeration of Pt/C Catalyst on Hydrogen Peroxide Formation, Electrochem. Solid-State Lett., 7 (2004) A474.

[42] A. Ohma, S. Yamamoto, K. Shinohara, Membrane degradation mechanism during open-circuit voltage hold test, J. Power Sources, 182 (2008) 39-47.

[43] S. Zhang, X.-Z. Yuan, R. Hiesgen, et al., Effect of open circuit voltage on degradation of a short proton exchange membrane fuel cell stack with bilayer membrane configurations, J. Power Sources, 205 (2012) 290-300.

[44] M.P. Rodgers, L.J. Bonville, H.R. Kunz, et al., Fuel Cell Perfluorinated Sulfonic Acid Membrane Degradation Correlating Accelerated Stress Testing and Lifetime, Chem. Rev., 112 (2012) 6075-6103.

[45] R. Singh, P.C. Sui, K.H. Wong, et al., Modeling the Effect of Chemical Membrane Degradation on PEMFC Performance, J. Electrochem. Soc., 165 (2018) F3328.

[46] M. Gummalla, V.V. Atrazhev, D. Condit, et al., Degradation of Polymer-Electrolyte Membranes in Fuel Cells: II. Theoretical model, J. Electrochem. Soc., 157 (2010) B1542.

[47] M. Inaba, T. Kinumoto, M. Kiriake, et al., Gas crossover and membrane degradation in polymer electrolyte fuel cells, Electrochim. Acta, 51 (2006).

[48] S. Rodosik, J.P. Poirot-Crouvezier, Y. Bultel, Impact of humidification by cathode exhaust gases recirculation on a PEMFC system for automotive applications, Int. J. Hydrogen Energy, 44 (2019) 12802-12817.

[49] X. Zhao, L. Xu, C. Fang, et al., Study on voltage clamping and self-humidification effects of pem fuel cell system with dual recirculation based on orthogonal test method, Int. J.

Hydrogen Energy, 43 (2018) 16268-16278.

[50] C.A. Reiser, L. Bregoli, T.W. Patterson, et al., A Reverse-Current Decay Mechanism for Fuel Cells, Electrochem. Solid-State Lett., 8 (2005) A273.

[51] C. Wang, J. Huang, B. Zhao, et al., Research progress of PEMFC degradation in full operating modes for electric vehicle, Journal of Automotive Safety and Energy, 7 (2016) 86-93.

[52] H. Tang, Z. Qi, M. Ramani, et al., PEM fuel cell cathode carbon corrosion due to the formation of air/fuel boundary at the anode, J. Power Sources, 158 (2006) 1306-1312.

[53] K. Eom, G. Kim, E. Cho, et al., Effects of Pt loading in the anode on the durability of a membrane–electrode assembly for polymer electrolyte membrane fuel cells during startup/shutdown cycling, Int. J. Hydrogen Energy, 37 (2012) 18455-18462.

[54] S. Maass, F. Finsterwalder, G. Frank, et al., Carbon support oxidation in PEM fuel cell cathodes, J. Power Sources, 176 (2008) 444-451.

[55] P. Mandal, B.K. Hong, J.-G. Oh, et al., Understanding the voltage reversal behavior of automotive fuel cells, J. Power Sources, 397 (2018) 397-404.

[56] A.P. Young, J. Stumper, E. Gyenge, Characterizing the Structural Degradation in a PEMFC Cathode Catalyst Layer: Carbon Corrosion, J. Electrochem. Soc., 156 (2009) B913.

[57] N. Macauley, D.D. Papadias, J. Fairweather, et al., Carbon Corrosion in PEM Fuel Cells and the Development of Accelerated Stress Tests, J. Electrochem. Soc., 165 (2018) F3148.

[58] S.R. Dhanushkodi, S. Kundu, M.W. Fowler, et al., Use of mechanistic carbon corrosion model to predict performance loss in Polymer Electrolyte Membrane fuel cells, J. Power Sources, 267 (2014) 171-181.

[59] L.M. Roen, C.H. Paik, T.D. Jarvi, Electrocatalytic Corrosion of Carbon Support in PEMFC

Cathodes, Electrochem. Solid-State Lett., 7 (2004) A19.

[60] P.T. Yu, Z. Liu, R. Makharia, Investigation of Carbon Corrosion Behavior and Kinetics in Proton Exchange Membrane Fuel Cell Cathode Electrodes, J. Electrochem. Soc., 160 (2013) F645.

[61] H. Schulenburg, B. Schwanitz, N. Linse, et al., 3D Imaging of Catalyst Support Corrosion in Polymer Electrolyte Fuel Cells, The Journal of Physical Chemistry C, 115 (2011) 14236-14243.

[62] Y. Yamashita, S. Itami, J. Takano, et al., Degradation Mechanisms of Carbon Supports under Hydrogen Passivation Startup and Shutdown Process for PEFCs, J. Electrochem. Soc., 164 (2017) F181.

[63] S. Takao, O. Sekizawa, G. Samjeské, et al., Observation of Degradation of Pt and Carbon Support in Polymer Electrolyte Fuel Cell Using Combined Nano-X-ray Absorption Fine Structure and Transmission Electron Microscopy Techniques, ACS Appl. Mater. Interfaces, 10 (2018) 27734-27744.

[64] Y. Ishigami, K. Takada, H. Yano, et al., Corrosion of carbon supports at cathode during hydrogen/air replacement at anode studied by visualization of oxygen partial pressures in a PEFC—Start-up/shut-down simulation, J. Power Sources, 196 (2011) 3003-3008.

[65] J. Durst, A. Lamibrac, F. Charlot, et al., Degradation heterogeneities induced by repetitive start/stop events in proton exchange membrane fuel cell: Inlet vs. outlet and channel vs. land, Applied Catalysis B: Environmental, 138-139 (2013) 416-426.

[66] S. Komini Babu, D. Spernjak, J. Dillet, et al., Spatially resolved degradation during startup and shutdown in polymer electrolyte membrane fuel cell operation, Appl. Energy, 254 (2019)

113659.

[67] R. Lin, X. Cui, J. Shan, et al., Investigating the effect of start-up and shut-down cycles on the performance of the proton exchange membrane fuel cell by segmented cell technology, Int. J. Hydrogen Energy, 40 (2015) 14952-14962.

[68] H.-S. Oh, J.-G. Oh, S. Haam, et al., On-line mass spectrometry study of carbon corrosion in polymer electrolyte membrane fuel cells, Electrochem. Commun., 10 (2008) 1048-1051.

[69] J. Speder, A. Zana, I. Spanos, et al., Comparative degradation study of carbon supported proton exchange membrane fuel cell electrocatalysts – The influence of the platinum to carbon ratio on the degradation rate, J. Power Sources, 261 (2014) 14-22.

[70] G.-B. Jung, K.-Y. Chuang, T.-C. Jao, et al., Study of high voltage applied to the membrane electrode assemblies of proton exchange membrane fuel cells as an accelerated degradation technique, Appl. Energy, 100 (2012) 81-86.

[71] S.V. Venkatesan, M. Dutta, E. Kjeang, Mesoscopic degradation effects of voltage cycled cathode catalyst layers in polymer electrolyte fuel cells, Electrochem. Commun., 72 (2016) 15-18.

[72] X. Zhang, Y. Yang, X. Zhang, et al., Performance Degradation of Proton Exchange Membrane Fuel Cell Caused by an Accelerated Stress Test, Fuel Cells, 19 (2019) 160-168.

[73] A.Z. Weber, R.L. Borup, R.M. Darling, et al., A Critical Review of Modeling Transport Phenomena in Polymer-Electrolyte Fuel Cells, J. Electrochem. Soc., 161 (2014) F1254.

[74] J.H. Kim, E.A. Cho, J.H. Jang, et al., Effects of Cathode Inlet Relative Humidity on PEMFC Durability during Startup–Shutdown Cycling: I. Electrochemical Study, J. Electrochem. Soc., 157 (2010) B104.

[75] T. Mittermeier, A. Weiß, F. Hasché, et al., PEM Fuel Cell Start-Up/Shut-Down Losses vs Relative Humidity: The Impact of Water in the Electrode Layer on Carbon Corrosion, J. Electrochem. Soc., 165 (2018) F1349.

[76] J. Kim, J. Lee, Y. Tak, Relationship between carbon corrosion and positive electrode potential in a proton-exchange membrane fuel cell during start/stop operation, J. Power Sources, 192 (2009) 674-678.

[77] T. Zhang, P. Wang, H. Chen, et al., A review of automotive proton exchange membrane fuel cell degradation under start-stop operating condition, Appl. Energy, 223 (2018) 249-262.

[78] C. Wang, S. Wang, L. Peng, et al., Recent Progress on the Key Materials and Components for Proton Exchange Membrane Fuel Cells in Vehicle Applications, Periodical 9 (2016).

[79] A. Ofstad, J. Davey, S. Sunde, et al., Carbon Corrosion of a PEMFC During Shut-down/Start-up when Using an Air Purge Procedure, ECS Trans., 16 (2008) 1301.

[80] W. Tokarz, P. Piela, Mitigation of catalysts degradation upon stopping work of polymer electrolyte membrane fuel cells for longer time, Int. J. Hydrogen Energy, 41 (2016) 15002-15006.

[81] Y. Yang, W. Li, R. Lin, et al., Impact of dummy load shut-down strategy on performance and durability of proton exchange membrane fuel cell stack, J. Power Sources, 404 (2018) 126-134.

[82] J.H. Park, S.-M. Hwang, G.-G. Park, et al., Variations in performance-degradation behavior of Pt/CNF and Pt/C MEAs for the same degree of carbon corrosion, Electrochim. Acta, 260 (2018) 674-683.

[83] W. Zhang, P. Sherrell, A.I. Minett, et al., Carbon nanotube architectures as catalyst supports for proton exchange membrane fuel cells, Energy & Environmental Science, 3 (2010) 1286-1293.

[84] R. Alipour MoghadamEsfahani, S.K. Vankova, E.B. Easton, et al., A hybrid Pt/NbO/CNTs catalyst with high activity and durability for oxygen reduction reaction in PEMFC, Renewable Energy, 154 (2020) 913-924.

[85] J.H. Kim, E.A. Cho, J.H. Jang, et al., Development of a Durable PEMFC Startup Process by Applying a Dummy Load: I. Electrochemical Study, J. Electrochem. Soc., 156 (2009) B955.

[86] F. Ettingshausen, J. Kleemann, A. Marcu, et al., Dissolution and Migration of Platinum in PEMFCs Investigated for Start/Stop Cycling and High Potential Degradation, Fuel Cells, 11 (2011) 238-245.

[87] A. Oyarce, E. Zakrisson, M. Ivity, et al., Comparing shut-down strategies for proton exchange membrane fuel cells, J. Power Sources, 254 (2014) 232-240.

[88] J.H. Kim, Y. Yeon Jo, E.A. Cho, et al., Effects of Cathode Inlet Relative Humidity on PEMFC Durability during Startup–Shutdown Cycling: II. Diagnostic Study, J. Electrochem. Soc., 157 (2010) B633.

[89] G. Samjeské, K. Higashi, S. Takao, et al., In Situ Techniques to Study the Effects of Anode or Cathode Gas-Exchange Cycles on the Deterioration of Pt/C Cathode Catalysts in PEFCs, ChemElectroChem, 2 (2015) 1595-1606.

[90] X. Zhang, Y. Yang, L. Guo, et al., Effects of carbon corrosion on mass transfer losses in proton exchange membrane fuel cells, Int. J. Hydrogen Energy, 42 (2017) 4699-4705.

[91] H. Chen, X. Zhao, B. Qu, et al., An evaluation method of gas distribution quality in

dynamic process of proton exchange membrane fuel cell, Appl. Energy, 232 (2018) 26-35.

[92] K.A. Page, J.W. Shin, S.A. Eastman, et al., In Situ Method for Measuring the Mechanical Properties of Nafion Thin Films during Hydration Cycles, ACS Appl. Mater. Interfaces, 7 (2015) 17874-17883.

[93] A. Kusoglu, A.M. Karlsson, M.H. Santare, et al., Mechanical behavior of fuel cell membranes under humidity cycles and effect of swelling anisotropy on the fatigue stresses, J. Power Sources, 170 (2007) 345-358.

[94] R. Mukundan, A.M. Baker, A. Kusoglu, et al., Membrane Accelerated Stress Test Development for Polymer Electrolyte Fuel Cell Durability Validated Using Field and Drive Cycle Testing, J. Electrochem. Soc., 165 (2018) F3085.

[95] A.S. Alavijeh, R.M.H. Khorasany, Z. Nunn, et al., Microstructural and Mechanical Characterization of Catalyst Coated Membranes Subjected to In Situ Hygrothermal Fatigue, J. Electrochem. Soc., 162 (2015) F1461.

[96] J. Zhao, S. Shahgaldi, X. Li, et al., Experimental Observations of Microstructure Changes in the Catalyst Layers of Proton Exchange Membrane Fuel Cells under Wet-Dry Cycles, J. Electrochem. Soc., 165 (2018) F3337.

[97] Y. Chang, J. Liu, R. Li, et al., Effect of humidity and thermal cycling on the catalyst layer structural changes in polymer electrolyte membrane fuel cells, Energy Conversion and Management, 189 (2019) 24-32.

[98] R.A. Silva, T. Hashimoto, G.E. Thompson, et al., Characterization of MEA degradation for an open air cathode PEM fuel cell, Int. J. Hydrogen Energy, 37 (2012) 7299-7308.

[99] G. Wang, F. Huang, Y. Yu, et al., Degradation behavior of a proton exchange membrane

fuel cell stack under dynamic cycles between idling and rated condition, Int. J. Hydrogen Energy, 43 (2018) 4471-4481.

[100] J. Kang, J. Kim, Membrane electrode assembly degradation by dry/wet gas on a PEM fuel cell, Int. J. Hydrogen Energy, 35 (2010) 13125-13130.

[101] S. Qu, X. Li, M. Hou, et al., The effect of air stoichiometry change on the dynamic behavior of a proton exchange membrane fuel cell, J. Power Sources, 185 (2008) 302-310.

[102] Z. Yang, K. Jiao, Z. Liu, et al., Investigation of performance heterogeneity of PEMFC stack based on 1+1D and flow distribution models, Energy Conversion and Management, 207 (2020) 112502.

[103] G. Zhang, X. Xie, B. Xie, et al., Large-scale multi-phase simulation of proton exchange membrane fuel cell, Int. J. Heat Mass Transfer, 130 (2019) 555-563.

[104] M. Narimani, J. DeVaal, F. Golnaraghi, Hydrogen emission characterization for proton exchange membrane fuel cell during oxygen starvation – Part 1: Low oxygen concentration, Int. J. Hydrogen Energy, 41 (2016) 4843-4853.

[105] M. Bodner, A. Schenk, D. Salaberger, et al., Air Starvation Induced Degradation in Polymer Electrolyte Fuel Cells, Fuel Cells, 17 (2017) 18-26.

[106] M. Gerard, J.-P. Poirot-Crouvezier, D. Hissel, et al., Oxygen starvation analysis during air feeding faults in PEMFC, Int. J. Hydrogen Energy, 35 (2010) 12295-12307.

[107] A. Taniguchi, T. Akita, K. Yasuda, et al., Analysis of degradation in PEMFC caused by cell reversal during air starvation, Int. J. Hydrogen Energy, 33 (2008) 2323-2329.

[108] T.W. Patterson, R.M. Darling, Damage to the Cathode Catalyst of a PEM Fuel Cell Caused by Localized Fuel Starvation, Electrochem. Solid-State Lett., 9 (2006) A183.

[109] J. Chen, J. Hu, J. Waldecker, Model-Based Analysis of Carbon Corrosion in Start-Up/Shutdown, Fuel Starvation, and Voltage Reversal of a Polymer Electrolyte Fuel Cell, ECS Trans., 77 (2017) 1473.

[110] C. Qin, J. Wang, D. Yang, et al., Proton Exchange Membrane Fuel Cell Reversal: A Review, Periodical 6 (2016).

[111] H. Chen, X. Zhao, T. Zhang, et al., The reactant starvation of the proton exchange membrane fuel cells for vehicular applications: A review, Energy Conversion and Management, 182 (2019) 282-298.

[112] D. Zhong, R. Lin, D. Liu, et al., Structure optimization of anode parallel flow field for local starvation of proton exchange membrane fuel cell, J. Power Sources, 403 (2018) 1-10.

[113] F. Jia, L. Guo, H. Liu, Mitigation strategies for hydrogen starvation under dynamic loading in proton exchange membrane fuel cells, Energy Conversion and Management, 139 (2017) 175-181.

[114] I. Pivac, D. Bezmalinović, F. Barbir, Catalyst degradation diagnostics of proton exchange membrane fuel cells using electrochemical impedance spectroscopy, Int. J. Hydrogen Energy, 43 (2018) 13512-13520.

[115] D. Bezmalinovic, B. Simic, F. Barbir, Characterization of PEM fuel cell degradation by polarization change curves, J. Power Sources, 294 (2015) 82-87.

[116] G.S. Harzer, J.N. Schwämmlein, A.M. Damjanović, et al., Cathode Loading Impact on Voltage Cycling Induced PEMFC Degradation: A Voltage Loss Analysis, J. Electrochem. Soc., 165 (2018) F3118.

[117] B. Wu, M. Zhao, W. Shi, et al., The degradation study of Nafion/PTFE composite

membrane in PEM fuel cell under accelerated stress tests, Int. J. Hydrogen Energy, 39 (2014) 14381-14390.

[118] A.A. Amamou, S. Kelouwani, L. Boulon, et al., A Comprehensive Review of Solutions and Strategies for Cold Start of Automotive Proton Exchange Membrane Fuel Cells, IEEE Access, 4 (2016) 4989-5002.

[119] R. Alink, D. Gerteisen, M. Oszcipok, Degradation effects in polymer electrolyte membrane fuel cell stacks by sub-zero operation—An in situ and ex situ analysis, J. Power Sources, 182 (2008) 175-187.

[120] Z. Zhan, H. Zhao, P.C. Sui, et al., Numerical analysis of ice-induced stresses in the membrane electrode assembly of a PEM fuel cell under sub-freezing operating conditions, Int. J. Hydrogen Energy, 43 (2018) 4563-4582.

[121] D. Zhong, R. Lin, Z. Jiang, et al., Low temperature durability and consistency analysis of proton exchange membrane fuel cell stack based on comprehensive characterizations, Appl. Energy, 264 (2020) 114626.

[122] A. Ozden, S. Shahgaldi, X. Li, et al., The impact of ionomer type on the morphological and microstructural degradations of proton exchange membrane fuel cell electrodes under freeze-thaw cycles, Appl. Energy, 238 (2019) 1048-1059.

[123] A. Ozden, S. Shahgaldi, J. Zhao, et al., Degradations in porous components of a proton exchange membrane fuel cell under freeze-thaw cycles: Morphology and microstructure effects, Int. J. Hydrogen Energy, 45 (2020) 3618-3631.

[124] S.-Y. Lee, H.-J. Kim, E. Cho, et al., Performance degradation and microstructure changes in freeze–thaw cycling for PEMFC MEAs with various initial microstructures, Int. J.

Hydrogen Energy, 35 (2010) 12888-12896.

[125] S. Kim, B.K. Ahn, M.M. Mench, Physical degradation of membrane electrode assemblies undergoing freeze/thaw cycling: Diffusion media effects, J. Power Sources, 179 (2008) 140-146.

[126] Y. Luo, K. Jiao, Cold start of proton exchange membrane fuel cell, Progr. Energy Combust. Sci., 64 (2018) 29-61.

[127] Q. Yan, H. Toghiani, Y.-W. Lee, et al., Effect of sub-freezing temperatures on a PEM fuel cell performance, startup and fuel cell components, J. Power Sources, 160 (2006) 1242-1250.

[128] K.-Y. Song, H.-T. Kim, Effect of air purging and dry operation on durability of PEMFC under freeze/thaw cycles, Int. J. Hydrogen Energy, 36 (2011) 12417-12426.

[129] S.-J. Lim, G.-G. Park, J.-S. Park, et al., Investigation of freeze/thaw durability in polymer electrolyte fuel cells, Int. J. Hydrogen Energy, 35 (2010) 13111-13117.

[130] M. Oszcipok, M. Zedda, D. Riemann, et al., Low temperature operation and influence parameters on the cold start ability of portable PEMFCs, J. Power Sources, 154 (2006) 404-411.

[131] X.G. Yang, Y. Tabuchi, F. Kagami, et al., Durability of Membrane Electrode Assemblies under Polymer Electrolyte Fuel Cell Cold-Start Cycling, J. Electrochem. Soc., 155 (2008) B752.

[132] S. Kim, M.M. Mench, Physical degradation of membrane electrode assemblies undergoing freeze/thaw cycling: Micro-structure effects, J. Power Sources, 174 (2007) 206-220.

[133] M. Oszcipok, D. Riemann, U. Kronenwett, et al., Statistic analysis of operational

influences on the cold start behaviour of PEM fuel cells, J. Power Sources, 145 (2005) 407-415.

[134] J. Mishler, Y. Wang, P.P. Mukherjee, et al., Subfreezing operation of polymer electrolyte fuel cells: Ice formation and cell performance loss, Electrochim. Acta, 65 (2012) 127-133.

[135] Z. Zhan, Z.Y. Lv, Y. Huang, et al., Research on PEMFC start-up at subzero temperature and performance decay, 33 (2011) 151-155.

[136] S. Kim, C. Chacko, R.P. Ramasamy, et al., Freeze-Induced Damage and Purge Based Mitigation in Polymer Electrolyte Fuel Cells, ECS Trans., 11 (2007) 577.

[137] Y. Lee, B. Kim, Y. Kim, et al., Effects of a microporous layer on the performance degradation of proton exchange membrane fuel cells through repetitive freezing, J. Power Sources, 196 (2011) 1940-1947.

[138] E. Pinton, Y. Fourneron, S. Rosini, et al., Experimental and theoretical investigations on a proton exchange membrane fuel cell starting up at subzero temperatures, J. Power Sources, 186 (2009) 80-88.

[139] K. Tajiri, Y. Tabuchi, C.-Y. Wang, Isothermal Cold Start of Polymer Electrolyte Fuel Cells, J. Electrochem. Soc., 154 (2007) B147.

[140] Y.S. Kim, S.I. Kim, N.W. Lee, et al., Study on a purge method using pressure reduction for effective water removal in polymer electrolyte membrane fuel cells, Int. J. Hydrogen Energy, 40 (2015) 9473-9484.

[141] H.-Y. Tang, A.D. Santamaria, J. Bachman, et al., Vacuum-assisted drying of polymer electrolyte membrane fuel cell, Appl. Energy, 107 (2013) 264-270.

[142] L. Li, S. Wang, L. Yue, et al., Cold-start method for proton-exchange membrane fuel cells

based on locally heating the cathode, Appl. Energy, 254 (2019) 113716.

[143] Z. Zhan, C. Yuan, Z. Hu, et al., Experimental study on different preheating methods for the cold-start of PEMFC stacks, Energy, 162 (2018) 1029-1040.

[144] G.A. Futter, A. Latz, T. Jahnke, Physical modeling of chemical membrane degradation in polymer electrolyte membrane fuel cells: Influence of pressure, relative humidity and cell voltage, J. Power Sources, 410-411 (2019) 78-90.

[145] T. Wilberforce, O. Ijaodola, E. Ogungbemi, et al., Technical evaluation of proton exchange membrane (PEM) fuel cell performance – A review of the effects of bipolar plates coating, Renewable and Sustainable Energy Reviews, 113 (2019) 109286.

[146] A. Pavlišič, P. Jovanovič, V.S. Šelih, et al., The influence of chloride impurities on Pt/C fuel cell catalyst corrosion, Chem. Commun. (Cambridge, U. K.), 50 (2014) 3732-3734.

[147] Z. Du, C. Liu, J. Zhai, et al., A Review of Hydrogen Purification Technologies for Fuel Cell Vehicles, Periodical 11 (2021).

[148] N. Zamel, X. Li, Effect of contaminants on polymer electrolyte membrane fuel cells, Progr. Energy Combust. Sci., 37 (2011) 292-329.

[149] K.H. Wong, E. Kjeang, Mitigation of Chemical Membrane Degradation in Fuel Cells: Understanding the Effect of Cell Voltage and Iron Ion Redox Cycle, ChemSusChem, 8 (2015) 1072-1082.

[150] J. Wu, X.Z. Yuan, J.J. Martin, et al., A review of PEM fuel cell durability: Degradation mechanisms and mitigation strategies, J. Power Sources, 184 (2008) 104-119.

[151] X. Luo, L. Ghassemzadeh, S. Holdcroft, Effect of free radical-induced degradation on water permeation through PFSA ionomer membranes, Int. J. Hydrogen Energy, 40 (2015)

16714-16723.

[152] S. Kundu, L.C. Simon, M.W. Fowler, Comparison of two accelerated Nafion™ degradation experiments, Polym. Degrad. Stab., 93 (2008) 214-224.

[153] J. Healy, C. Hayden, T. Xie, et al., Aspects of the Chemical Degradation of PFSA Ionomers used in PEM Fuel Cells, Fuel Cells, 5 (2005) 302-308.

[154] X. Wei, R.-Z. Wang, W. Zhao, et al., Recent research progress in PEM fuel cell electrocatalyst degradation and mitigation strategies, EnergyChem, 3 (2021) 100061.

[155] Z. Wang, E. Tada, A. Nishikata, In Situ Analysis of Chloride Effect on Platinum Dissolution by a Channel-Flow Multi-Electrode System, J. Electrochem. Soc., 161 (2014) F845.

[156] N. Hodnik, M. Zorko, B. Jozinović, et al., Severe accelerated degradation of PEMFC platinum catalyst: A thin film IL-SEM study, Electrochem. Commun., 30 (2013) 75-78.

[157] K. Jayasayee, J.A.R. Van Veen, E.J.M. Hensen, et al., Influence of chloride ions on the stability of PtNi alloys for PEMFC cathode, Electrochim. Acta, 56 (2011) 7235-7242.

[158] S. Geiger, S. Cherevko, K.J.J. Mayrhofer, Dissolution of Platinum in Presence of Chloride Traces, Electrochim. Acta, 179 (2015) 24-31.

[159] T. Varga, Á.T. Varga, G. Ballai, et al., One step synthesis of chlorine-free Pt/Nitrogen-doped graphene composite for oxygen reduction reaction, Carbon, 133 (2018) 90-100.

[160] L. Kaluža, M.J. Larsen, M. Zdražil, et al., Highly loaded carbon black supported Pt catalysts for fuel cells, Catal. Today, 256 (2015) 375-383.

[161] M. Saquib, A. Bharadwaj, H. Singh Kushwaha, et al., Chloride Corrosion Resistant

Nitrogen doped Reduced Graphene Oxide/Platinum Electrocatalyst for Hydrogen Evolution Reaction in an Acidic Medium, ChemistrySelect, 5 (2020) 1739-1750.

[162] T.M. Arruda, B. Shyam, J.M. Ziegelbauer, et al., Investigation into the Competitive and Site-Specific Nature of Anion Adsorption on Pt Using In Situ X-ray Absorption Spectroscopy, The Journal of Physical Chemistry C, 112 (2008) 18087-18097.

[163] L. Kaluža, M.J. Larsen, I.J. Morales, et al., Synthesis of Pt/C Fuel Cell Electrocatalysts: Residual Content of Chloride and Activity in Oxygen Reduction, Electrocatalysis, 7 (2016) 269-275.

[164] N. Job, M. Chatenet, S. Berthon-Fabry, et al., Efficient Pt/carbon electrocatalysts for proton exchange membrane fuel cells: Avoid chloride-based Pt salts!, J. Power Sources, 240 (2013) 294-305.

[165] V.F. Valdés-López, T. Mason, P.R. Shearing, et al., Carbon monoxide poisoning and mitigation strategies for polymer electrolyte membrane fuel cells – A review, Progr. Energy Combust. Sci., 79 (2020) 100842.

[166] R.J. Bellows, E.P. Marucchi-Soos, D.T. Buckley, Analysis of Reaction Kinetics for Carbon Monoxide and Carbon Dioxide on Polycrystalline Platinum Relative to Fuel Cell Operation, Ind. Eng. Chem. Res., 35 (1996) 1235-1242.

[167] W.A. Adams, J. Blair, K.R. Bullock, et al., Enhancement of the performance and reliability of CO poisoned PEM fuel cells, J. Power Sources, 145 (2005) 55-61.

[168] Y. Zhao, Y. Mao, W. Zhang, et al., Reviews on the effects of contaminations and research methodologies for PEMFC, Int. J. Hydrogen Energy, 45 (2020) 23174-23200.

[169] H.F. Oetjen, V.M. Schmidt, U. Stimming, et al., Performance Data of a Proton Exchange

Membrane Fuel Cell Using H_2 / CO as Fuel Gas, J. Electrochem. Soc., 143 (1996) 3838.

[170] G. Bender, M. Angelo, K. Bethune, et al., Quantitative analysis of the performance impact of low-level carbon monoxide exposure in proton exchange membrane fuel cells, J. Power Sources, 228 (2013) 159-169.

[171] B. Shabani, M. Hafttananian, S. Khamani, et al., Poisoning of proton exchange membrane fuel cells by contaminants and impurities: Review of mechanisms, effects, and mitigation strategies, J. Power Sources, 427 (2019) 21-48.

[172] N. Zamel, X. Li, Transient analysis of carbon monoxide poisoning and oxygen bleeding in a PEM fuel cell anode catalyst layer, Int. J. Hydrogen Energy, 33 (2008) 1335-1344.

[173] L.-Y. Sung, B.-J. Hwang, K.-L. Hsueh, et al., Comprehensive study of an air bleeding technique on the performance of a proton-exchange membrane fuel cell subjected to CO poisoning, J. Power Sources, 242 (2013) 264-272.

[174] Y. Matsuda, T. Shimizu, S. Mitsushima, Adsorption behavior of low concentration carbon monoxide on polymer electrolyte fuel cell anodes for automotive applications, J. Power Sources, 318 (2016) 1-8.

[175] D.N. Oko, J. Zhang, S. Garbarino, et al., Formic acid electro-oxidation at PtAu alloyed nanoparticles synthesized by pulsed laser ablation in liquids, J. Power Sources, 248 (2014) 273-282.

[176] K. Wang, H.A. Gasteiger, N.M. Markovic, et al., On the reaction pathway for methanol and carbon monoxide electrooxidation on Pt-Sn alloy versus Pt-Ru alloy surfaces, Electrochim. Acta, 41 (1996) 2587-2593.

[177] J.J. Baschuk, X. Li, Carbon monoxide poisoning of proton exchange membrane fuel cells, International Journal of Energy Research, 25 (2001) 695-713.

[178] K.A. Kuttiyiel, Y. Choi, K. Sasaki, et al., Tuning electrocatalytic activity of Pt monolayer shell by bimetallic Ir-M (M=Fe, Co, Ni or Cu) cores for the oxygen reduction reaction, Nano Energy, 29 (2016) 261-267.

[179] Z. Dong, Y. Nan, T. Tang, et al., Synergistically Mitigating Electron Back-Donation by Single-Atomic Fe–N–C and Alloying to Boost CO-Tolerance of Pt in Hydrogen Oxidation, ACS Catalysis, 13 (2023) 7822-7830.

[180] M. Götz, H. Wendt, Binary and ternary anode catalyst formulations including the elements W, Sn and Mo for PEMFCs operated on methanol or reformate gas, Electrochim. Acta, 43 (1998) 3637-3644.

[181] D.C. Papageorgopoulos, M. Keijzer, J.B.J. Veldhuis, et al., CO Tolerance of Pd-Rich Platinum Palladium Carbon-Supported Electrocatalysts : Proton Exchange Membrane Fuel Cell Applications, J. Electrochem. Soc., 149 (2002) A1400.

[182] D.C. Papageorgopoulos, M. Keijzer, F.A. de Bruijn, The inclusion of Mo, Nb and Ta in Pt and PtRu carbon supported electrocatalysts in the quest for improved CO tolerant PEMFC anodes, Electrochim. Acta, 48 (2002) 197-204.

[183] C. Jin, Y. Liao, A. Zhang, et al., Low-Pt anodes with gradient molybdenum isomorphism for high performance and anti-CO poisoning PEMFCs, Nano Energy, 122 (2024) 109305.

[184] G. He, M. Dou, Progress on effect of hydrogen impurities on the performance of automotive fuel cells, Chemical Industry and Engineering Progress, 40 (2021) 4815-4822.

[185] M.-V. Mathieu, M. Primet, Sulfurization and regeneration of platinum, Applied Catalysis,

9 (1984) 361-370.

[186] R. Mohtadi, W.k. Lee, S. Cowan, et al., Effects of Hydrogen Sulfide on the Performance of a PEMFC, Electrochem. Solid-State Lett., 6 (2003) A272.

[187] E. Najdeker, E. Bishop, The formation and behaviour of platinum sulphide on platinum electrodes, Journal of Electroanalytical Chemistry and Interfacial Electrochemistry, 41 (1973) 79-87.

[188] I. Urdampilleta, F. Uribe, T. Rockward, et al., PEMFC Poisoning with H2S: Dependence on Operating Conditions, ECS Trans., 11 (2007) 831.

[189] F. Garzon, T. Lopes, T. Rockward, et al., The Impact of Impurities on Long-Term PEMFC Performance, ECS Trans., 25 (2009) 1575.

[190] R. Mohtadi, W.K. Lee, J.W. Van Zee, The effect of temperature on the adsorption rate of hydrogen sulfide on Pt anodes in a PEMFC, Applied Catalysis B: Environmental, 56 (2005) 37-42.

[191] B.K. Kakati, A.R.J. Kucernak, Gas phase recovery of hydrogen sulfide contaminated polymer electrolyte membrane fuel cells, J. Power Sources, 252 (2014) 317-326.

[192] L. Franck-Lacaze, C. Bonnet, S. Besse, et al., Effects of Ozone on the Performance of a Polymer Electrolyte Membrane Fuel Cell, Fuel Cells, 9 (2009) 562-569.

[193] W. Shi, B. Yi, M. Hou, et al., Hydrogen sulfide poisoning and recovery of PEMFC Pt-anodes, J. Power Sources, 165 (2007) 814-818.

[194] F.A. Uribe, S. Gottesfeld, T.A. Zawodzinski, Effect of Ammonia as Potential Fuel Impurity on Proton Exchange Membrane Fuel Cell Performance, J. Electrochem. Soc., 149 (2002) A293.

[195] R. Halseid, P.J.S. Vie, R. Tunold, Effect of ammonia on the performance of polymer electrolyte membrane fuel cells, J. Power Sources, 154 (2006) 343-350.

[196] Y.A. Gomez, A. Oyarce, G. Lindbergh, et al., Ammonia Contamination of a Proton Exchange Membrane Fuel Cell, J. Electrochem. Soc., 165 (2018) F189.

[197] X. Zhang, U. Pasaogullari, T. Molter, Influence of ammonia on membrane-electrode assemblies in polymer electrolyte fuel cells, Int. J. Hydrogen Energy, 34 (2009) 9188-9194.

[198] K. Hongsirikarn, in, Clemson University, United States -- South Carolina, 2010, pp. 254.

[199] D. Imamura, Y. Matsuda, Y. Hashimasa, et al., Effect of Ammonia Contained in Hydrogen Fuel on PEMFC Performance, ECS Trans., 41 (2011) 2083.

[200] R. Halseid, T. Bystroň, R. Tunold, Oxygen reduction on platinum in aqueous sulphuric acid in the presence of ammonium, Electrochim. Acta, 51 (2006) 2737-2742.

[201] J.C.M. Silva, S.G. da Silva, R.F.B. De Souza, et al., PtAu/C electrocatalysts as anodes for direct ammonia fuel cell, Applied Catalysis A: General, 490 (2015) 133-138.

[202] U. Misz, A. Talke, A. Heinzel, et al., Sensitivity Analyses on the Impact of Air Contaminants on Automotive Fuel Cells, Fuel Cells, 16 (2016) 444-462.

[203] J. St-Pierre, Proton exchange membrane fuel cell contamination model: Competitive adsorption followed by a surface segregated electrochemical reaction leading to an irreversibly adsorbed product, J. Power Sources, 195 (2010) 6379-6388.

[204] F. Jing, M. Hou, W. Shi, et al., The effect of ambient contamination on PEMFC performance, J. Power Sources, 166 (2007) 172-176.

[205] R. Mohtadi, W.k. Lee, J.W. Van Zee, Assessing durability of cathodes exposed to common air impurities, J. Power Sources, 138 (2004) 216-225.

[206] D. Imamura, E. Yamaguchi, Effect of Air Contaminants on the Electrolyte Degradation in Polymer Electrolyte Membrane Fuel Cells, ECS Trans., 25 (2009) 813.

[207] B.D. Gould, O.A. Baturina, K.E. Swider-Lyons, Deactivation of Pt/VC proton exchange membrane fuel cell cathodes by SO2, H2S and COS, J. Power Sources, 188 (2009) 89-95.

[208] M.I. Awad, M.M. Saleh, T. Ohsaka, Impact of SO2 poisoning of platinum nanoparticles modified glassy carbon electrode on oxygen reduction, J. Power Sources, 196 (2011) 3722-3728.

[209] O.A. Baturina, K.E. Swider-Lyons, Effect of SO2 on the Performance of the Cathode of a PEM Fuel Cell at 0.5–0.7 V, J. Electrochem. Soc., 156 (2009) B1423.

[210] Y. Liu, L. Du, F. Kong, et al., Sulfur Dioxide-Tolerant Bimetallic PtRu Catalyst toward Oxygen Electroreduction, ACS Sustainable Chemistry & Engineering, 8 (2020) 1295-1301.

[211] D. Pillay, M.D. Johannes, Y. Garsany, et al., Poisoning of Pt3Co Electrodes: A Combined Experimental and DFT Study, The Journal of Physical Chemistry C, 114 (2010) 7822-7830.

[212] D. Pillay, M.D. Johannes, Effect of S on Pt(111) and Pt3Ni(111) Surfaces: A First Principles Study, The Journal of Physical Chemistry C, 112 (2008) 1544-1551.

[213] M. Xia, Y. Liu, L. Li, et al., A DFT study on PtMo resistance to SO2 poisoning, Science China Chemistry, 56 (2013) 1004-1008.

[214] Y. Ye, B. Chi, S. Jiang, et al., Enhancing the Durability of Membrane Electrode Assembly of Proton Exchange Membrane Fuel Cells, Progress in Chemistry, 31 (2019) 1637-1652.

[215] S. Ahmad, T. Nawaz, A. Ali, et al., An overview of proton exchange membranes for fuel cells: Materials and manufacturing, Int. J. Hydrogen Energy, 47 (2022) 19086-19131.

[216] D. Qiu, L. Peng, X. Lai, et al., Mechanical failure and mitigation strategies for the

membrane in a proton exchange membrane fuel cell, Renewable and Sustainable Energy Reviews, 113 (2019) 109289.

[217] E. Bakangura, L. Wu, L. Ge, et al., Mixed matrix proton exchange membranes for fuel cells: State of the art and perspectives, Prog. Polym. Sci., 57 (2016) 103-152.

[218] H. Wang, J. Zhang, X. Ning, et al., Recent advances in designing and tailoring nanofiber composite electrolyte membranes for high-performance proton exchange membrane fuel cells, Int. J. Hydrogen Energy, 46 (2021) 25225-25251.

[219] J. Gao, X. Dong, Q. Tian, et al., Carbon nanotubes reinforced proton exchange membranes in fuel cells: An overview, Int. J. Hydrogen Energy, 48 (2023) 3216-3231.

[220] K.D. Baik, B.K. Hong, M.S. Kim, Effects of operating parameters on hydrogen crossover rate through Nafion® membranes in polymer electrolyte membrane fuel cells, Renewable Energy, 57 (2013) 234-239.

[221] C.-K. Hwang, K.A. Lee, J. Lee, et al., Perpendicularly stacked array of PTFE nanofibers as a reinforcement for highly durable composite membrane in proton exchange membrane fuel cells, Nano Energy, 101 (2022) 107581.

[222] M. Breitwieser, C. Klose, A. Hartmann, et al., Cerium Oxide Decorated Polymer Nanofibers as Effective Membrane Reinforcement for Durable, High-Performance Fuel Cells, Advanced Energy Materials, 7 (2017) 1602100.

[223] G. Zhao, L. Shi, M. Zhang, et al., Self-assembly of metal-organic framework onto nanofibrous mats to enhance proton conductivity for proton exchange membrane, Int. J. Hydrogen Energy, 46 (2021) 36415-36423.

[224] C. Yin, B. Xiong, Q. Liu, et al., Lateral-aligned sulfonated carbon-nanotubes/Nafion

composite membranes with high proton conductivity and improved mechanical properties, J. Membr. Sci., 591 (2019) 117356.

[225] L. Liu, X. Li, Z. Liu, et al., High-performance fuel cells using Nafion composite membranes with alignment of sulfonated graphene oxides induced by a strong magnetic field, J. Membr. Sci., 653 (2022) 120516.

[226] Z. Li, G. He, B. Zhang, et al., Enhanced Proton Conductivity of Nafion Hybrid Membrane under Different Humidities by Incorporating Metal–Organic Frameworks With High Phytic Acid Loading, ACS Appl. Mater. Interfaces, 6 (2014) 9799-9807.

[227] W. Zhengbang, H. Tang, P. Mu, Self-assembly of durable Nafion/TiO2 nanowire electrolyte membranes for elevated-temperature PEM fuel cells, J. Membr. Sci., 369 (2011) 250-257.

[228] Q. Lin, X. Sun, X. Chen, et al., Effect of Pretreatment on Microstructure and Mechanical Properties of Nafion™ XL Composite Membrane, Fuel Cells, 19 (2019) 530-538.

[229] S. Feng, Z. Zhong, Y. Wang, et al., Progress and perspectives in PTFE membrane: Preparation, modification, and applications, J. Membr. Sci., 549 (2018) 332-349.

[230] E. Dhanumalayan, G.M. Joshi, Performance properties and applications of polytetrafluoroethylene (PTFE)—a review, Advanced Composites and Hybrid Materials, 1 (2018) 247-268.

[231] A. Ranjbarzadeh-Dibazar, P. Shokrollahi, J. Barzin, et al., Lubricant facilitated thermo-mechanical stretching of PTFE and morphology of the resulting membranes, J. Membr. Sci., 470 (2014) 458-469.

[232] Q.-L. Huang, C.-f. Xiao, X.-s. Feng, et al., Design of super-hydrophobic microporous

polytetrafluoroethylene membranes, New J. Chem., 37 (2013) 373-379.

[233] T. Zhou, Y. Yao, R. Xiang, et al., Formation and characterization of polytetrafluoroethylene nanofiber membranes for vacuum membrane distillation, J. Membr. Sci., 453 (2014) 402-408.

[234] J. Cheng, Q. Huang, Y. Huang, et al., Study on a novel PTFE membrane with regular geometric pore structures fabricated by near-field electrospinning, and its applications, J. Membr. Sci., 603 (2020) 118014.

[235] L. Liu, H. Li, G. Avgouropoulos, A review of porous polytetrafluoroethylene reinforced sulfonic acid-based proton exchange membranes for fuel cells, Int. J. Hydrogen Energy, (2023).

[236] S. Shi, A.Z. Weber, A. Kusoglu, Structure/property relationship of Nafion XL composite membranes, J. Membr. Sci., 516 (2016) 123-134.

[237] A. Sadeghi Alavijeh, S. Bhattacharya, O. Thomas, et al., Effect of hygral swelling and shrinkage on mechanical durability of fuel cell membranes, J. Power Sources, 427 (2019) 207-214.

[238] Y. Tang, A. Kusoglu, A.M. Karlsson, et al., Mechanical properties of a reinforced composite polymer electrolyte membrane and its simulated performance in PEM fuel cells, J. Power Sources, 175 (2008) 817-825.

[239] Y.S. Noh, H.Y. Jeong, S.J. Yoon, et al., Multilayered hydrocarbon ionomer/PTFE composite electrolytes with enhanced performance for energy conversion devices, Int. J. Hydrogen Energy, 48 (2023) 5288-5300.

[240] L. Liu, Y. Xing, Z. Fu, et al., Biased Expanded Polytetrafluoroethylene Reinforced

Composite Membranes with Naturally Formed 3D Surface Structures for High-Performance Proton Exchange Membrane Fuel Cells, ACS Sustainable Chemistry & Engineering, 11 (2023) 6319-6331.

[241] M. Zatoń, J. Rozière, D.J. Jones, Current understanding of chemical degradation mechanisms of perfluorosulfonic acid membranes and their mitigation strategies: a review, Sustainable Energy & Fuels, 1 (2017) 409-438.

[242] C. Yin, J. Li, Y. Zhou, et al., Enhancement in Proton Conductivity and Thermal Stability in Nafion Membranes Induced by Incorporation of Sulfonated Carbon Nanotubes, ACS Appl. Mater. Interfaces, 10 (2018) 14026-14035.

[243] C. Klose, M. Breitwieser, S. Vierrath, et al., Electrospun sulfonated poly(ether ketone) nanofibers as proton conductive reinforcement for durable Nafion composite membranes, J. Power Sources, 361 (2017) 237-242.

[244] M. Breitwieser, C. Klose, M. Klingele, et al., Simple fabrication of 12 µm thin nanocomposite fuel cell membranes by direct electrospinning and printing, J. Power Sources, 337 (2017) 137-144.

[245] H.-Y. Li, Y.-L. Liu, Nafion-functionalized electrospun poly(vinylidene fluoride) (PVDF) nanofibers for high performance proton exchange membranes in fuel cells, Journal of Materials Chemistry A, 2 (2014) 3783-3793.

[246] R. Sood, S. Cavaliere, D.J. Jones, et al., Electrospun nanofibre composite polymer electrolyte fuel cell and electrolysis membranes, Nano Energy, 26 (2016) 729-745.

[247] S. Shahgaldi, I. Alaefour, X. Li, The impact of short side chain ionomer on polymer electrolyte membrane fuel cell performance and durability, Appl. Energy, 217 (2018) 295-302.

[248] Z. Rui, J. Liu, Understanding of free radical scavengers used in highly durable proton exchange membranes, Progress in Natural Science: Materials International, 30 (2020) 732-742.

[249] D.E. Curtin, R.D. Lousenberg, T.J. Henry, et al., Advanced materials for improved PEMFC performance and life, J. Power Sources, 131 (2004) 41-48.

[250] Y. Cheng, H. Tang, M. Pan, A strategy for facile durability improvement of perfluorosulfonic electrolyte for fuel cells: Counter ion-assisted decarboxylation at elevated temperatures, J. Power Sources, 198 (2012) 190-195.

[251] H. Ben youcef, D. Henkensmeier, S. Balog, et al., Copolymer synergistic coupling for chemical stability and improved gas barrier properties of a polymer electrolyte membrane for fuel cell applications, Int. J. Hydrogen Energy, 45 (2020) 7059-7068.

[252] H. Bai, H. Peng, Y. Xiang, et al., Poly(arylene piperidine)s with phosphoric acid doping as high temperature polymer electrolyte membrane for durable, high-performance fuel cells, J. Power Sources, 443 (2019) 227219.

[253] J. Miyake, R. Taki, T. Mochizuki, et al., Design of flexible polyphenylene proton-conducting membrane for next-generation fuel cells, Science Advances, 3 (2017).

[254] T. Kwon, Y. Lim, J. Cho, et al., Antioxidant technology for durability enhancement in polymer electrolyte membranes for fuel cell applications, Materials Today, 58 (2022) 135-163.

[255] D. Zhao, B.L. Yi, H.M. Zhang, et al., MnO2/SiO2–SO3H nanocomposite as hydrogen peroxide scavenger for durability improvement in proton exchange membranes, J. Membr. Sci., 346 (2010) 143-151.

[256] C. D'Urso, C. Oldani, V. Baglio, et al., Immobilized transition metal-based radical

scavengers and their effect on durability of Aquivion® perfluorosulfonic acid membranes, J. Power Sources, 301 (2016) 317-325.

[257] M.J. Parnian, S. Rowshanzamir, A.K. Prasad, et al., High durability sulfonated poly (ether ether ketone)-ceria nanocomposite membranes for proton exchange membrane fuel cell applications, J. Membr. Sci., 556 (2018) 12-22.

[258] Z. Wang, H. Tang, H. Zhang, et al., Synthesis of Nafion/CeO2 hybrid for chemically durable proton exchange membrane of fuel cell, J. Membr. Sci., 421-422 (2012) 201-210.

[259] D. Banham, S. Ye, T. Cheng, et al., Effect of CeOx Crystallite Size on the Chemical Stability of CeOx Nanoparticles, J. Electrochem. Soc., 161 (2014) F1075.

[260] P. Trogadas, J. Parrondo, V. Ramani, CeO2 Surface Oxygen Vacancy Concentration Governs in Situ Free Radical Scavenging Efficacy in Polymer Electrolytes, ACS Appl. Mater. Interfaces, 4 (2012) 5098-5102.

[261] M. Danilczuk, F.D. Coms, S. Schlick, Visualizing Chemical Reactions and Crossover Processes in a Fuel Cell Inserted in the ESR Resonator: Detection by Spin Trapping of Oxygen Radicals, Nafion-Derived Fragments, and Hydrogen and Deuterium Atoms, The Journal of Physical Chemistry B, 113 (2009) 8031-8042.

[262] B.P. Pearman, N. Mohajeri, R.P. Brooker, et al., The degradation mitigation effect of cerium oxide in polymer electrolyte membranes in extended fuel cell durability tests, J. Power Sources, 225 (2013) 75-83.

[263] K.R. Yoon, K.A. Lee, S. Jo, et al., Mussel-Inspired Polydopamine-Treated Reinforced Composite Membranes with Self-Supported CeOx Radical Scavengers for Highly Stable PEM Fuel Cells, Adv. Funct. Mater., 29 (2019) 1806929.

[264] S. Yang, D. Kim, Antioxidant proton conductive toughening agent for the hydrocarbon based proton exchange polymer membrane for enhanced cell performance and durability in fuel cell, J. Power Sources, 393 (2018) 11-18.

[265] A.M. Baker, L. Wang, W.B. Johnson, et al., Nafion Membranes Reinforced with Ceria-Coated Multiwall Carbon Nanotubes for Improved Mechanical and Chemical Durability in Polymer Electrolyte Membrane Fuel Cells, The Journal of Physical Chemistry C, 118 (2014) 26796-26802.

[266] M. Vinothkannan, S. Ramakrishnan, A.R. Kim, et al., Ceria Stabilized by Titanium Carbide as a Sustainable Filler in the Nafion Matrix Improves the Mechanical Integrity, Electrochemical Durability, and Hydrogen Impermeability of Proton-Exchange Membrane Fuel Cells: Effects of the Filler Content, ACS Appl. Mater. Interfaces, 12 (2020) 5704-5716.

[267] M. Zatoń, J. Rozière, D.J. Jones, Mitigation of PFSA membrane chemical degradation using composite cerium oxide–PFSA nanofibres, Journal of Materials Chemistry A, 5 (2017) 5390-5401.

[268] C. D'Urso, C. Oldani, V. Baglio, et al., Towards fuel cell membranes with improved lifetime: Aquivion® Perfluorosulfonic Acid membranes containing immobilized radical scavengers, J. Power Sources, 272 (2014) 753-758.

[269] V.R. Stamenkovic, B. Fowler, B.S. Mun, et al., Improved Oxygen Reduction Activity on Pt3Ni(111) via Increased Surface Site Availability, Science, 315 (2007) 493-497.

[270] G. Xu, L. Yang, J. Li, et al., Strategies for improving stability of Pt-based catalysts for oxygen reduction reaction, Advanced Sensor and Energy Materials, 2 (2023) 100058.

[271] X. Tian, J. Luo, H. Nan, et al., Transition Metal Nitride Coated with Atomic Layers of Pt as

a Low-Cost, Highly Stable Electrocatalyst for the Oxygen Reduction Reaction, J. Am. Chem. Soc., 138 (2016) 1575-1583.

[272] L. Gan, M. Heggen, S. Rudi, et al., Core–Shell Compositional Fine Structures of Dealloyed PtxNi1–x Nanoparticles and Their Impact on Oxygen Reduction Catalysis, Nano Lett., 12 (2012) 5423-5430.

[273] E. Zhu, M. Wu, H. Xu, et al., Stability of Platinum-Group-Metal-Based Electrocatalysts in Proton Exchange Membrane Fuel Cells, Adv. Funct. Mater., 32 (2022).

[274] M. Wang, X. Qin, K. Jiang, et al., Electrocatalytic Activities of Oxygen Reduction Reaction on Pd/C and Pd–B/C Catalysts, The Journal of Physical Chemistry C, 121 (2017) 3416-3423.

[275] Y. Xiong, Y. Ma, L. Zou, et al., N-doping induced tensile-strained Pt nanoparticles ensuring an excellent durability of the oxygen reduction reaction, J. Catal., 382 (2020) 247-255.

[276] B.-A. Lu, L.-F. Shen, J. Liu, et al., Structurally Disordered Phosphorus-Doped Pt as a Highly Active Electrocatalyst for an Oxygen Reduction Reaction, ACS Catalysis, 11 (2021) 355-363.

[277] W.-Z. Li, B.-A. Lu, L. Gan, et al., High activity and durability of carbon-supported core-shell PtPx@Pt/C catalyst for oxygen reduction reaction, Chinese Journal of Catalysis, 42 (2021) 2173-2180.

[278] A.R.J. Kucernak, K.F. Fahy, V.N.N. Sundaram, Facile synthesis of palladium phosphide electrocatalysts and their activity for the hydrogen oxidation, hydrogen evolutions, oxygen reduction and formic acid oxidation reactions, Catal. Today, 262 (2016) 48-56.

[279] T. He, W. Wang, X. Yang, et al., Deposition of Atomically Thin Pt Shells on Amorphous Palladium Phosphide Cores for Enhancing the Electrocatalytic Durability, ACS Nano, 15 (2021) 7348-7356.

[280] L. Zhang, K. Doyle-Davis, X. Sun, Pt-Based electrocatalysts with high atom utilization efficiency: from nanostructures to single atoms, Energy & Environmental Science, 12 (2019) 492-517.

[281] X. Wang, S.-I. Choi, L.T. Roling, et al., Palladium–platinum core-shell icosahedra with substantially enhanced activity and durability towards oxygen reduction, Nat. Commun., 6 (2015) 7594.

[282] X. Wang, M. Vara, M. Luo, et al., Pd@Pt Core–Shell Concave Decahedra: A Class of Catalysts for the Oxygen Reduction Reaction with Enhanced Activity and Durability, J. Am. Chem. Soc., 137 (2015) 15036-15042.

[283] J. Hu, L. Wu, K.A. Kuttiyiel, et al., Increasing Stability and Activity of Core–Shell Catalysts by Preferential Segregation of Oxide on Edges and Vertexes: Oxygen Reduction on Ti–Au@Pt/C, J. Am. Chem. Soc., 138 (2016) 9294-9300.

[284] L. Tao, B. Huang, F. Jin, et al., Atomic PdAu Interlayer Sandwiched into Pd/Pt Core/Shell Nanowires Achieves Superstable Oxygen Reduction Catalysis, ACS Nano, 14 (2020) 11570-11578.

[285] M. Xie, Z. Lyu, R. Chen, et al., Pt-Co@Pt Octahedral Nanocrystals: Enhancing Their Activity and Durability toward Oxygen Reduction with an Intermetallic Core and an Ultrathin Shell, J. Am. Chem. Soc., 143 (2021) 8509-8518.

[286] H. Abe, F. Matsumoto, L.R. Alden, et al., Electrocatalytic Performance of Fuel Oxidation

by Pt3Ti Nanoparticles, J. Am. Chem. Soc., 130 (2008) 5452-5458.

[287] J. Li, S. Sun, Intermetallic Nanoparticles: Synthetic Control and Their Enhanced Electrocatalysis, Acc. Chem. Res., 52 (2019) 2015-2025.

[288] W. Xiao, W. Lei, M. Gong, et al., Recent Advances of Structurally Ordered Intermetallic Nanoparticles for Electrocatalysis, ACS Catalysis, 8 (2018) 3237-3256.

[289] T.Y. Yoo, J.M. Yoo, A.K. Sinha, et al., Direct Synthesis of Intermetallic Platinum–Alloy Nanoparticles Highly Loaded on Carbon Supports for Efficient Electrocatalysis, J. Am. Chem. Soc., 142 (2020) 14190-14200.

[290] X. Zhao, C. Xi, R. Zhang, et al., High-Performance Nitrogen-Doped Intermetallic PtNi Catalyst for the Oxygen Reduction Reaction, ACS Catalysis, 10 (2020) 10637-10645.

[291] C. He, Z. Ma, Q. Wu, et al., Promoting the ORR catalysis of Pt-Fe intermetallic catalysts by increasing atomic utilization and electronic regulation, Electrochim. Acta, 330 (2020) 135119.

[292] J. Liang, N. Li, Z. Zhao, et al., Tungsten-Doped L10-PtCo Ultrasmall Nanoparticles as a High-Performance Fuel Cell Cathode, Angewandte Chemie International Edition, 58 (2019) 15471-15477.

[293] P. Gao, M. Pu, Q. Chen, et al., Pt-Based Intermetallic Nanocrystals in Cathode Catalysts for Proton Exchange Membrane Fuel Cells: From Precise Synthesis to Oxygen Reduction Reaction Strategy, Catalysts, 11 (2021).

[294] J. Liang, Z. Zhao, N. Li, et al., Biaxial Strains Mediated Oxygen Reduction Electrocatalysis on Fenton Reaction Resistant L10-PtZn Fuel Cell Cathode, Advanced Energy Materials, 10 (2020) 2000179.

[295] S. Zhu, L. Yang, J. Bai, et al., Ultra-stable Pt5La intermetallic compound towards highly efficient oxygen reduction reaction, Nano Research, 16 (2023) 2035-2040.

[296] V.T. Ho, C.J. Pan, J. Rick, et al., Nanostructured Ti(0.7)Mo(0.3)O2 support enhances electron transfer to Pt: high-performance catalyst for oxygen reduction reaction, J. Am. Chem. Soc., 133 (2011) 11716-11724.

[297] S. Zaman, M. Wang, H. Liu, et al., Carbon-based catalyst supports for oxygen reduction in proton-exchange membrane fuel cells, Trends in Chemistry, 4 (2022) 886-906.

[298] D. Liu, S. Gao, J. Xu, et al., Boron induced strong metal-support interaction for high sintering resistance of Pt-based catalysts toward oxygen reduction reaction, Appl. Surf. Sci., 604 (2022) 154466.

[299] G. Lin, Q. Ju, Y. Jin, et al., Suppressing Dissolution of Pt-Based Electrocatalysts through the Electronic Metal–Support Interaction, Advanced Energy Materials, 11 (2021) 2101050.

[300] W. Gao, Z. Zhang, M. Dou, et al., Highly Dispersed and Crystalline Ta2O5 Anchored Pt Electrocatalyst with Improved Activity and Durability Toward Oxygen Reduction: Promotion by Atomic-Scale Pt–Ta2O5 Interactions, ACS Catalysis, 9 (2019) 3278-3288.

[301] G.-Y. Kim, K.R. Yoon, K. Shin, et al., Black Tungsten Oxide Nanofiber as a Robust Support for Metal Catalysts: High Catalyst Loading for Electrochemical Oxygen Reduction, Small, 17 (2021) 2103755.

[302] S. Li, J. Liu, J. Liang, et al., Tuning oxygen vacancy in SnO2 inhibits Pt migration and agglomeration towards high-performing fuel cells, Applied Catalysis B: Environmental, 320 (2023) 122017.

[303] G. Lin, Q. Ju, Y. Jin, et al., Suppressing Dissolution of Pt-Based Electrocatalysts through

the Electronic Metal–Support Interaction, Advanced Energy Materials, 11 (2021).

[304] W. Gao, Z. Zhang, M. Dou, et al., Highly Dispersed and Crystalline Ta2O5 Anchored Pt Electrocatalyst with Improved Activity and Durability Toward Oxygen Reduction: Promotion by Atomic-Scale Pt-Ta2O5 Interactions, ACS Catalysis, 9 (2019) 3278-3288.

[305] S. Li, J. Liu, J. Liang, et al., Tuning oxygen vacancy in SnO2 inhibits Pt migration and agglomeration towards high-performing fuel cells, Applied Catalysis B: Environmental, 320 (2023).

[306] J.D. Sinniah, W.Y. Wong, K.S. Loh, et al., Perspectives on carbon-alternative materials as Pt catalyst supports for a durable oxygen reduction reaction in proton exchange membrane fuel cells, J. Power Sources, 534 (2022) 231422.

[307] P. Stonehart, Carbon substrates for phosphoric acid fuel cell cathodes, Carbon, 22 (1984) 423-431.

[308] F. Coloma, A. Sepúlveda-Escribano, F. Rodríguez-Reinoso, Heat-treated carbon-blacks as supports for platinum catalysts, J. Catal., 154 (1995) 299-305.

[309] J. Zhang, Y. Yuan, L. Gao, et al., Stabilizing Pt-Based Electrocatalysts for Oxygen Reduction Reaction: Fundamental Understanding and Design Strategies, Adv. Mater., 33 (2021) 2006494.

[310] Z. Qiao, C. Wang, Y. Zeng, et al., Advanced Nanocarbons for Enhanced Performance and Durability of Platinum Catalysts in Proton Exchange Membrane Fuel Cells, Small, 17 (2021) 2006805.

[311] Y. Li, Y. Li, E. Zhu, et al., Stabilization of High-Performance Oxygen Reduction Reaction Pt Electrocatalyst Supported on Reduced Graphene Oxide/Carbon Black Composite, J. Am.

Chem. Soc., 134 (2012) 12326-12329.

[312] W.S. Jung, B.N. Popov, Improved durability of Pt catalyst supported on N-doped mesoporous graphitized carbon for oxygen reduction reaction in polymer electrolyte membrane fuel cells, Carbon, 122 (2017) 746-755.

[313] B.T. Sneed, D.A. Cullen, K.S. Reeves, et al., 3D Analysis of Fuel Cell Electrocatalyst Degradation on Alternate Carbon Supports, ACS Appl Mater Interfaces, 9 (2017) 29839-29848.

[314] Y. Shao, Y. Cheng, W. Duan, et al., Nanostructured Electrocatalysts for PEM Fuel Cells and Redox Flow Batteries: A Selected Review, ACS Catalysis, 5 (2015) 7288-7298.

[315] Y.-J. Wang, B. Fang, H. Li, et al., Progress in modified carbon support materials for Pt and Pt-alloy cathode catalysts in polymer electrolyte membrane fuel cells, Progress in Materials Science, 82 (2016) 445-498.

[316] E. Antolini, E.R. Gonzalez, Ceramic materials as supports for low-temperature fuel cell catalysts, Solid State Ionics, 180 (2009) 746-763.

[317] C. Kok Poh, S. Hua Lim, Z. Tian, et al., Pt-WxC nano-composites as an efficient electrochemical catalyst for oxygen reduction reaction, Nano Energy, 2 (2013) 28-39.

[318] J.L. Bott-Neto, W. Beck, L.C. Varanda, et al., Electrocatalytic activity of platinum nanoparticles supported on different phases of tungsten carbides for the oxygen reduction reaction, Int. J. Hydrogen Energy, 42 (2017) 20677-20688.

[319] M. Begum, M. Yurukcu, F. Yurtsever, et al., Pt-Ni/WC Alloy Nanorods Arrays as ORR Catalyst for PEM Fuel Cells, ECS Trans., 80 (2017) 919.

[320] Y.N. Regmi, G.R. Waetzig, K.D. Duffee, et al., Carbides of group IVA, VA and VIA

transition metals as alternative HER and ORR catalysts and support materials, Journal of Materials Chemistry A, 3 (2015) 10085-10091.

[321] O. Lori, S. Gonen, L. Elbaz, Highly Active, Corrosion-Resistant Cathode for Fuel Cells, Based on Platinum and Molybdenum Carbide, J. Electrochem. Soc., 164 (2017) F825.

[322] L. Elbaz, J. Phillips, K. Artyushkova, et al., Evidence of High Electrocatalytic Activity of Molybdenum Carbide Supported Platinum Nanorafts, J. Electrochem. Soc., 162 (2015) H681.

[323] S. Saha, J.A. Cabrera Rodas, S. Tan, et al., Performance evaluation of platinum-molybdenum carbide nanocatalysts with ultralow platinum loading on anode and cathode catalyst layers of proton exchange membrane fuel cells, J. Power Sources, 378 (2018) 742-749.

[324] E.E. Valenzuela, O. Savadogo, Nanostructured TiO2 Doped with Nb as a Novel Support for PEM Fuel Cells, ECS Meeting Abstracts, MA2011-01 (2011) 1960.

[325] Y. Liu, J.M. Szeifert, J.M. Feckl, et al., Niobium-Doped Titania Nanoparticles: Synthesis and Assembly into Mesoporous Films and Electrical Conductivity, ACS Nano, 4 (2010) 5373-5381.

[326] M.T. Anwar, X. Yan, S. Shen, et al., Enhanced durability of Pt electrocatalyst with tantalum doped titania as catalyst support, Int. J. Hydrogen Energy, 42 (2017) 30750-30759.

[327] H. Choi, J. Kim, G. Lee, et al., Nb-doped TiO2 support with enhanced durability as a cathode for polymer electrolyte membrane fuel cells, Nanotechnology, 31 (2020) 03LT01.

[328] L. Dubau, F. Maillard, M. Chatenet, et al., Durability of Alternative Metal Oxide Supports for Application at a Proton-Exchange Membrane Fuel Cell Cathode—Comparison of Antimony- and Niobium-Doped Tin Oxide, Energies, 13 (2020) 403.

[329] K. Kakinuma, K. Suda, R. Kobayashi, et al., Electronic States and Transport Phenomena of Pt Nanoparticle Catalysts Supported on Nb-Doped SnO2 for Polymer Electrolyte Fuel Cells, ACS Appl. Mater. Interfaces, 11 (2019) 34957-34963.

[330] Y. Senoo, K. Taniguchi, K. Kakinuma, et al., Cathodic performance and high potential durability of Ta-SnO2−δ-supported Pt catalysts for PEFC cathodes, Electrochem. Commun., 51 (2015) 37-40.

[331] J.M. Kim, Y.J. Lee, S.-h. Kim, et al., High-performance corrosion-resistant fluorine-doped tin oxide as an alternative to carbon support in electrodes for PEM fuel cells, Nano Energy, 65 (2019) 104008.

[332] P.K. Mohanta, C. Glökler, A.O. Arenas, et al., Sb doped SnO2 as a stable cathode catalyst support for low temperature polymer electrolyte membrane fuel cell, Int. J. Hydrogen Energy, 42 (2017) 27950-27961.

[333] K. Kakinuma, M. Uchida, T. Kamino, et al., Synthesis and electrochemical characterization of Pt catalyst supported on Sn0.96Sb0.04O2−δ with a network structure, Electrochim. Acta, 56 (2011) 2881-2887.

[334] I. Jiménez-Morales, F. Haidar, S. Cavaliere, et al., Strong Interaction between Platinum Nanoparticles and Tantalum-Doped Tin Oxide Nanofibers and Its Activation and Stabilization Effects for Oxygen Reduction Reaction, ACS Catalysis, 10 (2020) 10399-10411.

[335] C. Yao, F. Li, X. Li, et al., Fiber-like nanostructured Ti4O7 used as durable fuel cell catalyst support in oxygen reduction catalysis, J. Mater. Chem., 22 (2012) 16560-16565.

[336] Q. Li, L. Li, X. Yu, et al., Ultrafine platinum particles anchored on porous boron nitride enabling excellent stability and activity for oxygen reduction reaction, Chem. Eng. J., 399

(2020) 125827.

[337] H. Nan, D. Dang, X.L. Tian, Structural engineering of robust titanium nitride as effective platinum support for the oxygen reduction reaction, Journal of Materials Chemistry A, 6 (2018) 6065-6073.

[338] Z. Pan, Y. Xiao, Z. Fu, et al., Hollow and porous titanium nitride nanotubes as high-performance catalyst supports for oxygen reduction reaction, Journal of Materials Chemistry A, 2 (2014) 13966-13975.

[339] A. Perego, G. Giuffredi, P. Mazzolini, et al., Hierarchical TiN Nanostructured Thin Film Electrode for Highly Stable PEM Fuel Cells, ACS Applied Energy Materials, 2 (2019) 1911-1922.

[340] T.K. Chin, M.W. Liao, T.P. Perng, Enabling higher electrochemical activity of Pt nanoparticles uniformly coated on cubic titanium oxynitride by vertical forced-flow atomic layer deposition, J. Power Sources, 434 (2019).

[341] Y. Xiao, G. Zhan, Z. Fu, et al., Titanium cobalt nitride supported platinum catalyst with high activity and stability for oxygen reduction reaction, J. Power Sources, 284 (2015) 296-304.

[342] T.-K. Chin, M.-W. Liao, T.-P. Perng, Enabling higher electrochemical activity of Pt nanoparticles uniformly coated on cubic titanium oxynitride by vertical forced-flow atomic layer deposition, J. Power Sources, 434 (2019) 226716.

[343] V.T.T. Ho, C.J. Pan, J. Rick, et al., Nanostructured Ti0.7Mo0.3O2 support enhances electron transfer to Pt: High-performance catalyst for oxygen reduction reaction, J. Am. Chem. Soc., 133 (2011) 11716-11724.

[344] H. Liu, C. Koenigsmann, R.R. Adzic, et al., Probing ultrathin one-dimensional Pd-Ni nanostructures as oxygen reduction reaction catalysts, ACS Catalysis, 4 (2014) 2544-2555.

[345] X. Tian, J. Luo, H. Nan, et al., Binary transition metal nitrides with enhanced activity and durability for the oxygen reduction reaction, Journal of Materials Chemistry A, 3 (2015) 16801-16809.

[346] S. Jiang, B. Yi, H. Zhang, et al., Vertically Aligned Titanium Nitride Nanorod Arrays as Supports of Platinum-Palladium-Cobalt Catalysts for Thin-Film Proton Exchange Membrane Fuel Cell Electrodes, ChemElectroChem, 3 (2016) 734-740.

[347] X. Yang, L. Qin, L. Wang, et al., Scalable synthesis of quasi-monodispersed BN colloidal nanocrystals by “solvent cutting” and their anti-electrochemical corrosion coating, Chem. Eng. J., 333 (2018) 191-199.

[348] L. Fan, Z. Tu, S.H. Chan, Recent development of hydrogen and fuel cell technologies: A review, Energy Reports, 7 (2021) 8421-8446.

[349] R. Taherian, RETRACTED: A review of composite and metallic bipolar plates in proton exchange membrane fuel cell: Materials, fabrication, and material selection, J. Power Sources, 265 (2014) 370-390.

[350] X. Gao, J. Chen, R. Xu, et al., Research progress and prospect of the materials of bipolar plates for proton exchange membrane fuel cells (PEMFCs), Int. J. Hydrogen Energy, 50 (2024) 711-743.

[351] Z. Xu, D. Qiu, P. Yi, et al., Towards mass applications: A review on the challenges and developments in metallic bipolar plates for PEMFC, Progress in Natural Science: Materials International, 30 (2020) 815-824.

[352] N. Pilinski, C. Käding, A. Dushina, et al., Investigation of Corrosion Methods for Bipolar Plates for High Temperature Polymer Electrolyte Membrane Fuel Cell Application, Periodical 13 (2020).

[353] F. Bi, X. Li, P. Yi, et al., Characteristics of amorphous carbon films to resist high potential impact in PEMFCs bipolar plates for automotive application, Int. J. Hydrogen Energy, 42 (2017) 14279-14289.

[354] M. Kumagai, S.-T. Myung, S. Kuwata, et al., Corrosion behavior of austenitic stainless steels as a function of pH for use as bipolar plates in polymer electrolyte membrane fuel cells, Electrochim. Acta, 53 (2008) 4205-4212.

[355] V. Modanloo, H. Talebi-Ghadikolaee, V. Alimirzaloo, et al., Fracture prediction in the stamping of titanium bipolar plate for PEM fuel cells, Int. J. Hydrogen Energy, 46 (2021) 5729-5739.

[356] U.K. Chanda, A. Behera, S. Roy, et al., Evaluation of Ni-Cr-P coatings electrodeposited on low carbon steel bipolar plates for polymer electrolyte membrane fuel cell, Int. J. Hydrogen Energy, 43 (2018) 23430-23440.

[357] M. Zhang, K.H. Kim, Z. Shao, et al., Effects of Mo content on microstructure and corrosion resistance of arc ion plated Ti–Mo–N films on 316L stainless steel as bipolar plates for polymer exchange membrane fuel cells, J. Power Sources, 253 (2014) 201-204.

[358] X.-Z. Wang, M.-M. Zhang, D.-D. Shi, et al., Long-term polarization accelerated degradation of nano-thin C/Ti coated SS316L bipolar plates used in polymer electrolyte membrane fuel cells, Int. J. Hydrogen Energy, 47 (2022) 8974-8992.

[359] Q. Jia, Z. Mu, X. Zhang, et al., Electronic conductive and corrosion mechanisms of dual

nanostructure CuCr-doped hydrogenated carbon films for SS316L bipolar plates, Materials Today Chemistry, 21 (2021) 100521.

[360] G. Ma, J. Yuan, R. Chen, et al., Balancing the corrosion resistance and conductivity of Cr-Al-C coatings via annealing treatment for metal bipolar plates, Appl. Surf. Sci., 597 (2022) 153670.

[361] X. Li, L. Peng, D. Zhang, et al., The frequency of pulsed DC sputtering power introducing the graphitization and the durability improvement of amorphous carbon films for metallic bipolar plates in proton exchange membrane fuel cells, J. Power Sources, 466 (2020) 228346.

[362] P. Yi, D. Zhang, L. Peng, et al., Impact of Film Thickness on Defects and the Graphitization of Nanothin Carbon Coatings Used for Metallic Bipolar Plates in Proton Exchange Membrane Fuel Cells, ACS Appl. Mater. Interfaces, 10 (2018) 34561-34572.

[363] P. Yi, L. Peng, T. Zhou, et al., Composition optimization of multilayered chromium-nitride–carbon film on 316L stainless steel as bipolar plates for proton exchange membrane fuel cells, J. Power Sources, 236 (2013) 47-53.

[364] J. Jin, J. Zhang, M. Hu, et al., Investigation of high potential corrosion protection with titanium carbonitride coating on 316L stainless steel bipolar plates, Corros. Sci., 191 (2021) 109757.

[365] S. Wang, M. Hou, Q. Zhao, et al., Ti/(Ti,Cr)N/CrN multilayer coated 316L stainless steel by arc ion plating as bipolar plates for proton exchange membrane fuel cells, Journal of Energy Chemistry, 26 (2017) 168-174.

[366] T. Li, P.C. Zhang, K. Liu, et al., Performance of Tantalum Modified 316L Stainless Steel Bipolar Plate for Proton Exchange Membrane Fuel Cell, Fuel Cells, 19 (2019) 724-730.

[367] Z. Dong, T. Zhou, J. Liu, et al., Performance of surface chromizing layer on 316L stainless steel for proton exchange membrane fuel cell bipolar plates, Int. J. Hydrogen Energy, 44 (2019) 22110-22121.

[368] L. Wang, Y. Tao, Z. Zhang, et al., Molybdenum carbide coated 316L stainless steel for bipolar plates of proton exchange membrane fuel cells, Int. J. Hydrogen Energy, 44 (2019) 4940-4950.

[369] J. Li, Z. Xu, Y. Li, et al., Intergranular passivation of the TiC coating for enhancing corrosion resistance and surface conductivity in stainless-steel bipolar plates, J. Mater. Sci., 56 (2021) 8689-8703.

[370] F. Yan, B. Jiang, Z. Wang, et al., Thermal stabilization of nanocrystalline promoting conductive corrosion resistance of TiN–Ag films for metal bipolar plates, Vacuum, 195 (2022) 110631.

[371] W.-J. Lee, E.-Y. Yun, H.-B.-R. Lee, et al., Ultrathin effective TiN protective films prepared by plasma-enhanced atomic layer deposition for high performance metallic bipolar plates of polymer electrolyte membrane fuel cells, Appl. Surf. Sci., 519 (2020) 146215.

[372] H. Wang, J.A. Turner, Electrochemical nitridation of a stainless steel for PEMFC bipolar plates, Int. J. Hydrogen Energy, 36 (2011) 13008-13013.

[373] A.V. Ingle, V.S. Raja, J. Rangarajan, et al., Corrosion resistant quaternary Al–Cr–Mo–N coating on type 316L stainless steel bipolar plates for proton exchange membrane fuel cells, Int. J. Hydrogen Energy, 45 (2020) 3094-3107.

[374] N. Huang, C. Liang, H. Wang, et al., Corrosion Behavior of Passivated 316LSS with Ag Coating as PEMFC Bipolar Plate, International Journal of Corrosion, 2011 (2011) 103785.

[375] X.-Z. Wang, C.-P. Ye, D.-D. Shi, et al., Potential polarization accelerated degradation of interfacial electrical conductivity for Au/TiN coated 316L SS bipolar plates used in polymer electrolyte membrane fuel cells, Corros. Sci., 189 (2021) 109624.

[376] A. Kumar, M. Ricketts, S. Hirano, Ex situ evaluation of nanometer range gold coating on stainless steel substrate for automotive polymer electrolyte membrane fuel cell bipolar plate, J. Power Sources, 195 (2010) 1401-1407.

[377] W. Yoon, X. Huang, P. Fazzino, et al., Evaluation of coated metallic bipolar plates for polymer electrolyte membrane fuel cells, J. Power Sources, 179 (2008) 265-273.

[378] L. Fan, Z. Tu, S.H. Chan, Recent development in design a state-of-art proton exchange membrane fuel cell from stack to system: Theory, integration and prospective, Int. J. Hydrogen Energy, 48 (2023) 7828-7865.

[379] K. Jiao, X. Li, Water transport in polymer electrolyte membrane fuel cells, Progr. Energy Combust. Sci., 37 (2011) 221-291.

[380] Y. Tang, W. Yuan, M. Pan, et al., Feasibility study of porous copper fiber sintered felt: A novel porous flow field in proton exchange membrane fuel cells, Int. J. Hydrogen Energy, 35 (2010) 9661-9677.

[381] B.R. Friess, M. Hoorfar, Development of a novel radial cathode flow field for PEMFC, Int. J. Hydrogen Energy, 37 (2012) 7719-7729.

[382] S. Maharudrayya, S. Jayanti, A.P. Deshpande, Flow distribution and pressure drop in parallel-channel configurations of planar fuel cells, J. Power Sources, 144 (2005) 94-106.

[383] D.H. Jeon, S. Greenway, S. Shimpalee, et al., The effect of serpentine flow-field designs on PEM fuel cell performance, Int. J. Hydrogen Energy, 33 (2008) 1052-1066.

[384] J.P. Feser, A.K. Prasad, S.G. Advani, On the relative influence of convection in serpentine flow fields of PEM fuel cells, J. Power Sources, 161 (2006) 404-412.

[385] Y. Wu, J.I.S. Cho, T.P. Neville, et al., Effect of serpentine flow-field design on the water management of polymer electrolyte fuel cells: An in-operando neutron radiography study, J. Power Sources, 399 (2018) 254-263.

[386] I. khazaee, H. Sabadbafan, Effect of humidity content and direction of the flow of reactant gases on water management in the 4-serpentine and 1-serpentine flow channel in a PEM (proton exchange membrane) fuel cell, Energy, 101 (2016) 252-265.

[387] Q. Liu, F. Lan, C. Zeng, et al., A review of proton exchange membrane fuel cell's bipolar plate design and fabrication process, J. Power Sources, 538 (2022).

[388] C.W. Wu, W. Zhang, X. Han, et al., A systematic review for structure optimization and clamping load design of large proton exchange membrane fuel cell stack, J. Power Sources, 476 (2020) 228724.

[389] N. Akhtar, P.J.A.M. Kerkhof, Effect of channel and rib width on transport phenomena within the cathode of a proton exchange membrane fuel cell, Int. J. Hydrogen Energy, 36 (2011) 5536-5549.

[390] S. Lee, H. Jeong, B. Ahn, et al., Parametric study of the channel design at the bipolar plate in PEMFC performances, Int. J. Hydrogen Energy, 33 (2008) 5691-5696.

[391] Y.G. Yoon, W.Y. Lee, G.G. Park, et al., in: Int. J. Hydrogen Energy, 2005, pp. 1363-1366.

[392] W.-J. Yang, H.-Y. Wang, D.-H. Lee, et al., Channel geometry optimization of a polymer electrolyte membrane fuel cell using genetic algorithm, Appl. Energy, 146 (2015) 1-10.

[393] G. Varghese, V.B. K. P, T.V. Joseph, et al., Combined effect of channel to rib width ratio and gas diffusion layer deformation on high temperature – Polymer electrolyte membrane fuel cell performance, Int. J. Hydrogen Energy, 47 (2022) 33014-33026.

[394] Y. Kerkoub, A. Benzaoui, F. Haddad, et al., Channel to rib width ratio influence with various flow field designs on performance of PEM fuel cell, Energy Conversion and Management, 174 (2018) 260-275.

[395] L. Sun, P.H. Oosthuizen, K.B. McAuley, A numerical study of channel-to-channel flow cross-over through the gas diffusion layer in a PEM-fuel-cell flow system using a serpentine channel with a trapezoidal cross-sectional shape{star, open}{star, open}A preliminary version of this paper was presented at ICMM05: Third International Conference on Microchannels and Minichannels, held at University of Toronto, June 13-15, 2005, International Journal of Thermal Sciences, 45 (2006) 1021-1026.

[396] X.D. Wang, G. Lu, Y.Y. Duan, et al., in: Int. J. Hydrogen Energy, 2012, pp. 15778-15786.

[397] D.H. Ahmed, H.J. Sung, Effects of channel geometrical configuration and shoulder width on PEMFC performance at high current density, J. Power Sources, 162 (2006) 327-339.

[398] X. Zhu, Q. Liao, P.C. Sui, et al., Numerical investigation of water droplet dynamics in a low-temperature fuel cell microchannel: Effect of channel geometry, J. Power Sources, 195 (2010) 801-812.

[399] A. Mohammedi, Y. Sahli, H. Ben Moussa, 3D investigation of the channel cross-section configuration effect on the power delivered by PEMFCs with straight channels, Fuel, 263 (2020).

[400] Y. Zhou, B. Chen, Investigation of optimization and evaluation criteria for flow field in proton exchange membrane fuel cell: A critical review, Renewable and Sustainable Energy Reviews, 185 (2023) 113584.

[401] F. Mojica, M.A. Rahman, M. Sarker, et al., Study of converging-diverging channel induced convective mass transport in a proton exchange membrane fuel cell, Energy Conversion and Management, 237 (2021) 114095.

[402] Y. Zhou, B. Chen, W. Chen, et al., A novel opposite sinusoidal wave flow channel for performance enhancement of proton exchange membrane fuel cell, Energy, 261 (2022).

[403] Y. Zhou, K. Meng, W. Chen, et al., Experimental performance of proton exchange membrane fuel cell with novel flow fields and numerical investigation of water-gas transport enhancement, Energy Conversion and Management, 281 (2023).

[404] N. Akhtar, P.J.A.M. Kerkhof, Dynamic behavior of liquid water transport in a tapered channel of a proton exchange membrane fuel cell cathode, Int. J. Hydrogen Energy, 36 (2011) 3076-3086.

[405] J.N. Qiao, H. Guo, H. Chen, et al., Improving round-trip energy efficiency of a unitized regenerative fuel cell by adopting staircase flow channel and counter flow configuration, Energy Conversion and Management, 271 (2022).

[406] X. Chen, Z. Yu, C. Yang, et al., Performance investigation on a novel 3D wave flow channel design for PEMFC, Int. J. Hydrogen Energy, 46 (2021) 11127-11139.

[407] A. Ghanbarian, M.J. Kermani, Enhancement of PEM fuel cell performance by flow channel indentation, Energy Conversion and Management, 110 (2016) 356-366.

[408] A.A. Ebrahimzadeh, I. Khazaee, A. Fasihfar, Experimental and numerical investigation of

obstacle effect on the performance of PEM fuel cell, Int. J. Heat Mass Transfer, 141 (2019) 891-904.

[409] H. Heidary, M.J. Kermani, S.G. Advani, et al., in: Int. J. Hydrogen Energy, 2016, pp. 6885-6893.

[410] H. Heidary, M.J. Kermani, A.K. Prasad, et al., Numerical modelling of in-line and staggered blockages in parallel flowfield channels of PEM fuel cells, Int. J. Hydrogen Energy, 42 (2017) 2265-2277.

[411] Y. Wang, C. Guan, P. Zhang, et al., Optimal design of a cathode flow field with a new arrangement of baffle plates for a high clean power generation of a polymer electrolyte membrane fuel cell, Journal of Cleaner Production, 375 (2022).

[412] S.W. Perng, H.W. Wu, Non-isothermal transport phenomenon and cell performance of a cathodic PEM fuel cell with a baffle plate in a tapered channel, Appl. Energy, 88 (2011) 52-67.

[413] H. Chen, H. Guo, F. Ye, et al., An experimental study of cell performance and pressure drop of proton exchange membrane fuel cells with baffled flow channels, J. Power Sources, 472 (2020).

[414] Y. Yin, S. Wu, Y. Qin, et al., Quantitative analysis of trapezoid baffle block sloping angles on oxygen transport and performance of proton exchange membrane fuel cell, Appl. Energy, 271 (2020).

[415] J.P. Kloess, X. Wang, J. Liu, et al., Investigation of bio-inspired flow channel designs for bipolar plates in proton exchange membrane fuel cells, J. Power Sources, 188 (2009) 132-140.

[416] R. Roshandel, F. Arbabi, G.K. Moghaddam, Simulation of an innovative flow-field design

based on a bio inspired pattern for PEM fuel cells, Renewable Energy, 41 (2012) 86-95.

[417] S. Liu, T. Chen, Y. Xie, et al., Numerical simulation and experimental study on the effect of symmetric and asymmetric bionic flow channels on PEMFC performance under gravity, Int. J. Hydrogen Energy, 44 (2019) 29618-29630.

[418] H.C. Kang, K.M. Jum, Y.J. Sohn, Performance of unit PEM fuel cells with a leaf-vein-simulating flow field-patterned bipolar plate, Int. J. Hydrogen Energy, 44 (2019) 24036-24042.

[419] N. Guo, M.C. Leu, U.O. Koylu, Bio-inspired flow field designs for polymer electrolyte membrane fuel cells, Int. J. Hydrogen Energy, 39 (2014) 21185-21195.

[420] S. Kjelstrup, M.O. Coppens, J.G. Pharoah, et al., in: Energy and Fuels, 2010, pp. 5097-5108.

[421] M. Asadzade, A. Shamloo, Design and simulation of a novel bipolar plate based on lung-shaped bio-inspired flow pattern for PEM fuel cell, International Journal of Energy Research, 41 (2017) 1730-1739.

[422] J.I.S. Cho, J. Marquis, P. Trogadas, et al., Optimizing the architecture of lung-inspired fuel cells, Chem. Eng. Sci., 215 (2020) 115375.

[423] S.M. Senn, D. Poulikakos, Laminar mixing, heat transfer and pressure drop in tree-like microchannel nets and their application for thermal management in polymer electrolyte fuel cells, J. Power Sources, 130 (2004) 178-191.

[424] D. Lorenzini-Gutierrez, A. Hernandez-Guerrero, B. Ramos-Alvarado, et al., Performance analysis of a proton exchange membrane fuel cell using tree-shaped designs for flow distribution, Int. J. Hydrogen Energy, 38 (2013) 14750-14763.

[425] C.E. Damian-Ascencio, A. Saldaña-Robles, A. Hernandez-Guerrero, et al., Numerical modeling of a proton exchange membrane fuel cell with tree-like flow field channels based on an entropy generation analysis, Energy, 133 (2017) 306-316.

[426] M. Sauermoser, B.G. Pollet, N. Kizilova, et al., Scaling factors for channel width variations in tree-like flow field patterns for polymer electrolyte membrane fuel cells - An experimental study, Int. J. Hydrogen Energy, 46 (2021) 19554-19568.

[427] S. Zhang, S. Liu, H. Xu, et al., Performance of proton exchange membrane fuel cells with honeycomb-like flow channel design, Energy, 239 (2022).

[428] Y. Wang, C. Si, Y. Qin, et al., Bio-inspired design of an auxiliary fishbone-shaped cathode flow field pattern for polymer electrolyte membrane fuel cells, Energy Conversion and Management, 227 (2021) 113588.

[429] X. Xie, B. Yin, S. Xu, et al., Effects of microstructure shape parameters on water removal in a PEMFC lotus-like flow channel, Int. J. Hydrogen Energy, 47 (2022) 3473-3483.

[430] J. Wang, Theory and practice of flow field designs for fuel cell scaling-up: A critical review, Appl. Energy, 157 (2015) 640-663.

[431] F. Huang, D. Qiu, S. Lan, et al., Performance evaluation of commercial-size proton exchange membrane fuel cell stacks considering air flow distribution in the manifold, Energy Conversion and Management, 203 (2020) 112256.

[432] J. Wang, Barriers of scaling-up fuel cells: Cost, durability and reliability, Energy, 80 (2015) 509-521.

[433] H. Guo, M.H. Wang, J.X. Liu, et al., Temperature distribution on anodic surface of membrane electrode assembly in proton exchange membrane fuel cell with interdigitated flow

bed, J. Power Sources, 273 (2015) 775-783.

[434] D. Shi, L. Cai, C. Zhang, et al., Fabrication methods, structure design and durability analysis of advanced sealing materials in proton exchange membrane fuel cells, Chem. Eng. J., 454 (2023) 139995.

[435] R.-J. Yin, W.-C. Zeng, F. Bai, et al., Study on the effects of manifold structure on the gas flow distribution uniformity of anode of PEMFC stack with 140-cell, Renewable Energy, 221 (2024) 119693.

[436] J. Wang, Theory of flow distribution in manifolds, Chem. Eng. J., 168 (2011) 1331-1345.

[437] H. Liu, P. Li, Maintaining equal operating conditions for all cells in a fuel cell stack using an external flow distributor, Int. J. Hydrogen Energy, 38 (2013) 3757-3766.

[438] B.H. Lim, E.H. Majlan, W.R.W. Daud, et al., Effects of flow field design on water management and reactant distribution in PEMFC: a review, Ionics, 22 (2016) 301-316.

[439] J. Wang, H. Wang, Discrete method for design of flow distribution in manifolds, Applied Thermal Engineering, 89 (2015) 927-945.

[440] G. Su, D. Yang, Q. Xiao, et al., Effects of vortexes in feed header on air flow distribution of PEMFC stack: CFD simulation and optimization for better uniformity, Renewable Energy, 173 (2021) 498-506.

[441] R.J. Kee, P. Korada, K. Walters, et al., A generalized model of the flow distribution in channel networks of planar fuel cells, J. Power Sources, 109 (2002) 148-159.

[442] J.-H. Koh, H.-K. Seo, C.G. Lee, et al., Pressure and flow distribution in internal gas manifolds of a fuel-cell stack, J. Power Sources, 115 (2003) 54-65.

[443] W. Zhang, P. Hu, X. Lai, et al., Analysis and optimization of flow distribution in

parallel-channel configurations for proton exchange membrane fuel cells, J. Power Sources, 194 (2009) 931-940.

[444] R.A. Bajura, A Model for Flow Distribution in Manifolds, Journal of Engineering for Power, 93 (1971) 7-12.

[445] M.K. Bassiouny, H. Martin, Flow distribution and pressure drop in plate heat exchangers—I U-type arrangement, Chem. Eng. Sci., 39 (1984) 693-700.

[446] A. Acrivos, B.D. Babcock, R.L. Pigford, Flow distributions in manifolds, Chem. Eng. Sci., 10 (1959) 112-124.

[447] M.K. Bassiouny, H. Martin, Flow distribution and pressure drop in plate heat exchangers—II Z-type arrangement, Chem. Eng. Sci., 39 (1984) 701-704.

[448] F. Huang, D. Qiu, Z. Xu, et al., Analysis and improvement of flow distribution in manifold for proton exchange membrane fuel cell stacks, Energy, 226 (2021) 120427.

[449] J. Wang, H. Wang, Flow-Field Designs of Bipolar Plates in PEM Fuel Cells: Theory and Applications, Fuel Cells, 12 (2012) 989-1003.

[450] N. Midoux, D. Tondeur, The theory of parallel channels manifolds (Ladder networks) revisited part 1: Discrete mesoscopic modelling, The Canadian Journal of Chemical Engineering, 92 (2014) 1798-1821.

[451] N. Midoux, D. Tondeur, The theory of parallel channels manifolds (ladder networks) revisited part 2: Design for uniform cross-flow distribution, The Canadian Journal of Chemical Engineering, 93 (2015) 121-140.

[452] W. Pan, Z. Chen, X. Chen, et al., Analytical and numerical investigation of flow distribution in PEMFC stacks, Chem. Eng. J., 450 (2022) 137598.

[453] C.-H. Chen, S.-P. Jung, S.-C. Yen, Flow distribution in the manifold of PEM fuel cell stack, J. Power Sources, 173 (2007) 249-263.

[454] F. Huang, D. Qiu, L. Peng, et al., Optimization of entrance geometry and analysis of fluid distribution in manifold for high-power proton exchange membrane fuel cell stacks, Int. J. Hydrogen Energy, 47 (2022) 22180-22191.

[455] W. Lu, W. Pan, Z. Chen, et al., Structural optimization of distribution zone for large-sized PEMFC with high power density, Chem. Eng. Sci., 276 (2023) 118803.

[456] W. Pan, B. Wang, L. Tang, et al., A novel design of distribution zone in scaled-up PEM fuel cells based on active control of transverse flow, AIChE J., 69 (2023) e18178.

[457] Y. Qin, G. Liu, Y. Chang, et al., Modeling and design of PEM fuel cell stack based on a flow network method, Applied Thermal Engineering, 144 (2018) 411-423.

[458] B. Müller, S. Fischer, Epoxy ester resins as corrosion inhibitors for aluminium and zinc pigments, Corros. Sci., 48 (2006) 2406-2416.

[459] S. Müller, M. Kästner, J. Brummund, et al., A nonlinear fractional viscoelastic material model for polymers, Computational Materials Science, 50 (2011) 2938-2949.

[460] H.N. Yu, S.S. Kim, J.D. Suh, et al., Composite endplates with pre-curvature for PEMFC (polymer electrolyte membrane fuel cell), Composite Structures, 92 (2010) 1498-1503.

[461] Y.H. Yu, J.W. Lim, D.G. Lee, Composite sandwich endplates with a compliant pressure distributor for a PEM fuel cell, Composite Structures, 119 (2015) 505-512.

[462] G.M. Evertz J, Tribecraft A G., in: 2nd European PEFC Forum, Lucerne, Switzerland, 2003, pp. 469-482.

[463] B. Liu, M.Y. Wei, G.J. Ma, et al., Stepwise optimization of endplate of fuel cell stack

assembled by steel belts, Int. J. Hydrogen Energy, 41 (2016) 2911-2918.

[464] C.W. Wu, B. Liu, M.Y. Wei, et al., Mechanical response of a large fuel cell stack to impact: A numerical analysis, Fuel Cells, 15 (2015) 344-351.

[465] D. Qiu, P. Liang, L. Peng, et al., Material behavior of rubber sealing for proton exchange membrane fuel cells, Int. J. Hydrogen Energy, 45 (2020) 5465-5473.

[466] T. Cui, C.W. Lin, C.H. Chien, et al., Service life estimation of liquid silicone rubber seals in polymer electrolyte membrane fuel cell environment, J. Power Sources, 196 (2011) 1216-1221.

[467] B. Späth, T. Brückle, Seals for plastic components - Integrated seals contribute to greater functionality of plastic components, Sealing Technology, 2005 (2005) 6-7.

[468] S. Bhargava, K.A. O'Leary, T.C. Jackson, et al., Durability testing of silicone materials for proton exchange membrane fuel cell use, Rubber Chem. Technol., 86 (2013) 28-37.

[469] C.W. Lin, C.H. Chien, J. Tan, et al., Chemical degradation of five elastomeric seal materials in a simulated and an accelerated PEM fuel cell environment, J. Power Sources, 196 (2011) 1955-1966.

[470] G. Li, J.Z. Tan, J.M. Gong, Chemical Degradation of the Silicone Rubber in Simulated PEMFC Environments, Advanced Materials Research, 197-198 (2011) 741-748.

[471] F. Wu, B. Chen, Y. Yan, et al., Degradation of silicone rubbers as sealing materials for proton exchange membrane fuel cells under temperature cycling, Polymers, 10 (2018).

[472] J. Feng, Q. Zhang, Z. Tu, et al., Degradation of silicone rubbers with different hardness in various aqueous solutions, Polym. Degrad. Stab., 109 (2014) 122-128.

[473] P. Liang, D. Qiu, L. Peng, et al., Structure failure of the sealing in the assembly process

for proton exchange membrane fuel cells, Int. J. Hydrogen Energy, 42 (2017) 10217-10227.

[474] J. Zhang, Y. Hu, Sealing performance and mechanical behavior of PEMFCs sealing system based on thermodynamic coupling, Int. J. Hydrogen Energy, 45 (2020) 23480-23489.

[475] D.H. Ye, Z.G. Zhan, A review on the sealing structures of membrane electrode assembly of proton exchange membrane fuel cells, J. Power Sources, 231 (2013) 285-292.

[476] R.L.N.C. James, NY, US), Valentine, Seth D. (Edmond, OK, US), Liestra, James (Penfield, NY, US), in, GM Global Technology Operations LLC (Detroit, MI, US), United States, 2013.

[477] B.R.H. (CA), G.P.R. (CA), R.J.A. (CA), et al., in, BALLARD POWER SYSTEMS (CA); BARTON RUSSELL H (CA); GIBB PETER R (CA); RONNE JOEL A (CA); VOSS HENRY H (CA), 1999.

[478] L. Zhang, J. Li, R. Li, et al., Research on the Hydrogen Supply System of Fuel Cell for Vehicle, Journal of engineering thermophysics, 43 (2022) 1444-1459.

[479] Y. Li, H. Chen, T. Zhang, et al., Research on Control Strategies for Vehicle Fuel Cell Systems, Chinese Journal of Automotive Engineering, 1-20.

[480] A. Dalvi, M. Guay, Control and real-time optimization of an automotive hybrid fuel cell power system, Control Engineering Practice, 17 (2009) 924-938.

[481] X. Zheng, R. Lin, Summarization of Control Strategy for Proton Exchange Membrane Fuel Cell, Electrical Engineering, (2017) 1-5+24.

[482] H.-Y. Lee, H.-C. Su, Y.-S. Chen, A gas management strategy for anode recirculation in a proton exchange membrane fuel cell, Int. J. Hydrogen Energy, 43 (2018) 3803-3808.

[483] Z. Liu, J. Chen, H. Liu, et al., Anode purge management for hydrogen utilization and

stack durability improvement of PEM fuel cell systems, Appl. Energy, 275 (2020) 115110.

[484] H. Yuan, H. Dai, W. Wu, et al., A fuzzy logic PI control with feedforward compensation for hydrogen pressure in vehicular fuel cell system, Int. J. Hydrogen Energy, 46 (2021) 5714-5728.

[485] H. He, S. Quan, Y.-X. Wang, Hydrogen circulation system model predictive control for polymer electrolyte membrane fuel cell-based electric vehicle application, Int. J. Hydrogen Energy, 45 (2020) 20382-20390.

[486] S. Quan, Y.-X. Wang, X. Xiao, et al., Disturbance prediction-based enhanced stochastic model predictive control for hydrogen supply and circulating of vehicular fuel cells, Energy Conversion and Management, 238 (2021) 114167.

[487] B. Blunier, A. Miraoui, Proton Exchange Membrane Fuel Cell Air Management in Automotive Applications, Journal of Fuel Cell Science and Technology, 7 (2010).

[488] A. Akroot, Ö. Ekici, M. Köksal, Process modeling of an automotive pem fuel cell system, International Journal of Green Energy, 16 (2019) 778-788.

[489] V.M. Sanchez, R. Barbosa, L.G. Arriaga, et al., Real time control of air feed system in a PEM fuel cell by means of an adaptive neural-network, Int. J. Hydrogen Energy, 39 (2014) 16750-16762.

[490] Z. Liu, H. Chen, L. Peng, et al., Feedforward-decoupled closed-loop fuzzy proportion-integral-derivative control of air supply system of proton exchange membrane fuel cell, Energy, 240 (2022) 122490.

[491] T. Zeng, L. Xiao, J. Chen, et al., Feedforward-based decoupling control of air supply for vehicular fuel cell system: Methodology and experimental validation, Appl. Energy, 335 (2023)

120756.

[492] D. Zhao, F. Li, R. Ma, et al., An Unknown Input Nonlinear Observer Based Fractional Order PID Control of Fuel Cell Air Supply System, IEEE Trans. Ind. Appl., 56 (2020) 5523-5532.

[493] Y. Tian, Q. Zou, J. Liu, et al., Novel Hybrid Control Scheme of a Proton Exchange Membrane Fuel Cell Air Supply System, Energy Technology, 10 (2022) 2100906.

[494] K. Ou, Y.-X. Wang, Z.-Z. Li, et al., Feedforward fuzzy-PID control for air flow regulation of PEM fuel cell system, Int. J. Hydrogen Energy, 40 (2015) 11686-11695.

[495] J. Hou, Z. Yang, T. He, et al., Research progress on thermal management of proton exchange membrane fuel cells, Journal of Central South University (Science and Technology), 52 (2021) 19-30.

[496] Y. Wang, Q. Gao, T. Zhang, et al., Advances in Integrated Vehicle Thermal Management and Numerical Simulation, Energies, 10 (2017) 1636.

[497] G. Zhang, S.G. Kandlikar, A critical review of cooling techniques in proton exchange membrane fuel cell stacks, Int. J. Hydrogen Energy, 37 (2012) 2412-2429.

[498] A. Ozden, S. Shahgaldi, X. Li, et al., A review of gas diffusion layers for proton exchange membrane fuel cells—With a focus on characteristics, characterization techniques, materials and designs, Progr. Energy Combust. Sci., 74 (2019) 50-102.

[499] J. Xu, C. Zhang, Z. Wan, et al., Progress and perspectives of integrated thermal management systems in PEM fuel cell vehicles: A review, Renewable and Sustainable Energy Reviews, 155 (2022) 111908.

[500] X.R. Wang, Y. Ma, J. Gao, et al., Review on water management methods for proton

exchange membrane fuel cells, Int. J. Hydrogen Energy, 46 (2021) 12206-12229.

[501] Y. Wang, K. Wang, S. Zhong, et al., Research Progress on Durability Enhancement-oriented Electric Control Technology of Automotive Fuel Cell System, Automotive Engineering, 44 (2022) 545-559.

[502] H. Zhou, Y. Zhang, S. Song, et al., Research progress of proton exchange membrane fuel cell drainage technology, Chinese Journal of Power Sources, 44 (2020) 774-777.

[503] J. Li, Y. Li, T. Yu, Temperature Control of Proton Exchange Membrane Fuel Cell Based on Machine Learning, Frontiers in Energy Research, 9 (2021).

[504] C.-Q. Su, J.-F. Sun, G.-D. Meng, et al., Thermal management control strategy of liquid-cooled fuel cell vehicle, Energy Reports, 8 (2022) 141-153.

[505] J. Li, Y. Li, T. Yu, Distributed deep reinforcement learning-based multi-objective integrated heat management method for water-cooling proton exchange membrane fuel cell, Case Studies in Thermal Engineering, 27 (2021) 101284.

[506] S. Fu, D. Zhang, S.W. Cha, et al., An extreme gradient boosting-based thermal management strategy for proton exchange membrane fuel cell stacks, J. Power Sources, 558 (2023) 232617.

[507] N. Sulaiman, M.A. Hannan, A. Mohamed, et al., Optimization of energy management system for fuel-cell hybrid electric vehicles: Issues and recommendations, Appl. Energy, 228 (2018) 2061-2079.

[508] H.S. Das, C.W. Tan, A.H.M. Yatim, Fuel cell hybrid electric vehicles: A review on power conditioning units and topologies, Renewable and Sustainable Energy Reviews, 76 (2017) 268-291.

[509] V. Das, S. Padmanaban, K. Venkitusamy, et al., Recent advances and challenges of fuel cell based power system architectures and control – A review, Renewable and Sustainable Energy Reviews, 73 (2017) 10-18.

[510] Z. Fu, L. Zhu, F. Tao, et al., Optimization based energy management strategy for fuel cell/battery/ultracapacitor hybrid vehicle considering fuel economy and fuel cell lifespan, Int. J. Hydrogen Energy, 45 (2020) 8875-8886.

[511] K. Song, X. Wang, F. Li, et al., Pontryagin's minimum principle-based real-time energy management strategy for fuel cell hybrid electric vehicle considering both fuel economy and power source durability, Energy, 205 (2020) 118064.

[512] X. Tang, H. Zhou, F. Wang, et al., Longevity-conscious energy management strategy of fuel cell hybrid electric Vehicle Based on deep reinforcement learning, Energy, 238 (2022) 121593.

[513] J. Zhou, C. Feng, Q. Su, et al., The Multi-Objective Optimization of Powertrain Design and Energy Management Strategy for Fuel Cell–Battery Electric Vehicle, Sustainability, 14 (2022) 6320.

[514] C. Jia, W. Qiao, J. Cui, et al., Adaptive Model-Predictive-Control-Based Real-Time Energy Management of Fuel Cell Hybrid Electric Vehicles, IEEE Transactions on Power Electronics, 38 (2023) 2681-2694.

Declaration of interests

☒ The authors declare that they have no known competing financial interests or personal relationships that could have appeared to influence the work reported in this paper.

☐ The authors declare the following financial interests/personal relationships which may be considered as potential competing interests: